Final Report

FDOT Contract No.: BDK-75-977-25

UF Contract No.: 00083426

Resistance Factors for 100% Dynamic Testing, With and Without Static Load Tests

Principal Investigators: Michael C. McVay
Harald Klammler

Department of Civil and Coastal Engineering
University of Florida
Gainesville, Florida 32611-6580

Developed for the

Rodrigo Herrera, P.E., Project Manager
Peter Lai, P.E., Co-Project Manager

May 2011

DISCLAIMER

The opinions, findings, and conclusions expressed in this publication are those of the authors and not necessarily those of the Florida Department of Transportation or the U.S. Department of Transportation.

Prepared in cooperation with the State of Florida Department of Transportation and the U.S. Department of Transportation.

SI (MODERN METRIC) CONVERSION FACTORS (from FHWA)

APPROXIMATE CONVERSIONS TO SI UNITS

SYMBOL	WHEN YOU KNOW	MULTIPLY BY	TO FIND	SYMBOL
LENGTH				
in	inches	25.4	millimeters	mm
ft	feet	0.305	meters	m
yd	yards	0.914	meters	m
mi	miles	1.61	kilometers	km

SYMBOL	WHEN YOU KNOW	MULTIPLY BY	TO FIND	SYMBOL
AREA				
in^2	square inches	645.2	square millimeters	mm^2
ft^2	square feet	0.093	square meters	m^2
yd^2	square yard	0.836	square meters	m^2
ac	acres	0.405	hectares	ha
mi^2	square miles	2.59	square kilometers	km^2

SYMBOL	WHEN YOU KNOW	MULTIPLY BY	TO FIND	SYMBOL
VOLUME				
fl oz	fluid ounces	29.57	milliliters	mL
gal	gallons	3.785	liters	L
ft^3	cubic feet	0.028	cubic meters	m^3
yd^3	cubic yards	0.765	cubic meters	m^3
NOTE: volumes greater than 1000 L shall be shown in m^3				

SYMBOL	WHEN YOU KNOW	MULTIPLY BY	TO FIND	SYMBOL
MASS				
oz	ounces	28.35	grams	g
lb	pounds	0.454	kilograms	kg
T	short tons (2000 lb)	0.907	megagrams (or "metric ton")	Mg (or "t")

SYMBOL	WHEN YOU KNOW	MULTIPLY BY	TO FIND	SYMBOL
TEMPERATURE (exact degrees)				
°F	Fahrenheit	5 (F-32)/9 or (F-32)/1.8	Celsius	°C

SYMBOL	WHEN YOU KNOW	MULTIPLY BY	TO FIND	SYMBOL
ILLUMINATION				
fc	foot-candles	10.76	lux	lx
fl	foot-Lamberts	3.426	candela/m^2	cd/m^2

SYMBOL	WHEN YOU KNOW	MULTIPLY BY	TO FIND	SYMBOL
FORCE and PRESSURE or STRESS				
Lbf*	poundforce	4.45	newtons	N
kip	kip force	1000	pounds	lbf
lbf/in^2	poundforce per square inch	6.89	kilopascals	kPa

APPROXIMATE CONVERSIONS TO SI UNITS

SYMBOL	WHEN YOU KNOW	MULTIPLY BY	TO FIND	SYMBOL
		LENGTH		
mm	millimeters	0.039	inches	in
m	meters	3.28	feet	ft
m	meters	1.09	yards	yd
km	kilometers	0.621	miles	mi

SYMBOL	WHEN YOU KNOW	MULTIPLY BY	TO FIND	SYMBOL
		AREA		
mm^2	square millimeters	0.0016	square inches	in^2
m^2	square meters	10.764	square feet	ft^2
m^2	square meters	1.195	square yards	yd^2
ha	hectares	2.47	acres	ac
km^2	square kilometers	0.386	square miles	mi^2

SYMBOL	WHEN YOU KNOW	MULTIPLY BY	TO FIND	SYMBOL
		VOLUME		
mL	milliliters	0.034	fluid ounces	fl oz
L	liters	0.264	gallons	gal
m^3	cubic meters	35.314	cubic feet	ft^3
m^3	cubic meters	1.307	cubic yards	yd^3

SYMBOL	WHEN YOU KNOW	MULTIPLY BY	TO FIND	SYMBOL
		MASS		
g	grams	0.035	ounces	oz
kg	kilograms	2.202	pounds	lb
Mg (or "t")	megagrams (or "metric ton")	1.103	short tons (2000 lb)	T

SYMBOL	WHEN YOU KNOW	MULTIPLY BY	TO FIND	SYMBOL
		TEMPERATURE (exact degrees)		
°C	Celsius	1.8C+32	Fahrenheit	°F

SYMBOL	WHEN YOU KNOW	MULTIPLY BY	TO FIND	SYMBOL
		ILLUMINATION		
lx	lux	0.0929	foot-candles	fc
cd/m^2	candela/m^2	0.2919	foot-Lamberts	fl

SYMBOL	WHEN YOU KNOW	MULTIPLY BY	TO FIND	SYMBOL
		FORCE and PRESSURE or STRESS		
N	newtons	0.225	poundforce	lbf
kPa	kilopascals	0.145	poundforce per square inch	lbf/in^2

*SI is the symbol for International System of Units. Appropriate rounding should be made to comply with Section 4 of ASTM E380.
(Revised March 2003)

TECHNICAL REPORT DOCUMENTATION PAGE

1. Report No.	2. Government Accession No.	3. Recipient's Catalog No.

4. Title and Subtitle	5. Report Date
Resistance Factors for 100% Dynamic Testing, With and Without Static Load Tests	May 2011
	6. Performing Organization Code
7. Author(s)	8. Performing Organization Report No.
Michael McVay and Harald Klammler	UF Project 00083426
9. Performing Organization Name and Address	10. Work Unit No. (TRAIS)
Department of Civil and Coastal Engineering 365 Weil Hall – P.O. Box 116580 University of Florida Gainesville, FL 32611-6580	11. Contract or Grant No. BDK-75-977-25
12. Sponsoring Agency Name and Address	13. Type of Report and Period Covered
Florida Department of Transportation 605 Suwannee Street, MS 30 Tallahassee, FL 32399	Final Report 09/24/09 - 06/30/11
	14. Sponsoring Agency Code

15. Supplementary Notes

16. Abstract

Current department of transportation (DOT) and Federal Highway Administration (FHWA) practice has highly variable load and resistance factor design (LRFD) resistance factors, Φ, for driven piles from design (e.g., Standard Penetration Tests (SPT), Cone Penetrometer Test (CPT)) to construction (e.g., pile monitoring). Complicating the construction effort, are the number of piles monitored (e.g., 10% versus 100%), as well as the type of monitoring (e.g., high strain rate: Embedded Data Collector (EDC), Pile Driving Analyzer (PDA), static load test, etc.). Of great interest are quantifying the influence of number of piles within a group, number of piles monitored, as well as spatial variability on a pile group's uncertainty and associated LRFD Φ factors.

The work started with an investigation of probability of failure (POF) of a bridge in terms of its piers and underlying piles. It was discovered that the number of piles in a pier may have a large impact on POF of a pier, which is why the development of LRFD Φ should occur with respect to pier (i.e., pile group) level and include the total number of piles within the group as well as the distribution of monitored and unmonitored piles within the group. Next, the total uncertainty of the pier including spatial variability and error of the method (e.g., SPT, EDC/PDA, etc.) was investigated. The work started with spatial uncertainty of single pile resistance (side plus tip) from SPT data and then extended through kriging (considering different weights for individual borings) to group layouts (e.g., double, triple, quads, etc.) for assessing group resistance uncertainty, CV_R. Subsequently, the kriging group work was carried over to assessing uncertainty, i.e., spatial and method error (predicted versus static load test) for high strain rate field measurements. Equations and charts were developed to quantify group uncertainty, CV_R, and LRFD Φ for typical group layouts and monitoring. The latter approach was considered to be inflexible, and the spatial uncertainty (i.e., kriging) was replaced with hammer monitoring in conjunction with high strain rate monitoring. Using the uncertainty of monitoring method ($CV_{\varepsilon m}$) and a measured uncertainty of blow count regression ($CV_{\varepsilon h}$) versus high strain rate monitoring, an LRFD Φ equation was developed for pile groups considering the numbers of monitored and unmonitored piles. The developed expression was evaluated at two sites and gave reasonable predictions compared to current practice.

17. Key Words	18. Distribution Statement
LRFD Φ, pile monitoring, pile groups, EDC, PDA, and CAPWAP	No restrictions.

19. Security Classif. (of this report)	20. Security Classif. (of this page)	21. No. of Pages	22. Price
Unclassified	Unclassified	105	

Form DOT F 1700.7 (8-72) Reproduction of completed page authorized

EXECUTIVE SUMMARY

The departments of transportation (DOTs) and the Federal Highway Administration (FHWA) have moved away from an allowable stress design (ASD) to a load and resistance factor design (LRFD) based on probability of failure for deep foundations. In the case of driven piles, LRFD Φ factors vary significantly from design methods (e.g., American Association of State Highway and Transportation Officials (AASHTO, 2004): Standard Penetration Test (SPT): Φ = 0.45) to construction monitoring (Φ = 0.65 — Pile Driving Analyzer (PDA), Embedded Data Collector (EDC)). Complicating the construction effort, are the number of piles monitored (e.g., 10% versus 100%), as well as the type of monitoring (e.g., high strain rate: EDC, PDA; static load test, etc.). Of great interest are quantifying the influence of number of piles within a group, number of piles monitored, as well as spatial variability, on a pile group's resistance uncertainty and associated LRFD Φ factors.

The effort started with a discussion of probability of failure (POF) of a bridge and defines failure in terms of redundant and non-redundant systems. It was found that the number of piles in a pier may have a large impact on POF at the pier level. Therefore, it was decided to establish the LRFD Φ based on the POF of the whole pier which includes the total number of piles within the group as well as the distribution of monitored and unmonitored piles within the group.

Next, to establish an LRFD Φ, total uncertainty — which included spatial variability (i.e., monitored versus unmonitored) and method error (e.g., SPT, EDC/PDA versus static load test) — was investigated. The work started with spatial group uncertainty of a single pile resistance (side plus tip) from SPT data and was then extended through kriging (considering different weights for adjacent borings) to group layouts (e.g., double, triple, quads, etc.) to assess group uncertainty CV_R. Subsequently, the kriging group work was carried over to assessing

uncertainty, i.e., spatial and method error (predicted versus static load test) for high strain rate field measurements. The effort developed charts identifying the uncertainty (variance) reduction (α_e) for a specific group based on number and geometric configuration of piles monitored within a group, total piles within the group, and number of pile groups at the site. Unfortunately, no simple analytical expression for variance reduction in terms of pile group layouts could be developed and the approach had limited flexibility in the sense of assuming all piles had similar embedment depths or blow counts (i.e., also similar resistances) and the group design load was unknown apriori.

To overcome these problems associated with the spatial uncertainty, the use of hammer blow count data in combination with high strain rate measurements was introduced to assess a pile group's resistance uncertainty. Generally, good correlations were observed with static capacity by using Federal Highway Administration (FHWA) Gates dynamic formula (Paikowsky, 2004) or high strain rate test assessments. As with prior work, the uncertainty of the pile group was expressed in terms of the uncertainties of monitored ($CV_{\varepsilon m}$: high strain rate data: EDC, PDA, etc.) and unmonitored piles (hammer blow count measurements). In terms of the unmonitored piles within a group, their uncertainty ($CV_{\varepsilon h}$) was assessed by linear correlation between blow count data and EDC/PDA capacities. Subsequently, the total group resistance R_g, and its associated uncertainty in terms of the coefficient of variation CV_R, was assessed. Using the group uncertainty CV_R with a representative reliability of the group (e.g., $\beta = 3$), a relatively simple LRFD Φ expression was developed for a driven pile group depending on number of monitored and unmonitored piles in the group, and uncertainty of monitoring method ($CV_{\varepsilon m}$) as well as uncertainty of blow count regression ($CV_{\varepsilon h}$). The applicability of the developed LRFD Φ expression was evaluated on two separate sites with driven prestressed concrete piles. Interestingly, full monitoring gave LRFD Φ values similar to literature (i.e., AASHTO, 2009,

Florida Department of Transportation, 2009); however of great importance and not reported in the literature is the influence of pile group size and uncertainty of monitoring approach (i.e., $CV_{\varepsilon m}$, and $CV_{\varepsilon h}$). Finally, the proposed expression will allow different considerations, such as different degrees of method uncertainties (e.g., due to employing end of drive (EOD) versus beginning of redrive (BOR): variability of pile capacities; equipment, as well as site and soil conditions.

TABLE OF CONTENTS

LIST OF TABLES

LIST OF FIGURES

CHAPTER 1
INTRODUCTION

1.1 Background

The recommended load and resistance factor design (LRFD) Φ factor for the design of driven piles using in situ Standard Penetration Tests (SPT) varies from 0.35 to 0.45 (e.g., AASHTO Table 10.5.5.2.3-1 –Tomlinson versus Meyerhof). The value of Φ is a combination of uncertainty of design methods (i.e., Tomlinson versus Meyerhof) and number of borings as well as their locations relative to the pile. In the case of high strain rate field monitoring (e.g., Pile Driving Analyzer (PDA), Embedded Data Collector (EDC)), LRFD Φ factor increases to 0.65 according to FDOT Structures Design Guidelines if PDA and CAPWAP are used for approximately 10% of the piles during driving. In general, increasing LRFD Φ from 0.45 to 0.65 could potentially result in a 40% saving in pile length cost in uniform soil deposit without consideration of reduced driving times, equipment needs (e.g., bigger crane for longer piles), etc.

Recently, the Florida Department of Transportation (FDOT) funded the development of wireless pile monitoring, i.e., EDC, focusing on reducing pile monitoring cost/time and improved safety. Specifically, the technology uses: 1) wireless communication, which eliminates the need for personnel to climb (safety) pile leads (in some instances > 80 ft.) for gage attachment to the pile; 2) dual location of the instrumentation, which improves the "real time" assessment of dynamic stresses (e.g., pile damage during hard driving), static tip resistance (end bearing piles) for every hammer blow, as well as separation of side from tip resistance (dynamically and statically); and finally, 3) the wireless system, the instrumentation of which uses technologies developed for other mass markets (e.g., automotive, ITT, etc.) leading potentially to a larger number of monitored piles, e.g., 100% .

Of great interest is the appropriate LRFD Φ resistance value based on the number of piles monitored within a group. Obviously, monitoring every pile should increase Φ, but if the prediction method is non-conservative (e.g., biased) LRFD Φ should be less than one, whereas, for a conservative method Φ may be greater than one. In addition, if the designer/contractor decides to monitor just 50% of the piles, what are the recommended LRFD Φ factors given the soil/rock strength variability (coefficient of variation CV and spatial correlation, i.e., covariance)?

Current design practices suggested by AASHTO (2009) (Table 1-1) use pre-defined values of Φ depending on number of piles monitored, type of monitoring, and whether static load testing is performed. For example, Φ = 0.75 if all piles are monitored and Φ = 0.80 if 2% of the piles are monitored plus one static load test is performed. The table does consider older monitoring approaches (e.g., Gates, Φ = 0.40) based on hammer energy and measured blow counts. Evidently, all of the approaches do not explicitly account for the spatial heterogeneity that generally exists between individual piles (monitored and unmonitored) in a group, number of piles

Table 1-1. AASHTO 10.5.5.2.3-1 (2009)

Condition/Resistance Determination Method		Resistance Factor
Nominal bearing resistance of single pile–dynamic analysis and static load test method	Driving criteria established by successful static load test of at least one pile per site condition and dynamic testing of at least two piles per site condition, but no less than 2% of the production piles	0.8
	Driving criteria established by successful static load test of at least one pile per site condition without dynamic testing	0.75
	Driving criteria established by dynamic testing conducted on 100% of production piles	0.75
	Driving criteria established by dynamic test with signal matching at beginning of redrive (BOR) conditions only of at least one product pile per pier, but no less than the number of tests provided in Table 10.5.5.2.3-3	0.65
	Wave equation analysis, without pile dynamic measurements or load test, at end of drive (EOD) conditions only	0.4
	Federal Highway Administration (FHWA)-modified Gates dynamic pile formula (EOD conditions only)	0.4
	Engineering News-Record (as defined in Article 10.7.3.8.5) dynamic pile formula (EOD condition only)	0.1

monitored within a group, and if combined methods were used (i.e., high strain rate with hammer blow counts, etc.). Also, due to the typical dimensions of driven piles and expected vertical loads, piles are generally combined in a group underneath a rigid pile cap to form a foundation. For such a pile group foundation, if there are none, some, or all individual piles monitored, it will result in different pile group resistance uncertainties and, hence, different design LRFD resistance factors Φ of the group. Typically, the larger the number of piles monitored, the smaller the coefficient of variation of group resistance CV_R, thus leading to higher Φ for the group.

1.2 Scope of Research

The present work attempts to address the shortcomings of current assessment of LRFD Φ during construction by exploring a geostatistical approach, as well as combining monitored data with secondary information such as Standard Penetration Test / Cone Penetrometer Test (SPT/CPT) or hammer blow count data. In what follows, a brief discussion will be given on the general aspects of measurement bias and uncertainty as well as the probability of failure (reliability), the latter being perhaps the most fundamental parameter in reliability based design (Chapter 2). The work then proceeds to an investigation of the uncertainty of single driven pile resistances based on SPT/CPT data and the FB-Deep design method (Chapter 3). Further, geospatial kriging approaches are presented for pile groups with nearby SPT/CPT data (Chapter 4) and for partially or fully monitored pile groups (Chapter 5). Finally, the work focuses on correlation between monitored pile resistances and hammer blow count data. The latter is found to significantly simplify the geospatial approach and make it more flexible in the sense that less restrictive assumptions are required (Chapter 6). Although different chapters are related to each other and a consistent nomenclature is used, deviations may occur and all variables are defined in their respective chapters.

CHAPTER 2
GENERAL ASPECTS OF DEEP FOUNDATION RELIABILITY ASSESSMENT

2.1 Estimation Bias and Uncertainty

Ideally, pile resistance measurements would be obtained from static load tests on each and every pile, as they represent a direct replication of pile behavior under service with sufficiently non-transient (e.g., excluding impact loads) conditions. The static load test measurements are generally considered as the "true" values. However, static load tests are costly and time-consuming. Consequently, faster and cheaper methods (SPT/CPT, EDC, PDA, etc.) have been developed to predict the resistance measured in a top down static load test. Any prediction method may be biased as well as imprecise, i.e., contain uncertainty. Bias generally refers to systematic errors between the predictor and true measure (e.g., load test) which remain after unit conversion (e.g., from SPT blow counts to resistance) and may be corrected for by a deterministic relationship (i.e., a formula). Imprecision or uncertainty of the method relates to a random prediction error (variance σ_ε^2) which remains after bias correction and is due to purely random components of the measurement process (e.g., instrument errors, imperfections in pile geometry, etc.).

A bias correction formula applied after unit conversion is equivalent to improving (correcting) the unit conversion formula itself. Figure 2-1 shows scatterplots of predicted values (a) before bias correction P' and (b) after bias correction P versus true values T. It may be seen that P is a good predictor of T in the sense that the prediction error $\varepsilon = P - T$ is zero on average. The residual scatter of the data points about the 45° line represents the random prediction error (uncertainty) and is described by the variance σ_ε^2 of the residuals ε.

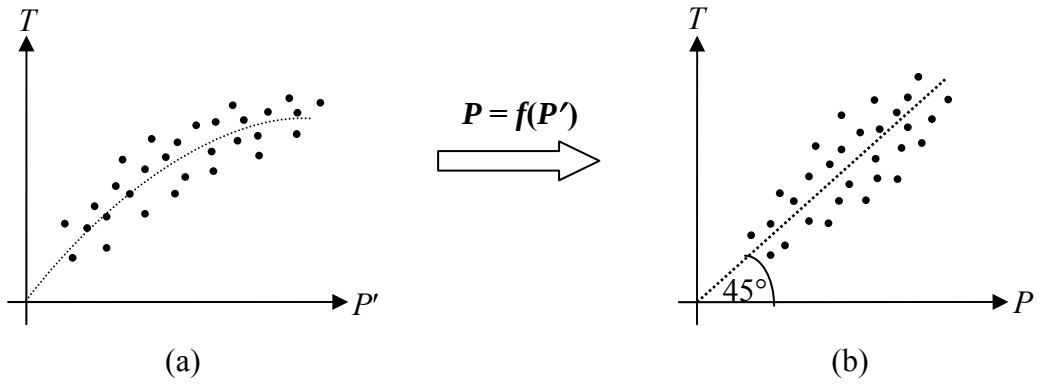

Figure 2-1. Scatterplots of predicted values: (a) before bias correction P'; and (b) after bias correction P versus true values T.

From this it is seen that "bias correction" is equivalent to finding the relationship between P and P' (e.g., $P = a + b\,P'$, $P = \ln(P')$, etc.) as indicated in Figure 2-1. For this purpose, both the type of relationship (e.g., linear, logarithmic, etc.) as well as its coefficients (e.g., a and b) need to be investigated. Once P is known, σ_ε^2 is obtained as the variance of the random prediction error ($\varepsilon = P - T$) distribution. The random prediction error σ_ε^2 may be a constant or depend on T; for example, if σ_ε is directly proportional to T, then the coefficient of variation of error ($CV_\varepsilon = \sigma_\varepsilon/\mu_\varepsilon$ = standard deviation divided by mean) is a constant.

Note that different bias relationships may apply to different combinations of prediction method, construction methods, and soil conditions. Sufficient predicted versus true data pairs are required to define bias relationships and values of σ_ε^2 for the largest possible number of prediction-construction-soil scenarios. Once bias is corrected for, P is known to be equal to T except for some random error of variance σ_ε^2 which allows for subsequent (geo-) statistical treatment.

2.2. Probability of Failure

The probability of failure (POF) and reliability index β are related by definition through the normal cumulative distribution function as illustrated in Figure 2-2.

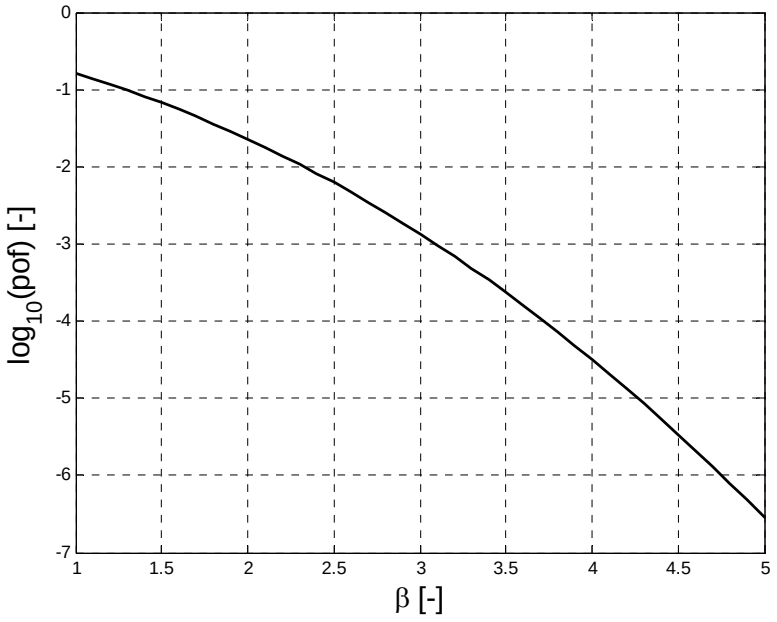

Figure 2-2. Probability of failure (POF) versus reliability index β. Here, $p_f = G(-\beta)$ where $G(\ )$ is the normal cumulative distribution function.

The POF p_b of a whole bridge is determined by the POFs and the level of redundancy of its individual components. Limiting our attention to foundation failure only (i.e., not considering failure of other structural bridge components), then p_b becomes a mere function of the individual POFs p_{ri} of each of its n_r piers. The level of redundancy expresses how many piers must simultaneously fail in order to cause the whole bridge to fail. Full redundancy means that all piers must fail for the bridge to fail; this is not a reasonable assumption for bridges, but may be so for other structures. For such a case,

$$p_b = \prod_{i=1}^{n_r} p_{ri} = p_r^{n_r} \tag{2.1}$$

where Π denotes the product operator (i.e., successive multiplication of terms) and the last term is obtained if $p_{ri} = p_r$ for all i, i.e., if all pier POFs are the same. In the case of no redundancy, failure of a single pier or multiple piers causes the whole bridge to fail. This is more likely to be the case with bridges and p_b is obtained as

$$p_b = 1 - \prod_{i=1}^{n_r} (1 - p_{ri}) = 1 - (1 - p_r)^{n_r} \tag{2.2}$$

where the last term is again the case where all piers have the same POF p_r. The term $1 - p_{ri}$ represents the probability of pier i not failing and, hence, the term $\prod_{i=1}^{n_r} (1 - p_{ri})$ is the probability of none of the piers to fail. The term $1 - \prod_{i=1}^{n_r} (1 - p_{ri})$ represents the probability that one or more piers fails and, hence, the bridge fails. An intermediate level of redundancy would be the scenario of bridge failure caused by simultaneous failure of two, three or more piers, which may be required to occur at adjacent locations or not. The laws of combination / permutation may be used to establish a general equation for this situation which will contain Equations 2.1 and 2.2 as limiting cases. For cases when bridge failure requires failure of more than a single pier, additional complexity may be added by the fact that failure of one pier may increase the POF of other (e.g., immediately adjacent) piers through load redistribution. This behavior may be captured by making use of conditional POF's, i.e., values of p_{ri} which depend on the number and locations of previously failed piers.

The very same discussion of bridges applies to the relationship between POFs of a pier and the individual piles beneath the pier. Let pier i consist of n_{li} piles, then Equations 2.1 and 2.2 may be rewritten as

$$p_{ri} = \prod_{j=1}^{n_{li}} p_{lj} = p_l^{n_{li}} \tag{2.3}$$

if all piles must fail for the pier to fail, and

$$p_{ri} = 1 - \prod_{j=1}^{n_{li}} \left(1 - p_{lj}\right) = 1 - \left(1 - p_l\right)^{n_{li}} \tag{2.4}$$

if failure of one or more piles cause pier failure. Here p_{lj} is the POF of the j-th pile, which is equal to p_l if it is the same for all piles. Note that indices "b", "r" and "l" are used for bridge, pier and pile, respectively, and "i" and "j" are running indices for piers and piles, respectively. Equations 2.3 and 2.4 may be substituted into Equations 2.1 and 2.2 to obtain a relationship between individual pile and bridge POF for full and no redundancy. Generally in bridge design, very stiff pile caps introduce a high level of redundancy among individual piles while almost no redundancy exists between individual piers. For this situation and assuming all pile POFs are equal to p_l and that all piers have the same number n_l of piles such that all pier POFs are equal as well, we get by substituting Equation 2.3 (full redundancy) into Equation 2.2 (no redundancy)

$$p_b = 1 - \left(1 - p_l^{n_l}\right)^{n_r} \tag{2.5}$$

Overall, it may be observed that a high level of redundancy of piers leads to a decreased POF of a bridge and a higher level of redundancy of piles leads to a decreased POF of a pier (Equations 2.1 and 2.3). This decrease becomes stronger with more elements that must fail simultaneously for the system to fail. On the other hand, a low level of redundancy of piers leads to increased POF of a bridge and so is of piles for a pier (Equations 2.2 and 2.4). This is due to the fact that failure of a single (or a few) out of many elements causes the system to fail. The larger the total number of elements involved and the smaller the number of elements whose simultaneous failure causes the system to fail, the larger the increase in POF. Figure 2-3 illustrates this by graphically representing the relationship of Equation 2.5 for three different values of p_l (10^{-2}, 10^{-3} and 10^{-4}). It is seen that for the typical values of p_l, the selected n_l has a

dominant influence on p_b over n_r, i.e., the number of piles in a pier is an important magnitude. For $n_l = 1$, however, it is seen that $p_b < p_l$, while for $n_l > 1$, $p_b > p_l$ up to rather large values of n_r (not shown here). For bridges founded on multiple pile piers with a target POF assigned to individual piles, the POF of the whole bridge is seen to be very conservative (i.e., very much smaller than the target value).

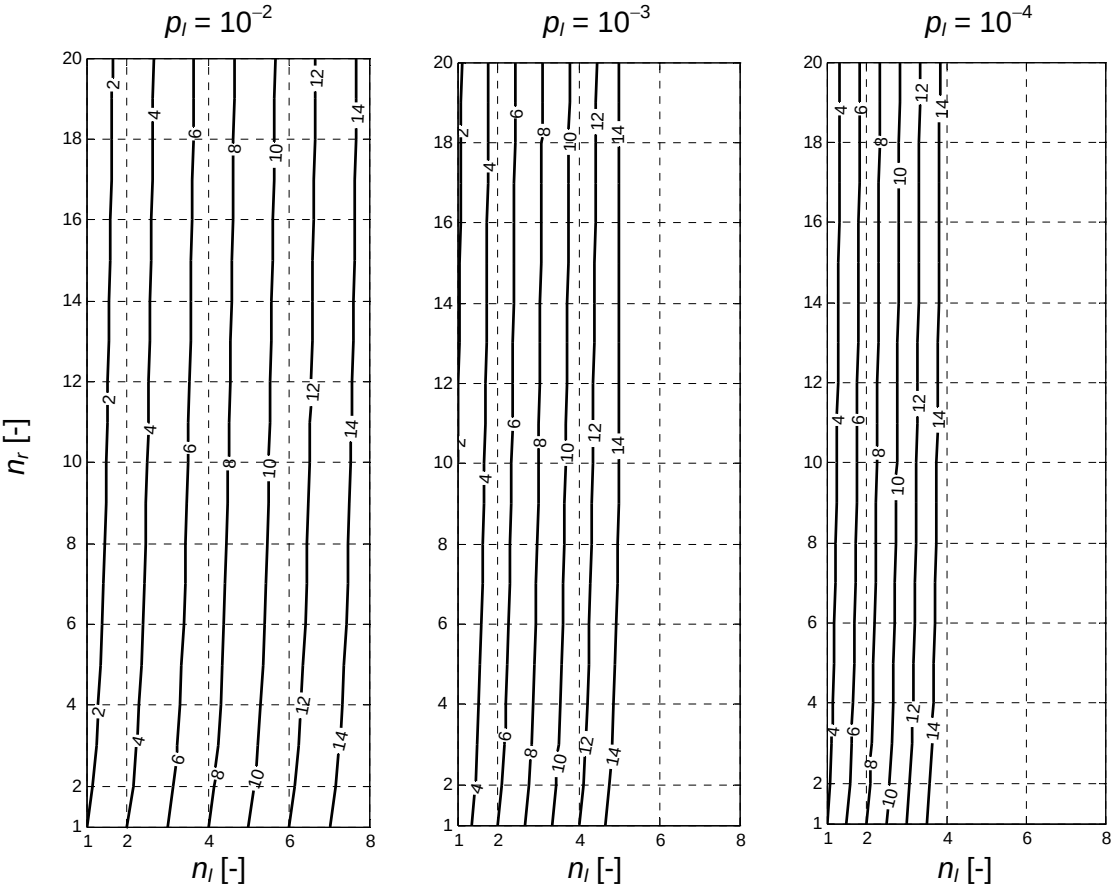

Figure 2-3. Contour lines of $-\log_{10}(p_b)$ as a function of p_l, n_l, and n_r from Equation 2.5.

As a consequence, it is fundamental to know what structural level (e.g., pile, pier, bridge) a certain POF or reliability β that the analysis is considering. Ideally, it may be desired to design a bridge such that a maximum allowable POF at the entire bridge level is met (or for a whole highway between points A and B). However, the number of structural elements involved at

bridge level is quite large and generally outside the geotechnical field. Based on the latter and the fact that design loads are typically given at the bridge pier level (rather than bridge level), it is understood in what follows that values of POF β and, hence Φ, always correspond to the pier level (i.e., for entire pile groups).

CHAPTER 3
SPATIAL UNCERTAINTY OF FB-DEEP SPT/CPT CAPACITY ASSESSMENT

3.1 Background

For different combinations of soil conditions (e.g., sand, clay, etc.) and the type of borehole data available (e.g., SPT or CPT), FB-Deep uses a series of simple relationships to estimate total resistances of driven piles. Since it is assumed that a pile is driven at a particular boring location (data along center line of pile), values of Φ only consider the uncertainty of the estimation method. However, a pile may be driven at a random location at a site (i.e., without collocated data) over which several SPT/CPT soundings may have been obtained. Quantification of Φ in this case requires accounting for spatial variability, the effect of which is investigated in the present chapter. For this purpose, the effect of method uncertainty is neglected, however, it may be added back in without loss of applicability. For simplicity, a single geological layer is assumed, which allows for deriving closed form solutions and facilitating some insight into spatial upscaling of side friction and end bearing separately, as well as in combination (side-tip correlation). Note, however, that the results are only applicable to the FB-Deep methods identified.

3.2 Theory

Figure 3-1 shows a schematic of a driven pile of length L and diameter D along the center line of which SPT or CPT data are available. Following the linear model implemented in FB-Deep, mean unit side friction f_s is estimated by

$$f_s = \frac{1}{n_L}\sum_{i=1}^{n_L} SN_i = \frac{S}{L}\int_0^L N(z)dz \tag{3.1}$$

where N_i is the number of blow-counts per depth interval for SPT or the mean driving force over a depth interval for CPT. The term n_L represents the number of depth intervals over the pile length L and S is a constant conversion factor from SPT or CPT data to unit side friction.

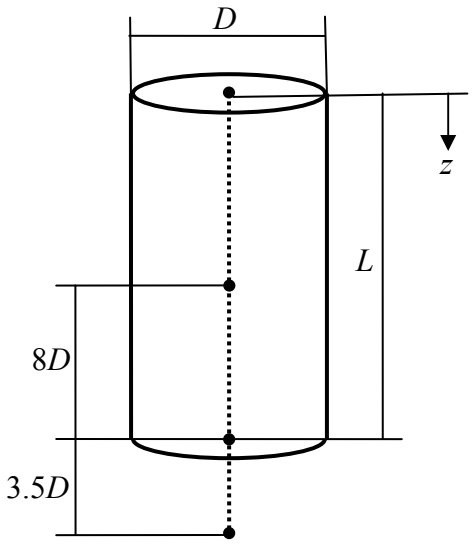

Figure 3-1. Schematic of driven pile (circular or square) with SPT or CPT data available along center line (dashed) for use in FB-Deep method.

Without loss of generality, depth intervals may be considered arbitrarily short leading to the integral form of Equation 3.1 (i.e., line averaging) on the far right-hand-side, where z is the vertical coordinate as indicated in Figure 3-1. From this, predicted pile side friction resistance R_s results as

$$R_s = DL\pi f_s = DS\pi \int_0^L N(z)dz \tag{3.2}$$

For predicting unit tip resistance q_t (in a single layer), a linear FB-Deep model uses

$$q_t = \frac{1}{2}\left(\frac{1}{n_{8D}} \sum_{i=1}^{n_{8D}} TN_i + \frac{1}{n_{3.5D}} \sum_{j=1}^{n_{3.5D}} TN_j \right) = \frac{1}{2}\left(\frac{T}{8D} \int_{L-8D}^{L} N(z)dz + \frac{T}{3.5D} \int_{L}^{L+3.5D} N(z)dz \right) \tag{3.3}$$

where n_{8D} and $n_{3.5D}$ are the number of depth intervals over distances 8D and 3.5D immediately above and below the center of the pile tip as illustrated in Figure 3-1. Term T is a constant conversion factor between SPT or CPT data and unit tip resistance. Predicted tip resistance R_t results as

$$R_t = \frac{D^2 \pi q_t}{4} = \frac{DT\pi}{64}\left(\int_{L-8D}^{L} N(z)dz + \frac{8}{3.5} \int_{L}^{L+3.5D} N(z)dz \right) \tag{3.4}$$

Summing Equations 3.2 and 3.4 leads to the total pile resistance R as

$$R = D\pi \left[S\int_{0}^{L} N(z)dz + \frac{T}{64}\left(\int_{L-8D}^{L} N(z)dz + \frac{8}{3.5} \int_{L}^{L+3.5D} N(z)dz \right) \right] \tag{3.5}$$

which is a weighted integral of N over $0 \leq z \leq (L + 3.5D)$ and can be written equivalently as

$$R = D\pi \int_{0}^{L+3.5D} g(z)N(z)dz \tag{3.6}$$

where

$$g(z) = \begin{cases} S & \text{for } 0 \leq z < L - 8D \\ S + \dfrac{T}{64} & \text{for } L - 8D \leq z < L \\ \dfrac{T}{28} & \text{for } L \leq z \leq L + 3.5D \end{cases} \tag{3.7}$$

Regarding N as a spatially random function in a geostatistical sense with mean μ_N, variance σ_N^2 and spatial covariance function C_N, then the mean μ_R and variance σ_R^2 of total pile resistance, R may be found. Taking the mean (expectation) of Equation 3.6 gives

$$\mu_R = D\pi\mu_N \int_0^{L+3.5D} g(z)dz = D\pi\mu_N\left(SL + \frac{TD}{4}\right) = DL\pi S\mu_N + \frac{D^2\pi}{4}T\mu_N \tag{3.8}$$

where the last two terms on the right-hand-side represent the means μ_{Rs} and μ_{Rt} of R_s and R_t, respectively.

The variance of the weighted sum in Equation 3.6 is known as

$$\sigma_R^2 = D^2\pi^2 \int_0^{L+3.5D}\int_0^{L+3.5D} g(z_1)g(z_2)C_N(z_1 - z_2)dz_1dz_2 \tag{3.9}$$

which is the sum of C_N for all possible location pairs over $0 \le z \le (L + 3.5D)$ weighted by the product of the respective values of $g(z)$ at both locations. Note that for side friction only, $T = 0$ and the integral in Equation 3.9 reduces to the form used for variance reduction of the line shaft approximation in previous work (Klammler 2010a and b). In order to eventually obtain values of LRFD Φ for a desired reliability through the AASHTO equation, it is of interest to express the coefficient of variation $CV_R = \sigma_R/\mu_R$ of R as a function of the coefficient of variation $CV_N = \sigma_N/\mu_N$ of N or

$$CV_R = \sqrt{\alpha}CV_N \tag{3.10}$$

Using Equations 3.8 and 3.9, the dimensionless conversion factor α is obtained as

$$\alpha = \frac{\int_0^{L+3.5D}\int_0^{L+3.5D} g(z_1)g(z_2)\,C'_N(z_1 - z_2)dz_1dz_2}{\left(LS + \frac{DT}{4}\right)^2} \tag{3.11}$$

where $C'_N = C_N/\sigma_N^2$ is the spatial covariance function of N normalized to unit sill (which makes it the spatial correlation function).

Combining Equations 3.7 and 3.11 α may be written as

$$\alpha = \frac{16}{\left(4LS + DT\right)^2}\left(I_1 + I_2 + I_3 + 2I_4 + 2I_5 + 2I_6\right) \tag{3.12}$$

which is proportional to the sum of the following six integrals:

$$\begin{aligned}
I_1 &= S^2 \int_0^L \int_0^L C_N'(z_1 - z_2)dz_1 dz_2 \\
I_2 &= \frac{T^2}{64^2} \int_{L-8D}^{L} \int_{L-8D}^{L} C_N'(z_1 - z_2)dz_1 dz_2 \\
I_3 &= \frac{T^2}{28^2} \int_{L}^{L+3.5D} \int_{L}^{L+3.5D} C_N'(z_1 - z_2)dz_1 dz_2 \\
I_4 &= \frac{ST}{64} \int_0^L \int_{L-8d}^{L} C_N'(z_1 - z_2)dz_1 dz_2 \\
I_5 &= \frac{ST}{28} \int_0^L \int_{L}^{L+3.5D} C_N'(z_1 - z_2)dz_1 dz_2 \\
I_6 &= \frac{T^2}{28 \cdot 64} \int_{L-8D}^{L} \int_{L}^{L+3.5D} C_N'(z_1 - z_2)dz_1 dz_2
\end{aligned} \tag{3.13}$$

Using Equation 3.13 with Equation 3.9, it may be seen that I_1 and I_2 correspond to the respective variances of the side and tip resistance along the pile; I_3 corresponds to the average below the tip; and I_4, I_5, and I_6 correspond to the respective covariances. As mentioned above, for side friction only $T = 0$ and only I_1 remains non-zero. Furthermore, the sum $I_2 + I_3 + 2I_6$ corresponds to the variance of R_t while the sum $I_4 + I_5$ corresponds to the covariance between R_s and R_t. Thus, by splitting up the integral in Equation 3.9 (e.g., as done in Equation 3.13) different variance and covariance components may be isolated. For example, $I_4 = I_{41} + I_{42}$ may be written with

$$\begin{aligned}
I_{41} &= \frac{ST}{64} \int_{L-8D}^{L} \int_{L-8D}^{L} C_N'(z_1 - z_2)dz_1 dz_2 \\
I_{42} &= \frac{ST}{64} \int_{0}^{L-8D} \int_{L-8D}^{L} C_N'(z_1 - z_2)dz_1 dz_2
\end{aligned} \tag{3.14}$$

With this, the integrals in I_1, I_2, I_3, and I_{41} are of the form $A = \int_a^b \int_a^b C'_N(z_1 - z_2)dz_1 dz_2$, while I_{42}, I_5 and I_6 are of the form $B = \int_a^b \int_b^c C'_N(z_1 - z_2)dz_1 dz_2$, where a, b and c are variable integration limits. Assuming that C_N is of the spherical type

$$C'_N(h) = \begin{cases} 1 - 1.5h + 0.5h^3 & \text{for } h < 1 \\ 0 & \text{for } h \geq 1 \end{cases} \tag{3.15}$$

where $h = |z_1 - z_2|/a_v$ and a_v is the vertical correlation length of N, the integral of type A has been solved in Appendix B of Final Project Report BD-545-76. Although mathematically simple, use of Equation 3.15 in the sequel requires lengthy algebraic manipulations and numerous case distinctions due to the separate definition of C_N on the intervals $h < 1$ and $h < 1$. Therefore, the exponential covariance function

$$C'_N(h) = e^{-3h} \tag{3.16}$$

is used in the analytical development hereafter. For direct numerical integration of Equation 3.11, however, both Equations 3.15 and 3.16 will be evaluated. As shown in Final Project Report BD-545-76 (Figures 3-1 and 3-2) in a closely related context, differences between Equations 3.15 and 3.16 when used with same a_v are negligible for all practical purposes. Moreover, the decision whether Equation 3.15 or 3.16 (or some other covariance model) is most adequate is mostly based on limited data (experimental variogram) and, hence, rather arbitrary or subjective.

Integral A will be solved here using $L_{ab} = |a - b|/a_v$ by transforming the double integral in dz_1 and dz_2 into a single integral in dh giving

$$A = \int_0^{L_{ab}} 2\left(L_{ab} - h\right) C'_N(h)dh \tag{3.17}$$

That is, instead of effectively pairing up all possible locations z_1 and z_2 over L_{ab} in the double integral, Equation 3.17 uses the frequency of occurrence of each separation distance h between all possible location pairs on L_{ab} (see Figure 3-2) which is equal to $2(L_{ab} - h)$ as apparent in the integrand of Equation 3.17. Combining Equations 3.16 and 3.17 and knowing that $\int xe^{kx}dx = \frac{e^{kx}}{k^2}(kx-1)$ gives

$$A = \frac{2L_{ab}}{3}\left[1 - \frac{1}{3L_{ab}}\left(1 - e^{-3L_{ab}}\right)\right] \tag{3.18}$$

This result may be validated against results of numerical integration shown in Figure 3-2 (for $D/a_h = 0$) of Final Project Report BD-545-76 (note that their $\alpha = A/L_{ab}^2$ here).

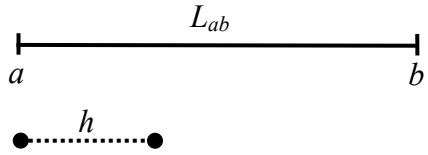

Figure 3-2. Illustration of how the double integral in A may be converted into a single integral using the frequency of occurrence of location pairs on L_{ab}, which are separated by distance h.

Integral B may be solved using L_{ab} as above and $L_{bc} = |b - c|/a_v$, where $L_{bc} \le L_{ab}$ is assumed without loss of generality (the order of integration in all double integrals above may be switched without affecting the results). The double integral in dz_1 and dz_2 may be transformed into a single integral in dh giving

$$B = \int_0^{L_{bc}} hC_N{}'(h)dh + \int_{L_{bc}}^{L_{ab}} L_{bc}\, C_N'(h)dh + \int_{L_{ab}}^{L_{ab}+L_{bc}} \left(L_{ab} + L_{bc} - h\right) C_N'(h)dh \tag{3.19}$$

Instead of effectively pairing up all possible location z_1 and z_2 in the double integral, Equation 3.19 uses the frequency of occurrence of each separation distance h between all possible location pairs of one point on L_{ab} and the other point on L_{bc}. This is illustrated in Figure 3-3 and the coefficients inside the integrands of Equation 3.19 indicate that separation distances between zero and L_{bc} occur h times, between L_{bc} and L_{ab} they occur L_{bc} times, and between L_{ab} and $L_{ab} + L_{bc}$ they occur $L_{ab} + L_{bc} - h$ times. Location pairs of $h > L_{ab} + L_{bc}$ cannot occur.

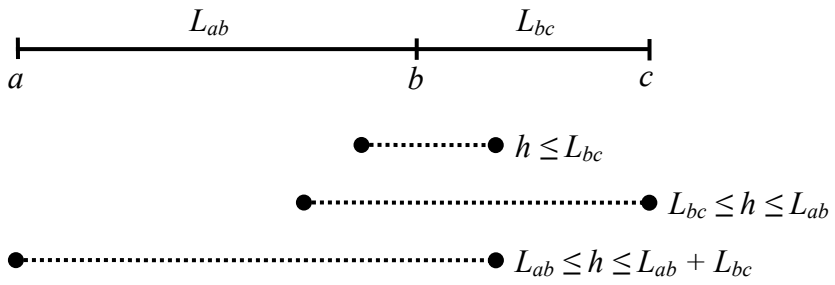

Figure 3-3. Illustration of how the double integral in B may be converted into a single integral using the frequency of occurrence of location pairs between L_{ab} and L_{bc}, which are separated by distance h.

Combining Equations 3.16 and 3.19 gives after some manipulations

$$B = \frac{1}{9}\left[1 - e^{-3L_{ab}} - e^{-3L_{bc}} + e^{-3(L_{ab}+L_{bc})}\right] \tag{3.20}$$

which shows the convenient fact that the condition $L_{bc} \le L_{ab}$ established for building Equation 3.19 becomes irrelevant (L_{ab} and L_{bc} may be switched in Equation 3.20 without affecting B).

Using Equations 3.18 and 3.20, the integrals of Equations 3.13 and 3.14 may be found using $L' = L/a_v$, $D' = D/a_v$ and the following equivalences: $L_{ab} = L'$ in A for I_1; $L_{ab} = 8D'$ in A for I_2; $L_{ab} = 3.5D'$ for A in I_3; $L_{ab} = 8D'$ in A for I_{41}; $L_{ab} = L' - 8D'$ and $L_{bc} = 8D'$ in B for I_{42}; $L_{ab} = L'$ and $L_{bc} = 3.5D'$ for B in I_5; and $L_{ab} = 8D'$ and $L_{bc} = 3.5D'$ in B for I_6. Substituting the results into Equation 3.12 gives

$$\alpha = \left[\frac{1}{3D'\left(\frac{1}{4}+\frac{R_{LD}}{R_{TS}}\right)}\right]^2 \left[\begin{array}{l} -\frac{193}{2048\cdot 49}+\frac{9}{32\cdot 7R_{TS}}-\frac{2}{R_{TS}^2}+\frac{6}{R_{TS}^2}L'+\frac{3}{2}\left(\frac{23}{128\cdot 7}+\frac{1}{R_{TS}}\right)D'- \\ -\left(\frac{9}{32\cdot 7R_{TS}}-\frac{2}{R_{TS}^2}\right)e^{-3L'}-\left(\frac{9}{2048\cdot 7}-\frac{1}{32R_{TS}}\right)e^{-24D'}+ \\ +\left(\frac{9}{128\cdot 49}-\frac{1}{14R_{TS}}\right)e^{-10.5D'}+\frac{1}{128\cdot 7}e^{-34.5D'}+\frac{1}{14R_{TS}}e^{-3(L'+3.5D')}- \\ -\frac{1}{32R_{TS}}e^{-3(L'-8D')} \end{array}\right] \quad (3.21)$$

where $R_{LD} = L/D = L'/D'$ and $R_{TS} = T/S$. As to be expected, α is not a function of T and S separately, but of their ratio R_{TS}.

3.3 Example of FB-Deep Spatial Uncertainty of a Pile/shaft in Sands

For SPT data in sand, for example, FB-Deep uses $S = 0.019$ and $T = 1.07$ (for output in tsf) such that $R_{TS} = 56.3$. With this, Equation 3.21 becomes

$$\alpha = \left[\frac{18.8}{14.1D'+L'}\right]^2 \left[\begin{array}{l} -1.92\cdot 10^{-3}+1.89\cdot 10^{-3}L'+6.51\cdot 10^{-2}D'-8.27\cdot 10^{-5}e^{-3L'}- \\ -7.27\cdot 10^{-5}e^{-24D'}+1.66\cdot 10^{-4}e^{-10.5D'}+1.12\cdot 10^{-3}e^{-34.5D'}+ \\ +1.27\cdot 10^{-3}e^{-3(L'+3.5D')}-5.55\cdot 10^{-4}e^{-3(L'-8D')} \end{array}\right] \quad (3.22)$$

Assuming a typical situation with a pile of $L = 30$ ft., $D = 1$ ft. and $a_v = 5$ ft., such that $L' = 6$, $D' = 0.2$, and $R_{LD} = 30$ the terms in Equation 3.22 become

$$\alpha = 4.54 \left[\begin{array}{l} -1.84\cdot 10^{-3}+1.13\cdot 10^{-2}+1.30\cdot 10^{-2}-1.25\cdot 10^{-12}- \\ -\mathbf{5}.96\cdot 10^{-7}+2.03\cdot 10^{-5}+1.12\cdot 10^{-6}+ \\ +2.34\cdot 10^{-12}-5.06\cdot 10^{-11} \end{array}\right] \quad (3.23)$$

which shows that, under this and similar situations, only the first three terms in the brackets are significant. Interesting to note is also that none of the significant terms depends on the actual

shape of the spatial covariance function (i.e., the exponential function in this case), but merely contain L' and D' expressing how many times L and D contain a_v. With this an approximation of Equation 3.22 may be written in a rational form as

$$\alpha \approx \frac{0.668L' + 23.0D' - 0.679}{\left(L' + 14.1D'\right)^2} \tag{3.24}$$

Figures 3-4 and 3-5 graphically represent results of Equations 3.22 and 3.24 for $L/D \geq 8$. The dashed line in Figure 3-4 is from Equation 3.22, where T was previously set to zero in Equation 3.21. Term $T = 0$ means that end bearing is excluded from consideration and the problem is based on side friction along a vertical line only ("line shaft approximation"). The dashed line appears to act as an upper bound for the continuous lines of $T > 0$, however, this is not generally true for other values of S and T. The approximations in Figure 3-5 are seen to be valid for $L/a_v > 1.5$, which is reasonable for practice. Figures 3-6 and 3-7 are analogous to Figures 3-4 and 3-5, with the exception that a spherical covariance model (Equation 3.15) is used instead of an exponential covariance model (Equation 3.16) and that graphs are obtained from numerical integration of Equation 3.11. In order for Equation 3.24 to be also a good approximation for the spherical covariance model, $\alpha^{1/2}$ from Equation 3.24 must be multiplied by 1.07. Note also that Figures 3-4 through 3-7 may be directly plugged into quadrant charts developed in previous work (Final Project Report BD-545-76) which allows for direct determination of required pile length L for given D, μ_N, CV_N, reliability β and design load Q_{des}. The corresponding design situation would be of possessing exhaustive sample data of N over a site associated with a random pile location.

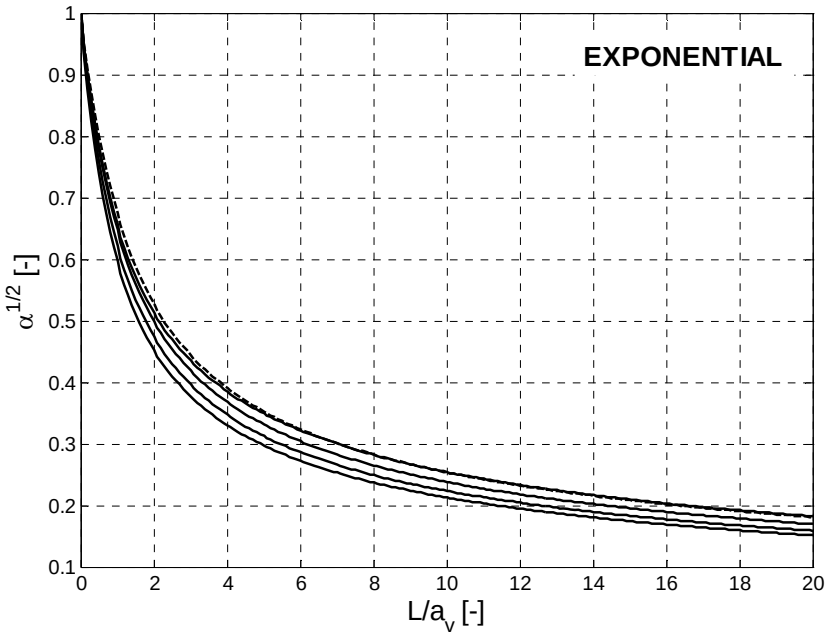

Figure 3-4. $\alpha^{1/2}$ from Equation 3.22 for exponential covariance function (Equation 3.16). Continuous lines from bottom up are for $L/D = \{8, 10, 15, \geq 30\}$. Dashed line is for $T = 0$, i.e., side friction only ("line shaft approximation").

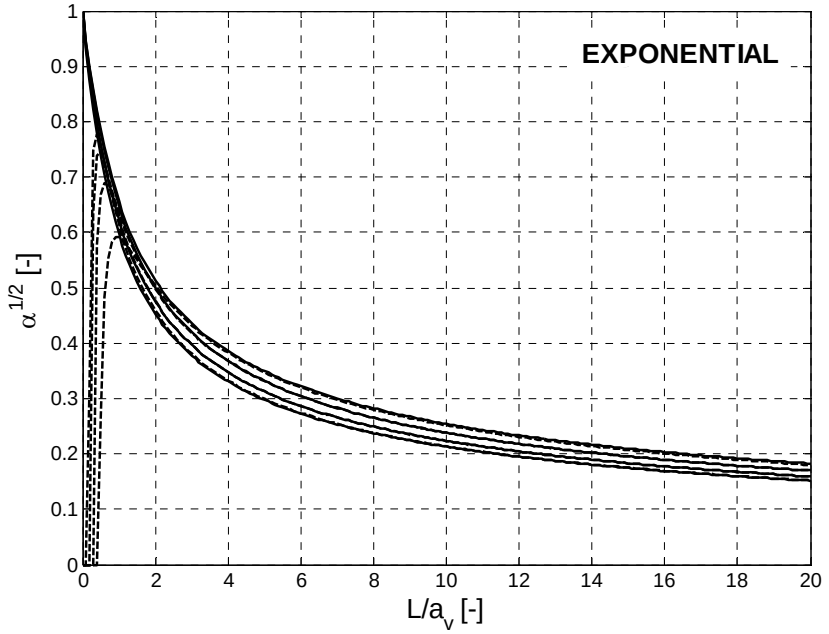

Figure 3-5. $\alpha^{1/2}$ from Equation 3.22 (continuous) and its rational approximation from Equation 3.24 (dashed) valid for $L/a_v > 1.5$. Lines from bottom up are for $L/D = \{8, 10, 15, \geq 30\}$.

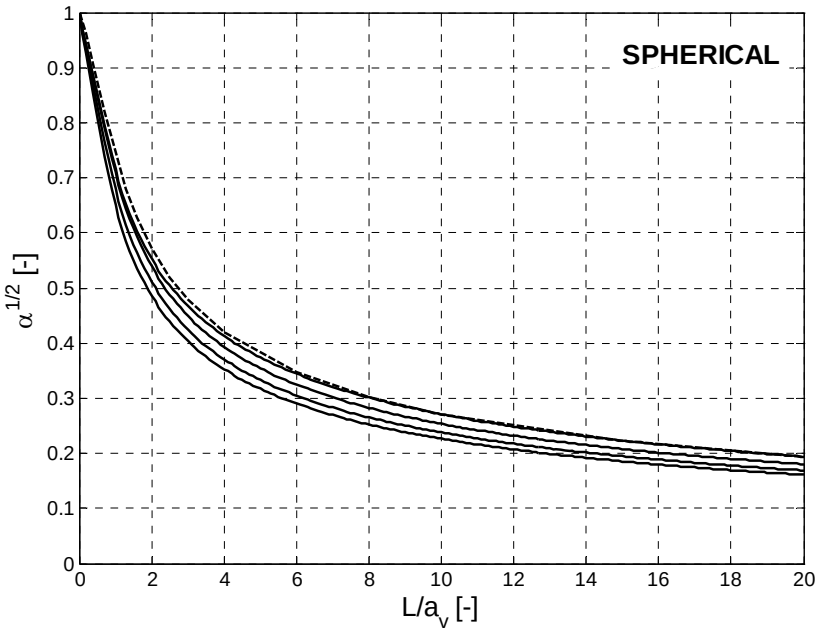

Figure 3-6. $\alpha^{1/2}$ from numerical integration of Equation 3.11 for spherical covariance function (Equation 3.15). Continuous lines from bottom up are for $L/D = \{8, 10, 15, \geq 30\}$. Dashed line is for $T = 0$, i.e., side friction only ("line shaft approximation").

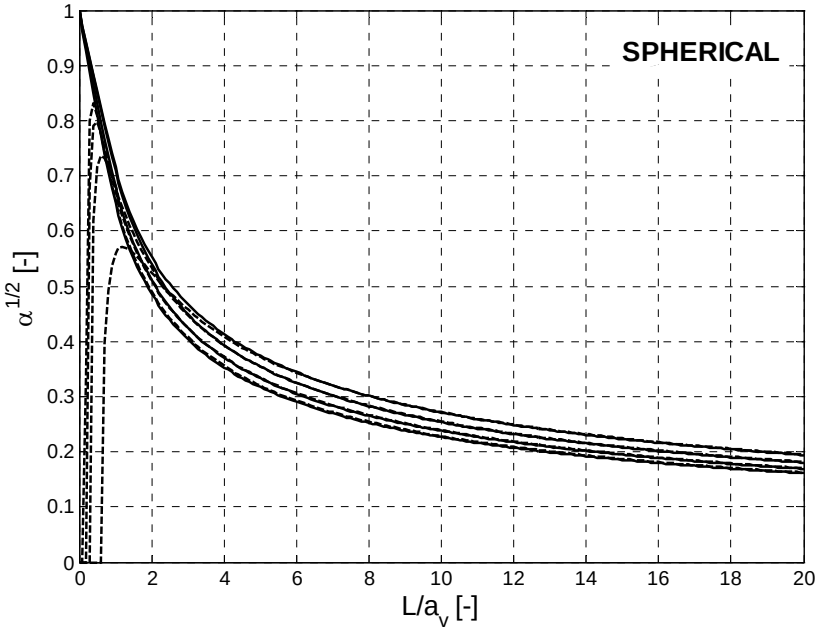

Figure 3-7. $\alpha^{1/2}$ from numerical integration of Equation 3.11 (continuous) and a rational approximation as 1.07 times α from Equation 3.24 (dashed). Approximation valid for $L/a_v > 1.5$ with $L/D \geq 15$ and for $L/a_v > 3$ with $L/D > 15$. Lines from bottom up are for $L/D = \{8, 10, 15, \geq 30\}$.

CHAPTER 4
PILE GROUP SPATIAL UNCERTAINTY WITH NEARBY SPT/CPT DATA

4.1 Background

The previous chapter considers exhaustive borehole (i.e., SPT or CPT) data available at a site where the influence of spatial variability on total pile resistance is investigated. The pile was considered to be randomly located or, equivalently, located beyond the spatial correlation range from available data. The present chapter expands on this by assuming SPT/CPT data from a limited number of borings, where spatial correlation between a "nearby" boring and the foundation may be present. Moreover, the analysis is generalized to allow for one or more piles in a group with tip resistance neglected until the next chapter for simplicity. As such, results are equally applicable to single or groups of drilled shafts with local strength data available from a number of borings which is the scenario providing the terminology used in the remainder of this chapter. A detailed discussion and analysis of worst case scenarios for unknown horizontal correlation lengths is illustrated by an example calculation at the conclusion of the chapter.

4.2 Notation

The term $q(x)$ denotes a spatially variable (random) function for local ground (i.e., soil or rock) strength with x being a spatial coordinate vector. The term $q(x)$ — or in short q — is described by a mean μ_q, variance σ_q^2 and a spatial covariance function $C_q(h)$ — or in short C_q — with h being a spatial separation vector between two locations x_1 and x_2. Variable C_q may be anisotropic with a range a_h in all horizontal directions and a range a_v in the vertical direction. A normalized spatial covariance function $C_q'(h_i) = C_q(h_i)/\sigma_q^2$ of unit sill and unit isotropic range may be defined by using $h_i = \sqrt{(h_h/a_h)^2 + (h_v/a_v)^2}$ where h_h and h_v are the horizontal and vertical

separation vector components, respectively, between two locations. The term f_s with mean μ_s and variance σ_s^2 is a random function used to describe the mean unit side friction over the lateral surface of area A_s of a single shaft of diameter D and embedment length L. Similarly, f_f with mean μ_f and variance σ_f^2 is a random function used to represent the mean unit side friction over the lateral surface area A_f of all n_s shafts of diameter D, length L and fundamental center-to-center separation distance D_s in the foundation or group. Finally, R_n and CV_R denote the foundation or group nominal resistance (defined as the mean of the random foundation resistance R) due to side friction and the respective coefficient of variation as a measure of uncertainty used in determining the LRFD resistance factor Φ.

4.3 Multiple Shaft Foundations without Conditioning Data

As opposed to single shaft foundations, failure of multiple shaft foundations in a group from axial loads may occur in one of two different forms: (1) along the set of disjoint lateral surfaces encompassing all of the individual shafts; or (2) along a single surface enclosing all shafts of a foundation or group (block failure). For $D_s/D > 2$ block failure may not be expected to occur (Zhang et al. 2001) and scenario (1) will be investigated in the present work with results presented for a typical value of $D_s/D = 3$. As in Klammler et al. (2010a), it is assumed in this section that the geostatistical parameters of q (i.e., μ_q, σ_q^2 and C_q) within a geostatistically homogeneous site (or subzone thereof) are well known which may be the case due to exhaustive rock core sampling, SPT/CPT soil testing, etc. Equation 4.1 describes the simple relationship between f_f and R

$$R = A_f f_f \tag{4.1}$$

where $A_f = n_s LD\pi$ is considered deterministic, i.e., with negligible uncertainty compared to f_f. R and f_f are random variables linked to q by the spatial upscaling (arithmetic averaging) process

$$f_f = \frac{1}{A_f} \int_{A_f} q \cdot dA \tag{4.2}$$

By taking the expectation and variance of Equation 4.2, the parameters μ_f and σ_f^2 are found as (Journel and Huijbregts 1978)

$$\mu_f = \mu_q \tag{4.3}$$

$$\sigma_f^2 = \frac{\sigma_q^2}{A_f^2} \int_{A_f} \int_{A_f} C_q' dA_1 dA_2 \tag{4.4}$$

where a variance reduction factor α_{qf} between local strength q and mean foundation unit side friction f_f may be defined as

$$\alpha_{qf} = \frac{\sigma_f^2}{\sigma_q^2} = \alpha_{sf} \frac{\sigma_s^2}{\sigma_q^2} = \alpha_{sf} \alpha_{qs} \tag{4.5}$$

which links the variability in local strength q to the uncertainty in foundation or group resistance R by $CV_R = \alpha_{qf}^{1/2} CV_q$ ("CV" being the notation for coefficient of variation of the variable in the index). Term α_{sf} in Equation 4.5 denotes an intermediate variance reduction factor between single shaft unit side friction f_s and the foundation unit side friction f_f. Furthermore, α_{qs} quantifies the variance reduction between local strength q and f_s as studied by Klammler et al. (2010a). The double integral in Equation 4.4 is nothing but the summation of the normalized covariance values between all possible combinations of point pairs on the n_s lateral shaft surfaces (i.e., the sum of all elements in the variance–covariance matrix between all possible point pairs) and may be evaluated numerically by discretizing each shaft surface into a large enough number of points (Journel and Huijbregts 1978). Calculations may hereby be accelerated by recognizing

that center-to-center separation distances between different shaft pairs are limited to a certain pattern (e.g., 3*D* for all shaft pairs on a side of a quadruple square foundation and $3\sqrt{2}D$ for shaft pairs on a diagonal). Thus, normalized covariances $C'_s(h_s) = C_s(h_s)/\sigma_s^2$ between upscaled single shaft resistances f_s (with h_s representing the horizontal separation distance between shaft centers) may be determined for these separation distances by using Equation 4.6 (Journel and Huijbregts 1978) to populate a respective variance–covariance matrix between all individual shafts in a foundation through

$$C'_s(h_s) = \frac{\sigma_q^2}{\sigma_s^2 A_{s1} A_{s2}} \int_{A_{s1}} \int_{A_{s2}} C'_q \, dA_1 dA_2 \tag{4.6}$$

where A_{s1} and A_{s2} are the lateral surface areas of two horizontally offset shafts. Equation 4.6 is, in fact, a generalization of Equation 4.4 (normalized to σ_s^2, i.e., unit sill) which is obtained by setting $A_{s1} = A_{s2} = A_f$, i.e., the total of all shafts' lateral surfaces. For $A_{s1} = A_{s2} = LD\pi$, i.e., a single shaft's lateral surface or zero separation between two shafts, Equation 4.6 reduces to the upscaled variance of f_s for single shafts as in Klammler et al. (2010a).

Figure 4-1 shows an example of a quadruple square configuration (hereafter called "*Q*") with respective shaft separation and variance–covariance matrices. The matrix in Figure 4-1c is based on numerical integration of Equation 4.6 where a spherical covariance function C_q is used with parameters $L/a_v = 5$ and $D/a_h = 0.1$. Based on the same principle of Equation 4.6, the average of all the elements in the variance–covariance matrix of all shafts directly results in the respective variance reduction factor α_{sf} defined in Equation 4.5. The shape of C'_s from Equation 4.6 is not easily described analytically; however, its horizontal correlation range is known to be equal to $a_h + D$ corresponding to the minimum horizontal separation distance between shaft centers for which all location pairs between shafts are beyond a_h and, thus, uncorrelated. Based

on this, an approximation to C_s', i.e., Equation 4.7, is proposed in the form of a spherical covariance function of range $a_h + D$, which avoids the numerical integration of Equation 4.6 and allows for a quick and direct population of the respective shaft variance–covariance matrix as shown in Figure 4-1d.

$$C_s'(h_s) \approx \begin{cases} 1 - 1.5\left(\dfrac{h_s}{a_h + D}\right) + 0.5\left(\dfrac{h_s}{a_h + D}\right)^3 & \text{for } \dfrac{h_s}{a_h + D} < 1 \\ 0 & \text{for } \dfrac{h_s}{a_h + D} \geq 1 \end{cases} \tag{4.7}$$

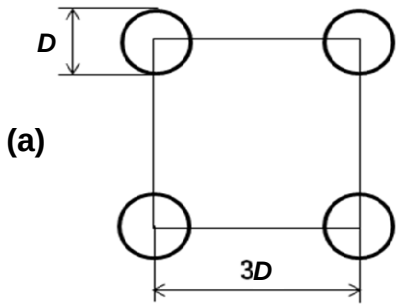

(b)	1	2	3	4
1	0	3	4.2	3
2	3	0	3	4.2
3	4.2	3	0	3
4	3	4.2	3	0

(c)	1	2	3	4
1	1	0.68	0.48	0.68
2	0.68	1	0.68	0.48
3	0.48	0.68	1	0.68
4	0.68	0.48	0.68	1

(d)	1	2	3	4
1	1	0.60	0.45	0.60
2	0.60	1	0.60	0.45
3	0.45	0.60	1	0.60
4	0.60	0.45	0.60	1

Figure 4-1. (a) Example of quadruple "*Q*" square configuration with (b) respective shaft separation matrix in multiples of *D*, and (c) and (d) are variance–covariance matrices in multiples of the upscaled single shaft variance σ_s^2. Part (c) is from numerical evaluation of Equation 4.6, while Part (d) assumes a spherical covariance function of range $a_h + D$ to approximate the horizontal covariance function C_s (Equation 4.7). A spherical covariance function for q and $L/a_v = 5$ and $a_h/D = 10$ are used. Bold italic numbers indicate shaft numeration and are used to label rows and columns of the matrices.

In addition to the quadruple configuration of Figure 4-1a, Figure 4-2 illustrates further multiple shaft configurations considered in this work (*D*1, *T*1 and *T*2). In analogy to Figure 4-1, for every configuration considered here and associated shaft separation distances, the variance–covariance matrices may be constructed using Equation 4.6 or 4.7 and α_{sf} may be found by averaging of all matrix elements. The averaging of the matrix elements may be summarized by the following equations where the type of foundation is indicated in the subscripts. Extensions to other group configurations not considered herein are straightforward.

$$\begin{aligned}
\alpha_{sf,D} &= 0.5\,C_s'(0) + 0.5\,C_s'(D_s) \\
\alpha_{sf,T1} &= 0.33(0) + 0.44\,C_s'(D_s) + 0.22\,C_s'(2D_s) \\
\alpha_{sf,T2} &= 0.33\,C_s'(0) + 0.67\,C_s'(D_s) \\
\alpha_{sf,Q} &= 0.25\,C_s'(0) + 0.5\,C_s'(D_s) + 0.25\,C_s'(\sqrt{2}D_s)
\end{aligned} \tag{4.8}$$

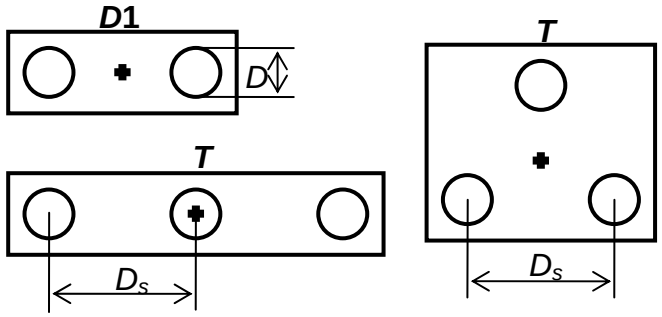

Figure 4-2. Further examples of multiple shaft configurations with rigid pile caps and possible center borings (crosses).

For the exact solution of Equation 4.6, values of C_s' and α_{sf} in Equation 4.8 are a function of L/a_v, D/a_h and D_s/D. For a typical value of $D_s/D = 3$ and using Equations 4.5 and 4.8, Figure 4-3 graphically represents the outcome of the exact solution of $\alpha_{qf}^{1/2}$ for different shaft configurations (single shafts "*S*" from Klammler et al. 2010b is included for reference). Using the approximation of Equation 4.7 (not shown for clearness of charts) instead of Equation 4.6

results in maximum errors in $\alpha_{qf}^{1/2}$ (and hence CV_R for a given CV_q) of approximately ±5 %. Errors are close to zero for $D/a_h < 0.05$, $D/a_h \approx 0.15$ and $D/a_h > 0.5$. For $0.05 < D/a_h < 0.15$ errors are negative (i.e., unconservative, which may be avoided by multiplication of $\alpha_{qf}^{1/2}$ by 1.05 in this range), while for $0.15 < D/a_h < 0.5$ errors are positive. Maximum positive and negative errors of the approximation also decrease as D_s/D increases and unconservative errors do not exceed 5% down to a theoretical value of $D_s/D = 1$ (results not shown).

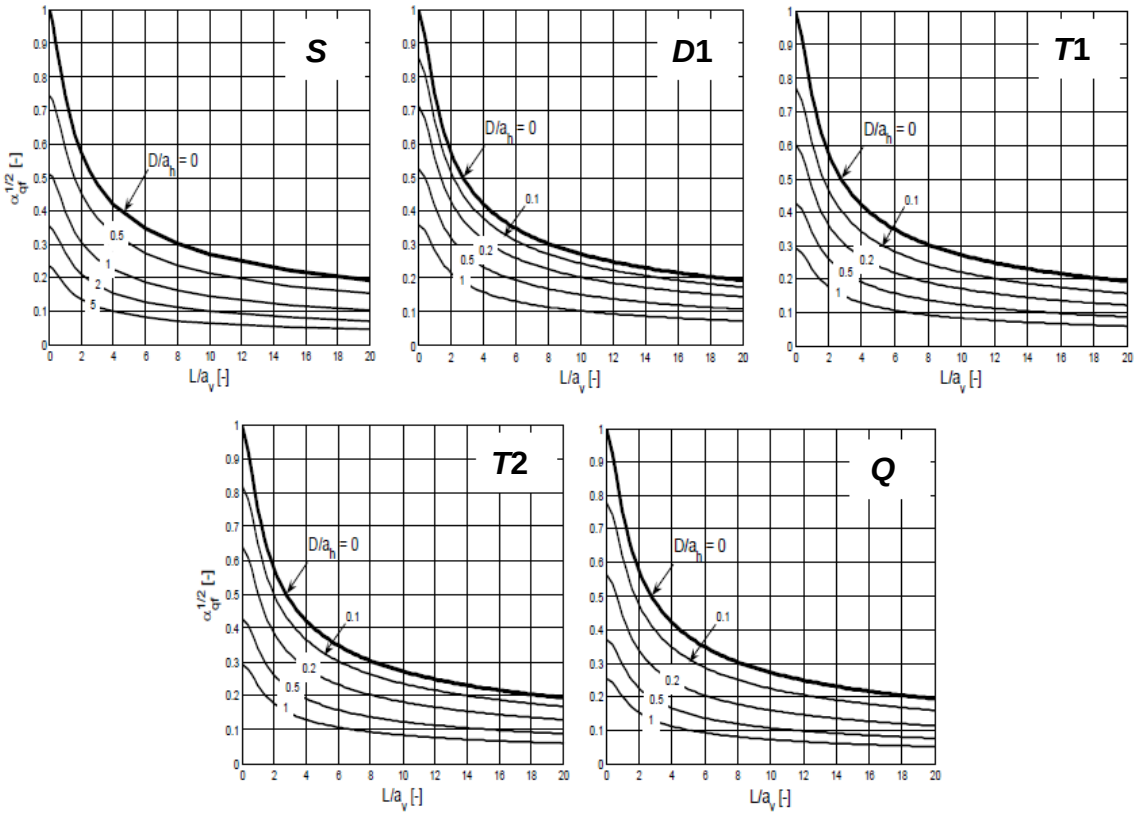

Figure 4-3. $\alpha_{qf}^{1/2}$ as a function of L/a_v for single and multiple shaft configurations of Figures 4-1 and 4-2 with $D_s/D = 3$. Thick graph corresponds to line shaft approximation $\alpha_0^{1/2}$.

The top graphs (case of $D/a_h = 0$) in Figure 4-3 are all identical; in this case the variance reduction is independent of the number and arrangement of shafts and equal to variance reduction α_0 for averaging over a vertical line of length L (termed "line shaft approximation" in Klammler et al. 2010a and b)

$$\alpha_0 = 1 - \frac{L}{2a_v} + \frac{L^3}{20a_v^3} \qquad \text{for} \quad 0 \le \frac{L}{a_v} \le 1$$
$$\alpha_0 = \frac{3a_v}{4L} - \frac{a_v^2}{5L^2} \qquad \text{for} \quad \frac{L}{a_v} \ge 1 \tag{4.9}$$

This is seen to be the common worst case scenario (maximum α_{qf} and CV_R) for all configurations in the case of potentially unknown a_h. For $D/a_h > 0.5$ correlation between individual shafts is zero and α_{sf} from shaft to foundation level becomes equal to $1/n_s$. Based on the assumption of lognormality for foundation resistance and computed CV_R, determination of LRFD resistance factor Φ may be achieved along the lines of Klammler et al. (2010a) by the following AASHTO (2004) formulae:

$$\Phi = \frac{\lambda_R \left(\gamma_D \frac{Q_D}{Q_L} + \gamma_L \right) \sqrt{\frac{1+CV_Q^2}{1+CV_R^2}}}{\left(\lambda_{QD} \frac{Q_D}{Q_L} + \lambda_{QL} \right) \exp\left\{ \beta \sqrt{\ln\left[\left(1+CV_R^2\right)\left(1+CV_Q^2\right) \right]} \right\}} \tag{4.10}$$

$$CV_Q^2 = \frac{\left(\frac{Q_D}{Q_L} \lambda_{QD} CV_{QD} \right)^2 + \left(\lambda_{QL} CV_{QL} \right)^2}{\left(\frac{Q_D}{Q_L} \lambda_{QD} \right)^2 + 2 \frac{Q_D}{Q_L} \lambda_{QD} \lambda_{QL} + \lambda_{QL}^2} \tag{4.11}$$

The term CV_Q hereby denotes the coefficient of variation of the random load and β is a user selected reliability index depending on the importance of a structure (admissible probability of failure). The remaining dimensionless parameters in Equations 4.10 and 4.11 may be chosen according to AASHTO (2004) for load cases I, II, and IV where dead load factor $\gamma_D = 1.25$, live load factor $\gamma_L = 1.75$, and the Federal Highway Administration (FHWA) recommended values of dead-to-live load ratio $Q_D/Q_L = 2$, resistance bias factor $\lambda_R = 1.06$, dead load bias factor $\lambda_{QD} = 1.08$, live load bias factor $\lambda_{QL} = 1.15$, dead load coefficient of variation $CV_{QD} = 0.128$ and live load coefficient of variation $CV_{QL} = 0.18$. It is worthwhile noting that Φ from Equation 4.10 is

based on CV_R of the whole foundation and, as such, assures a target probability of failure of the whole foundation and not just of a single shaft of the group (which would not be the actual design goal).

4.4 Single and Multiple Shaft Foundations with Conditioning Data

Knowing the exact locations of each foundation in the design process allows for collection of additional boring data inside or near the footprint (e.g., at the center as indicated by crosses in Figures 4-1 and 4-2 and considered hereafter) of a foundation to decrease uncertainty in predicted foundation resistances. In order to incorporate the influence of such collocated boring data, spatial correlation (conditioning) between data and the foundation is explored. The geostatistical tool used for this purpose is ordinary kriging (Journel and Huijbregts 1978), which delivers a predicted mean unit side friction f_f^* with an error variance σ_{fk}^2 between f_f^* and its true counterpart f_f. The resulting problem may be studied in a two-dimensional (horizontal) plane where each of n_b borings on a site is represented by a point associated to a data value equal to the mean q_{bi} (i = 1, 2… n_b) of the local strength observations in that boring (assuming that all borings are of approximately same length L). The foundation is represented by its horizontal cross section centered on one of the borings as illustrated by Figure 4-4.

Figure 4-4. Typical plan view of borehole (crosses) and foundation locations (e.g., quadruple shaft foundation for a bridge site). Not to scale.

For a full ordinary kriging solution, the horizontal covariances among all the borings themselves and between all the borings and the foundation would be required in order to

determine a specific kriging weight w_i ($\Sigma w_i = 1$) for each boring. The term f_f as given by Equation 4.2 is then predicted in the well known form by

$$f_f^* = \sum_{i=1}^{n_b} w_i q_{bi} \tag{4.12}$$

with a variance σ_{fk}^2 of the prediction error $f_f^* - f_f$ as

$$\sigma_{fk}^2 = \sigma_f^2 + \sum_{i=1}^{n_b}\sum_{j=1}^{n_b} w_i w_j C_b(x_i - x_j) - 2\sum_{i=1}^{n_b} w_i C_{bf}(x_i - x_f) \tag{4.13}$$

where C_b is the horizontal covariance function of q_b (i.e., a vertically upscaled version of C_q according to Equation 4.6) between boring locations x_i and x_j, and C_{bf} is the horizontal covariance function between q_b and f_f with x_f denoting the (center) location of the foundation. It is hereby assumed that the borings are sampled at intervals smaller than a_v such that additional sampling in a boring would only deliver highly redundant (i.e., correlated) information. With this, each boring may be considered as continuously sampled over depth and the actual numbers of samples per boring become irrelevant (i.e., do not appear in Equations 4.12 and 4.13). The three terms on the right-hand-side of Equation 4.13 are the variance σ_f^2 of f_f (Equation 4.4), the variance σ_{f*}^2 of f_{f*} and twice the covariance $C(f_f^*, f_f)$ between f_f^* and f_f whose negative sign reflects the benefit of conditioning data on prediction uncertainty. All terms may be directly obtained from Equation 4.6 with respective choices of A_1 and A_2.

In typical design situations, n_b borings at a site may consist of n_1 largely spaced borings from preliminary site investigation (i.e., previous to definition of foundation locations) and n_2 subsequent borings at potential foundation locations. In such cases, it may be reasonable to assume that no correlation exists between the borings at a site (i.e., $C_b(x_i\text{-}x_j) = C_b(0)$ for $i = j$ and equal to zero otherwise), except for when a preliminary boring happens to be in the vicinity of a future foundation location where a collocated boring is also obtained. In such a case, it is

conservative to consider full correlation between such nearby pairs of borings and reduce them to one "effective" boring by averaging (a non-simplified ordinary kriging solution would do the same). Thus, a conservative "effective" number of uncorrelated borings is obtained as $n_{be} \leq n_b$ (e.g., in Figure 4-4 $n_b = 8$ and $n_{be} = 6$). With the further assumption that only the collocated boring ($i = 1$) presents possible spatial correlation with f_f (i.e., $C_{bf}(x_i\text{-}x_f) = C_{bf}(x_1\text{-}x_f)$ for $i = 1$ and zero otherwise, a very simple ordinary kriging system may be constructed for determination of the kriging weights w_i as represented by Equation 4.14. The term w_1 represents the weight for the collocated boring, $w_2 = (1 - w_1)/(n_{be} - 1)$ the equal weights for all other borings ($w_i = w_2$ for $i > 1$), and μ is a Lagrangian operator.

$$\begin{bmatrix} C_b(0) & 0 & \cdots & 0 & 1 \\ 0 & C_b(0) & \ddots & \vdots & \vdots \\ \vdots & \ddots & \ddots & 0 & \vdots \\ 0 & \cdots & 0 & C_b(0) & 1 \\ 1 & \cdots & \cdots & 1 & 0 \end{bmatrix} \begin{bmatrix} w_1 \\ w_2 \\ \vdots \\ w_{be} \\ \mu \end{bmatrix} = \begin{bmatrix} C_{bf}(x_1 - x_f) \\ 0 \\ \vdots \\ 0 \\ 1 \end{bmatrix} \tag{4.14}$$

Solving for w_1 and w_2 gives

$$w_1 = \frac{1 + (n_{be} - 1)r}{n_{be}}$$
$$w_2 = \frac{1 - r}{n_{be}} \tag{4.15}$$

where $r = C_{bf}(x_1\text{-}x_f)/C_b(0)$ is a normalized covariance between q_{b1} (collocated boring) and f_f (foundation). With Equation 4.15 and $q_{bm} = 1/n_{be}\,\Sigma q_{bi}$ denoting the mean of all $i = 1, 2, \ldots, n_{be}$, effective borehole data Equation 4.12 may be written as

$$f_f^* = r q_{b1} + (1-r) q_{bm} \tag{4.16}$$

For $r = 0$, the collocated boring has no more predictive power than the other borings and $f_f^* = q_{bm}$, while for $r = 1$ the collocated boring is a perfect predictor such that $f_f^* = q_{b1}$. Substituting Equation 4.15 into Equation 4.13 under the above assumptions about C_b and C_{bf}, simplifying and dividing by σ_q^2 gives

$$\alpha_{qfk} = \frac{\sigma_{fk}^2}{\sigma_q^2} = \alpha_0 \left[\frac{(1-r)^2}{n_{be}} - r^2 \right] + \alpha_{qf} \tag{4.17}$$

as a respective variance reduction factor which accounts for limited data through n_{be} and data conditioning through r. Theoretically perfect prediction with $r = 1$ is possible only if the foundation is reduced to a vertical line (identical to the collocated boring), such that $\alpha_{qf} = \alpha_0$ correctly leading to $\alpha_{qfk} = 0$. For the opposite case of $r = 0$ (no conditioning to nearby data or random/unknown foundation location) and the conservative line shaft approximation ($\alpha_{qf} = \alpha_0$) Equation 4.17 reduces to a respective expression developed in Klammler et al. (2010b) for the presence of a limited number of test borings. Finally, Equation 4.17 is seen to correctly reduce to $\alpha_{qfk} = \alpha_{qf}$ of the previous section for $r = 0$ and $n_{be} >> 1$, i.e., no data conditioning and exhaustive data set available.

Equations 4.16 and 4.17 are directly valid for any type of single or multiple shaft foundation and required values of α_0 and α_{qf} may be readily obtained from Figure 4-3 and/or Equation 4.9. What remains to be determined is the correlation parameter r, which is obtained from Equation 4.6 with A_1 being a vertical line of length L (collocated boring) and A_2 being the total lateral foundation surface A_f. As such, Equations 4.16 and 4.17 are generally valid for arbitrary boring locations inside or nearby the foundation footprint. For the particular (but quite

typical) case of a boring at the center of the footprint (i.e., $x_1 = x_f$), results from numerical integration of Equation 4.6 are graphically represented in Figure 4-5 as a function of a_h/D for various shaft configurations. As to be expected, spatial correlation in the vertical direction only has a small influence on the horizontal correlation parameter r with this influence becoming quite insignificant for $L/a_v > 1$. The latter is also the range encountered in practical applications for which Figure 4-5 is valid ($L/a_v < 1$ would be reflected by a non-stationary variogram over the foundation depths and would be handled by subtraction of a deterministic trend function such that $L/a_v > 1$ is again the case for the random residuals).

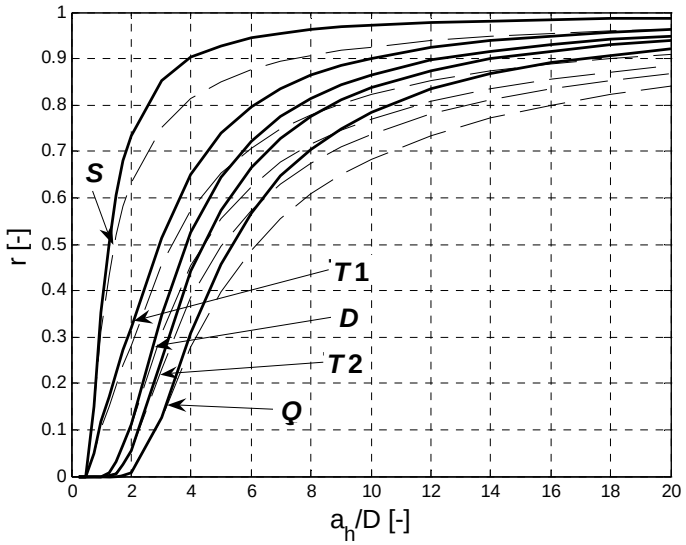

Figure 4-5. The term $r = C_{bf}(0)/C_b(0)$ as a function of a_h/D for $L/a_v > 1$ (continuous), $L/a_v = 0$ (dashed) and different shaft configurations ($D_s = 3D$).

For given foundation types (S, $D1$, $T1$, $T2$ or Q), dimensions (D and L; $D_s = 3D$) and site conditions (q_{b1}, q_{bm}, CV_q, a_v and a_h) Figure 4-5 with Equations 4.16 and 4.17 can be used to find a nominal resistance R_n equal to

$$R_n = A_f f_f^* \tag{4.18}$$

A respective coefficient of variation CV_R results as

$$CV_R = \frac{\sigma_{qfk}}{f_f^*} = \frac{\sqrt{\alpha_{qfk}}}{1 + r\left(\frac{q_{b1}}{q_{bm}} - 1\right)} CV_q \tag{4.19}$$

permitting evaluation of Equation 4.10 to find Φ. However, as already discussed in the previous section, the horizontal correlation range a_h is a potentially unknown parameter due to a generally limited number of borings (i.e., horizontal information) at a site. One way of dealing with this problem is to adopt hypothetical values of a_h within a reasonable practical range and conservatively choose to design according to the worst case scenario, i.e., where the resulting design load or the product $R_n\Phi$ are a minimum. The equations for (numerically) minimizing $R_n\Phi$ are given above; however, results will depend on a large number of case specific parameters such as foundation type n_{be}, q_{b1}/q_{bm}, CV_q, β and many more in Equations 4.10 and 4.11.

Of interest is a simpler and more general method to conservatively minimize $R_n\Phi$ by minimizing each factor R_n and Φ, separately. From Equation 4.16 it is immediately seen that R_n is minimized to R_{nw} by equating f_f^* to the lower value between q_{b1} and q_{bm}.

$$R_{nw} = A_f \min(q_{b1}, q_{bm}) \tag{4.20}$$

On the other hand, knowing that Φ for any value of β is a monotonically decreasing function in CV_R, Φ is minimized by maximizing CV_R to CV_{Rw} as

$$CV_{Rw} = \frac{\sqrt{\alpha_{qfkw}}}{R_{nw}} CV_q A_f q_{bm} \tag{4.21}$$

where α_{qfkw} is obtained by maximizing Equation 4.17 as a function of a_h. This is best done numerically for different parameter combinations of foundation type n_{be} and L/a_v. Knowing from Figure 4-3 that α_{qf} in Equation 4.17 may be well approximated by $k\alpha_0$ where k is primarily a function of a_h/D and, hence, r (not so much of L/a_v) an equation of the form

$$\alpha_{qfkw} \approx \left(A + \frac{B}{n_{be}} \right) \alpha_0 \tag{4.22}$$

is sought to approximate α_{qfkw}. For D_s = 3D and with maximum errors in CV_{Rw} of approximately 1% on the unconservative and 5% on the conservative side, respective values of the coefficients A and B for each foundation type indicated in the index are obtained by trial and error fitting to exact numerical results as: $A_S = 0.17$, $B_S = 0.98$; $A_D = 0.30$, $B_D = 0.90$; $A_{T1} = 0.10$, $B_{T1} = 0.90$; $A_{T2} = 0.21$, $B_{T2} = 0.95$; $A_Q = 0.18$, $B_Q = 0.97$. Hereby, it may be consistently observed that the worst case scenarios for each individual foundation type occur for maximum values of a_h where r is still zero or small (Figure 4-5), i.e., where spatial averaging on A_f is limited and correlation to data in the footprint is equal or close to zero. Results of $(A + B/n_{be})^{1/2}$ of different foundation types are graphically illustrated in Figure 4-6 (continuous) together with a previous solution for no center boring from Klammler et al. (2010b) for comparison (dashed). Finally, it is noted that the worst case scenario of Equation 4.22 is independent of D, which contributes to maintaining the design process as simple as possible.

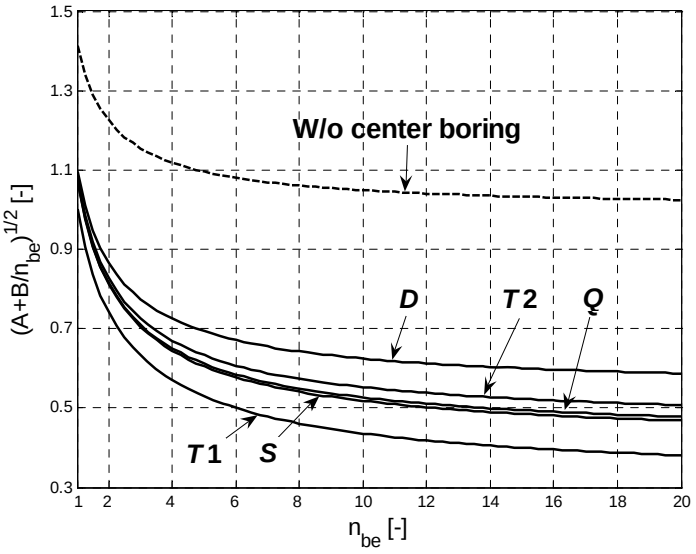

Figure 4-6. Performance of different shaft configurations under the worst case scenario of Equations 21 and 22 for unknown a_h in the presence of a center boring. Dashed line for comparison from Klammler et al. (2010b) without a center boring.

4.5 Discussion of Results

The results developed above are valid for both single and multiple shaft foundations with unknown or known foundation locations. In the latter case, nearby data may be considered to decrease resistance prediction uncertainty through spatial correlation (conditioning) where particular results given are for borehole data at the center of a foundation's footprint. Equations 4.16 and 4.17 are general in the sense that they encompass all of these scenarios and correctly collapse to the solution of Equations 4.6 and 4.8 for $n_{be} >> 1$ and no data conditioning. However, explicit results for this particular scenario as summarized in Figure 4-3 are still valuable as input for the more general formulation, since it provides the parameter α_{qf} for Equation 4.17. In Figure 4-3, the expected general tendency may be confirmed that the variance reduction monotonically increases as both L/a_v or D/a_h grow, i.e., as the degree of spatial averaging increases. In the same way, it may also be observed that increasing the number (n_s) of shafts in a foundation lowers resistance uncertainty. However, a direct comparison between different shaft configurations is not straightforward as equal values of L and D lead to different values of A_f and, hence, nominal resistances for each case. In other words, different types of foundations are typically designed with different shaft dimensions. An exception to this are the triple shaft configurations "$T1$" (row) and "$T2$" (triangle) which perform identically for $D/a_h \geq 0.5$ (no correlation between individual shafts) and where "$T1$" slightly outperforms "$T2$" for $0 < D/a_h < 0.5$ due to the larger horizontal spreading of shafts in "$T1$". Under the common practical situation of unknown horizontal correlation range a_h, Figure 4-3 indicates that a respective worst case scenario exists by adopting $D/a_h = 0$ which reduces all foundation types to the same line shaft approximation of Klammler et al. (2010a and b). Finally, independent of foundation type, shaft diameter, and correlation ranges, a general conclusion may be drawn from Figure 4-3 that vertical averaging may be very efficiently explored up to $L/a_v \approx 4$ (steep portions

of curves), while for $L/a_v > 4$ the benefits of increasing shaft length on uncertainty reduction (in absolute terms) become small.

As reflected by Equations 4.17 or 4.22, the latter conclusion remains valid in the presence of a center boring in the footprint of a single or multiple shaft foundation. Moreover, a center boring has the benefit of leading to considerably more favorable worst case scenarios for unknown a_h as reflected by Figure 4-6 where continuous graphs correspond to results from Equation 4.22 and the dashed line represents $(1 + 1/n_{be})^{1/2}$ as derived in Klammler et al. (2010b) for an unknown foundation location (i.e., no center boring). This remains true even if no actual data conditioning between the center boring and the foundation exists (i.e., $r = 0$, such as considered for unknown foundation location) which is due to the mere fact that data was collected inside the foundation footprint and used in Equation 4.16. Figure 4-6 demonstrates that for a given number of borings n_{be}, the benefit of a center boring is a 50% reduction in CV_R. Provided a center boring is available, Figure 4-6 also illustrates the performance of different shaft configurations in terms of resistance uncertainty. As above, a direct comparison is not straightforward due to generally different shaft dimensions for each configuration, but assuming equal L/a_v (i.e., α_0 in Equation 4.22) some observations may be made. Independent of n_{be}, the configuration "*T*1" (triple row) performs clearly best among all foundation types considered. "*T*1" is followed by "*S*" (single), "*Q*" (quadruple) and "*T*2" (triple triangle) which show similar behaviors and, finally, "*D*1" (double). The perhaps unexpectedly good performance of "*T*1" may be attributed to the fact that the center boring falls exactly into the footprint of the center shaft, which reduces uncertainty substantially. In other words, data conditioning starts at lower a_h (compare Figure 4-5) when horizontal averaging is still more effective as well. Another interesting observation from Figure 4-6 is that prediction uncertainty may be efficiently reduced up to $n_{be} \approx 4$ (steep portions of graphs), while for $n_{be} > 4$ the benefit of additional borings on

uncertainty reduction decreases. This fact is very important for sites which are not statistically homogenous, i.e., where (horizontal) division into sub-zones is required for separate geostatistical treatment such that the n_{be} for each sub-zone become smaller (e.g., 5 instead of 15). Moreover, in the (actual or potential) presence of smooth horizontal trends over a site, n_{be} may be limited without significantly inflating uncertainty to a small number of nearest borings which are used for design of a foundation ("moving window approach," Journel and Rossi 1989). This may avoid making crucial decisions about the presence and shape of horizontal deterministic trend functions. Finally, in the presence of vertical layering and/or nested variogram structures, the approach of Klammler et al. (2010a) remains valid which is based on separate treatment of individual layers and/or variogram components with subsequent addition of predictions and prediction variances.

4.6 Practical Example

In order to demonstrate the application of the results presented, the 17th Street Bridge case study of Klammler et al. (2010a) is extended by considering a triangle ("*T*2") foundation with $L = 9$ m, $D = 0.4$ m and the presence or not of a center boring. A total of 136 local rock strength measurements from 6 borings is available, where $q_{bm} = 2.28$ MPa with $CV_q = 0.50$. A spherical covariance function is adopted with correlation ranges of $a_v = 1.5$ m and $a_h = 4.5$ m for 80% of σ_q^2 plus $a_v = \infty$ and $a_h = 4.5$ m for the remaining 20% (i.e., 20% of the variability in q is only contained in the horizontal direction — "random areal trend." For the purpose of illustrating the present approach, the 6 borings are assumed spatially uncorrelated among each other such that $n_{eb} = 6$.

In a first design step with unknown foundation location or before obtaining data from a center boring $R_n = A_f q_{bm} = 77.31$ MN, where $A_f = 3 \cdot 0.4 \cdot \pi \cdot 9 = 33.91$ m^2. Assuming a_h and,

consequently, $D/a_h = 0.4/4.5 = 0.09$ are known, Figure 4-3 immediately gives a variance reduction factor for the first variogram component with $L/a_v = 9/1.5 = 6$ of $\alpha_{qf1} = 0.31^2$ and for the second variogram component with $L/a_v = 9/\infty = 0$ of $\alpha_{qf2} = 0.84^2$. Applying a result of Klammler et al. (2010a) α_{qf1} and α_{qf2} may be combined to a total variance reduction factor by taking the weighted average $\alpha_{qf} = 0.8\alpha_{qf1} + 0.2\alpha_{qf2} = 0.22$ such that further $CV_R = 0.22^{1/2} \cdot 0.5 = 0.23$ and $\Phi = 0.63$ from Equation 4.10 (**ΦR_n = 48.71 MN**). In case a_h is not reliably known, the same chart of Figure 4-3 gives worst case values of $\alpha_{01} = 0.35^2$ and $\alpha_{02} = 1$ by using $D/a_h = 0$. By the same relationships from above this leads to $\alpha_0 = 0.30$, $CV_R = 0.27$ and a reduced $\Phi = 0.56$ (**ΦR_n = 43.29 MN**). These results are very similar to those obtained for a single shaft in Klammler et al. (2010a) which may be attributed to the reduced shaft diameter for the triple configuration in order to achieve equal R_n.

In a more advanced stage of the design process, data from a center boring at a foundation location may be available. Assuming that a_h is known and that the mean local strength observed in the center boring is $q_{b1} = 1.70$ MPa, respective values of $r_1 = 0.87$ (continuous line for $L/a_v = 6 > 1$) and $r_2 = 0.77$ (dashed line for $L/a_v = 0$) are obtained from Figure 4-5 which may be combined by the same process of variance weighted averaging to a total value of $r = 0.8r_1 + 0.2r_2 = 0.85$. Equations 4.16 and 4.18 then give $f_f^* = 0.85 \cdot 1.70 + 0.15 \cdot 2.28 = 1.79$ MPa and $R_n = 33.91 \cdot 1.79 = 60.70$ MN. Furthermore, Equation 4.17 may be evaluated with all parameters known from above as $\alpha_{qfk}^{1/2} = [0.30(0.15^2/6 - 0.85^2) + 0.22]^{1/2} = 0.07$. Equation 4.19 then gives $CV_R = 0.07 \cdot 0.5/(1 - 0.25 \cdot 0.85) = 0.044$ which translates into $\Phi = 0.98$ by Equation 4.10 such that **ΦR_n = 59.49 MN**. This is significantly larger than 48.71 MN obtained above in the absence of a center boring and with known $a_h = 4.5$ m even though R_n is 25% smaller.

Under the same scenario of a center boring, but with a_h unknown, Figure 4-7 graphically represents results of the design variables (with $A_f q_{bm}$ normalized to unity) as a function of a_h/D and for four different values of q_{b1}/q_{bm} which reflects the previous results for $q_{b1}/q_{bm} = 0.75$ and $a_h/D = 4.5/0.4 = 11.15$.

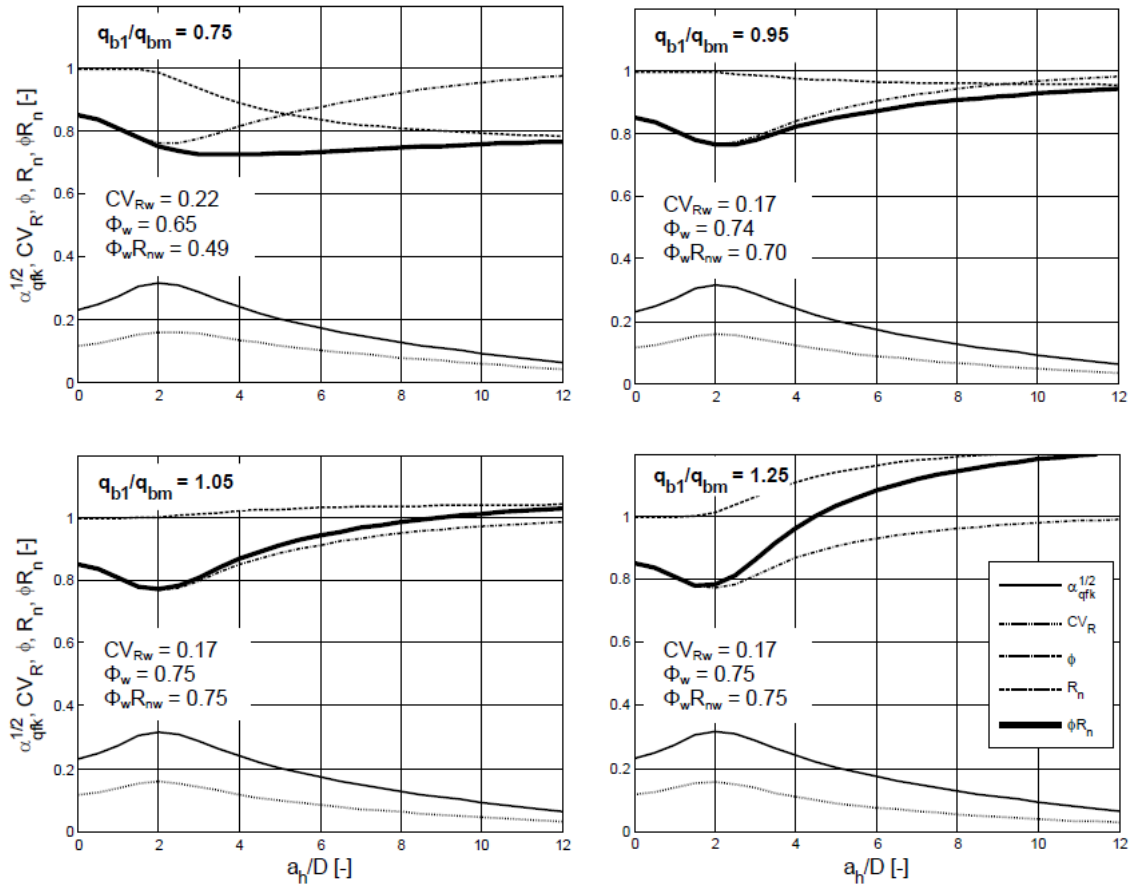

Figure 4-7. Worst case scenarios for example problem and different values of q_{b1}/q_{bm}. Exact results are shown in the graphs, while approximate results are given in the text inserts.

Most interesting to notice are the minima in ΦR_n (thick continuous lines), which can be explored in design as worst case scenarios for unknown a_h. While for q_{b1}/q_{bm} close to or above one, these minima are mainly conditioned by minima in Φ (i.e., prediction uncertainty) and consistently occur near the point where correlation between center boring and foundation starts; for q_{b1}/q_{bm} significantly smaller than one, the minima may occur for very large values of a_h/D,

thus being conditioned by small values of R_n without significant prediction uncertainty ($CV_R \approx 0$). In the above case of $q_{b1}/q_{bm} = 0.75$, for example, $\boldsymbol{\Phi R_n} = 0.73\ A_f q_{bm} =$ **56.44 MN** is obtained being only slightly smaller than 59.49 MN for $a_h = 4.5$ m from above. As evident from Figure 4-7, the potential increase in ΦR_n due to a known a_h becomes larger as q_{b1}/q_{bm} grows. Considering only worst case scenarios, however, benefits in ΦR_n due to larger q_{b1}/q_{bm} (i.e., stronger ground at the foundation location) are not very significant in the present case. An improvement upon the minima in ΦR_n of Figure 4-7 can be possible by explicitly taking into account the spatial correlation structures between all borings (i.e., improving on the conservative assumption that two nearby borings are fully correlated) and by allowing for correlation between more than a single boring with the foundation. However, this would quickly lead to an increased computational complexity, since an ordinary kriging system has to be solved for every value of a_h/D instead of the simplified Equations 4.16 and 4.17. Even evaluation of worst case scenarios as in Figure 4-7 based on Equations 4.16 and 4.17 may soon become a tedious task without computational aid and even more conservative worst case scenarios are indicated inside the charts based on the approximate Equations 4.20, 4.21 and 4.22. For the example problem with $q_{b1}/q_{bm} = 0.75$, this results in $R_{nw} = 0.75\ A_f q_{bm} = 57.99$ MN, $\alpha_{qfkw} = (0.21 + 0.95/6) \cdot 0.30 = 0.11$, $CV_{Rw} = 0.11^{1/2} \cdot 0.5 / 0.75 = 0.22$, $\Phi_w = 0.65$ and $\boldsymbol{\Phi_w R_{nw}} =$ **37.69 MN**, which presents a relatively large decrease in admissible load with respect to 56.44 MN from above based on simultaneous minimization of the product ΦR_n rather than of each factor separately. However, as illustrated by Figure 4-7, this conservative difference decreases quickly as q_{b1}/q_{bm} approaches or exceeds unity. This indicates that an additional mathematical effort to directly minimize the product ΦR_n may be quite compensating, especially for $q_{b1}/q_{bm} < 1$.

CHAPTER 5
UNMONITORED, PARTIALLY AND FULLY MONITORED PILE GROUPS – KRIGING APPROACH

5.1 Background

The present chapter further generalizes the kriging approach from Chapter 4 for the particular scenario of partially monitored (including unmonitored and fully monitored) pile groups. Total pile resistance R_p (i.e., side + tip) is hereby considered as a spatially random variable, as this avoids individual treatment of side and tip resistances with subsequent addition (problem of side-tip correlation). Note, this data is generally available from high strain rate pile monitoring systems and is generally used to set pile lengths, blow counts, etc. For this development, the following assumptions are considered:

- Data used are total pile resistances such that each pile represents a point location in the horizontal plane (no more horizontal and vertical averaging over pile surfaces);
- Different numbers and configurations of piles may be monitored in a group; and
- The number and configuration of monitored piles may be different from group to group.

5.2 List of Variables for Chapter Five

To assist with the description of monitored and unmonitored pile variables, uncertainties, etc., the following variable descriptions are provided:

i	Index from 1 to n_g denoting pile groups; $i = 1$ denotes pile group to be designed such that indexation of i changes depending on what pile group is being designed (refer to Figure 5-2).
j, k	Indices from 1 to n_{pi} denoting piles in group i; piles from j, $k = 1$ to n_{mi} are monitored, while piles from j, $k = n_{mi} + 1$, $n_{mi} + 2$, …, n_{pi} are unmonitored (refer to Figure 5-1).
n_g	Number of pile groups in a site (homogeneous subzone), where at least one pile is monitored.
n_{pi}	Number of piles in pile group i.
n_{mi}	Number of monitored piles in pile group i.

D_s Fundamental center-to-center pile separation distance within a group (e.g., 3 times pile diameter)

R_p Random function in the horizontal plane representing true total (side + tip) pile resistance.

$R_{p\varepsilon}$ R_p plus random measurement error of monitoring method (result of measurements).

σ_ε^2 Variance of random measurement error of monitoring method.

α_ε $\sigma_\varepsilon^2 / \sigma_p^2$.

μ_p Mean of $R_{p(\varepsilon)}$.

σ_p^2 Variance of R_p.

$\sigma_{p\varepsilon}^2$ Variance of $R_{p\varepsilon}$ ($\sigma_p^2 + \sigma_\varepsilon^2$).

CV_{Rp} Coefficient of variation of σ_p/μ_p of R_p.

$C(h)$ Spatial covariance function of R_p (isotropic).

$C_\varepsilon(h)$ Spatial covariance function of $R_{p\varepsilon}$ (isotropic).

$\gamma(h)$ Variogram of R_p.

$\gamma_\varepsilon(h)$ Variogram of $R_{p\varepsilon}$.

a_h Horizontal correlation length.

h Spatial lag separation distance.

h_{jk} Spatial lag separation distance between piles j and k within a pile group.

R_{pij} Total (side + tip) true (e.g., from static load test) pile resistance of the j-th pile in the i-th pile group.

$R_{p\varepsilon ij}$ Total (side +tip) monitored pile resistance of the j-th pile in the i-th pile group (containing measurement error).

R_{mi} Mean of monitored pile resistances in group i.

R_{m1} Mean of monitored pile resistances in group $i = 1$.

σ_{mi}^2 Variance about R_{mi} for $\sigma_\varepsilon^2 = 0$.

σ_{m1}^2 Variance about R_{m1} for $\sigma_\varepsilon^2 = 0$.

α_{m1} $\sigma_{m1}^2 / \sigma_p^2$.

R_{g1} Mean pile resistance of pile group $i = 1$ to be designed.

σ_{g1}^2 Variance about R_{g1}.

α_{g1} $\sigma_{g1}^2 / \sigma_p^2$.

R_{g1}^* Unbiased (ordinary kriging) estimate of R_{g1}.

R_{g1w}^* Worst case estimate of R_{g1} for unknown a_h.

R_n Nominal LRFD resistance given by $n_{p1} R^*_{g1}$ or $n_{p1} R^*_{g1w}$.

w_i Ordinary kriging weights of all R_{mi}.

W_1 Weight of R_{m1} against μ_p.

W_{1min} Minimum value of W_1 for unknown a_h.

W_{1max} Maximum value of W_1 for unknown a_h.

μ Lagrangian operator.

σ^2_{mg1} Covariance between R_{m1} and R_{g1}.

α_{mg1} $\sigma^2_{mg1} / \sigma^2_p$.

σ^2_e Variance of estimation error $R^*_{g1} - R_{g1}$.

α_e σ^2_e / σ^2_p.

α_{ew} Worst case value of α_e for unknown a_h.

CV_{Rg1} Coefficient of variation of estimation error $\sigma_e / R^*_{g1} = \alpha_e^{1/2} CV_{Rp}$ for finding Φ.

CV_{Rg1w} Worst case value of CV_{Rg1w} for unknown a_h.

Φ LRFD resistance factor for pile group $i = 1$ ($Q < \Phi R^*_{g1(w)}$).

Φ_w Worst case Φ for unknown a_h.

Q Mean of random design load for pile group $i = 1$.

Q_w Worst case Q for unknown a_h.

β LRFD reliability index.

5.3 Predicting Pile Group Resistance from Monitored Piles Using Kriging

It is common practice in pile driving that once the minimum tip elevation is reached (e.g., for lateral load requirements) then final unmonitored pile lengths are set by the hammer blow count. If all piles are driven to the (approximately) same number of hammer blows per foot with approximately the same embedment depth, then the total pile resistance R_p may be considered as a random function in the horizontal plane. Randomization of R_p is due to uncertainties of the "hammer blow count approach" (or spatial variability of R_p for constant embedment depth), which may or may not depend on the spatial soil properties. As such, R_p may or may not be spatially correlated and sampled values of R_p are available as $R_{p\varepsilon ij}$ at monitored pile locations,

where the subscript "ε" indicates the presence of a random measurement error of the monitoring method. The magnitude (variance) of this measurement error is denoted by σ_ε^2. If the hammer blow count is used as the common property of all piles, then the actual pile embedment depths are irrelevant.

An arbitrary number of piles may be monitored within a pile group as indicated by the black circles in the examples of Figure 5-1. Also, one or more pile groups may be present within a site (or homogeneous subzone thereof). The index *i* is used to denote the individual pile groups as shown in Figure 5-2, where $i = 1$ always indicates the pile group under consideration, i.e., the one for which the allowable design load Q is to be found. The numbering of the other pile groups may be arbitrary. The total number of pile groups present with at least one pile monitored is n_g (subscript "*g*" for group level). Each pile group may consist of a different number of piles, which is denoted by n_{pi} (subscript "*p*" for pile level and index "*i*" showing the group number).

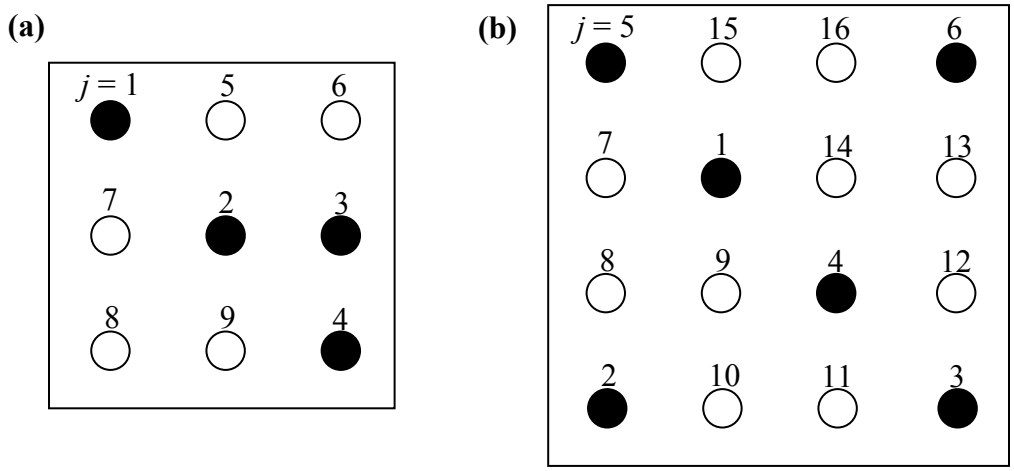

Figure 5-1. Examples of an (a) 3 × 3 ($n_{pi} = 9$) and a (b) 4 × 4 ($n_{pi} = 16$) pile group with monitoring configurations (black circles) and pile numbering using index *j*. The lower numbers may be arbitrarily assigned to the monitored piles, while the higher numbers may be arbitrarily assigned to the unmonitored piles.

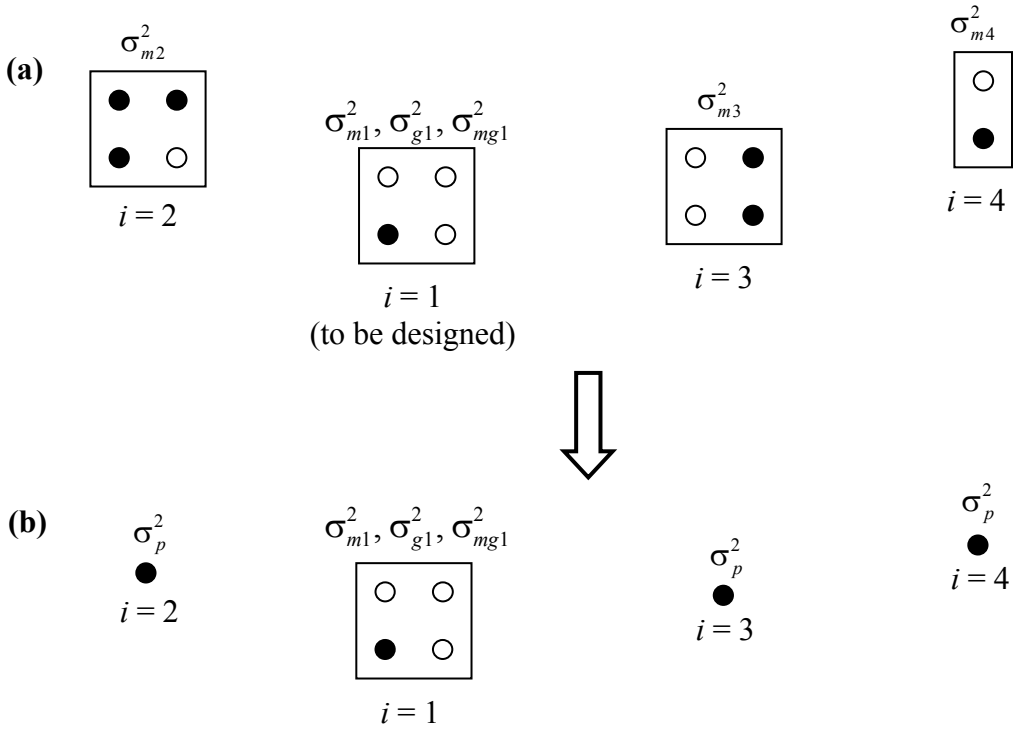

Figure 5-2. (a) Example of pile groups and monitoring configurations (black circles) for $n_g = 4$ (Term $i = 1$ is used for the pile group under consideration, while $i > 1$ may be arbitrarily assigned to the other pile groups); (b) Simplified model corresponding to Equation 5.9.

R_{pij} stands for the total true (i.e., without measurement error, e.g., from static load test) resistance of the j-th pile in the i-th pile group. The numbering of piles within a group may be arbitrary with the exception that the lower indices are assigned to monitored piles, while the higher indices are assigned to unmonitored piles. Using n_{mi} as the number of monitored piles in the i-th group (subscript "m" for monitored and index "i" again for group number), this means that $j = 1, 2, \ldots, n_{mi}$ indicate monitored piles, while $j = n_{mi} + 1, n_{mi} + 2, \ldots, n_{pi}$ indicate unmonitored piles (compare Figure 5-1).

The true pile resistance mean R_{g1} in the pile group of interest ($i = 1$) is given by

$$R_{g1} = \frac{1}{n_{p1}} \sum_{j=1}^{n_{p1}} R_{p1j} \tag{5.1}$$

and the nominal LRFD pile group resistance R_n is equal to $n_{p1}R_{g1}$. As n_{p1} is known, it is the goal to predict R_{g1} as well as the corresponding coefficient of variation CV_{Rg1} to determine LRFD Φ and allowable design load Q of the group. For this prediction we use the mean resistances R_{mi} of all monitored piles in each individual pile group (i.e., every pile group possesses its own value of R_{mi}) given by

$$R_{mi} = \frac{1}{n_{mi}} \sum_{j=1}^{n_{mi}} R_{p\varepsilon ij} \tag{5.2}$$

Mean μ_p and variance $\sigma^2_{p\varepsilon}$ of $R_{p\varepsilon}$ for all pile groups may be obtained as

$$\mu_p = \sum_{i=1}^{n_g} \sum_{j=1}^{n_{mi}} \frac{R_{p\varepsilon ij}}{n_g n_{mi}} = \frac{1}{n_g} \sum_{i=1}^{n_g} R_{mi} \tag{5.3}$$

$$\sigma^2_{p\varepsilon} = \sum_{i=1}^{n_g} \sum_{j=1}^{n_{mi}} \frac{\left(R_{p\varepsilon ij} - \mu_p\right)^2}{n_g n_{mi}} \tag{5.4}$$

where the product $n_g n_{mi}$ may be identified as declustering weights, similar to those of cell declustering (Isaaks and Srivastava 1989). Variogram analysis of all available data $R_{p\varepsilon ij}$ leads to the variogram $\gamma_\varepsilon(h)$ of $R_{p\varepsilon}$ and to the spatial covariance function $C_\varepsilon(h) = \sigma^2_{p\varepsilon} - \gamma_\varepsilon(h)$. The spatial covariance including the measurement error $C_\varepsilon(h)$ is assumed to be isotropic, i.e., $C_\varepsilon(h)$ is the same in all horizontal directions. Due to the random (and typically spatially uncorrelated) measurement error, the spatial covariance function $C(h)$ of true pile resistance R_p is known to be identical to $C_\varepsilon(h)$, except for a nugget variance of σ^2_ε at the origin. This is illustrated in Figure 5-3 and means that $C(h) = C_\varepsilon(h)$ for $h > 0$ and $C(0) = C_\varepsilon(0) - \sigma^2_\varepsilon$. Note that the issue of zonal anisotropies between the horizontal and vertical directions (e.g., random layering or random areal trends) is no longer relevant as the vertical direction is eliminated from the problem (no more vertical upscaling).

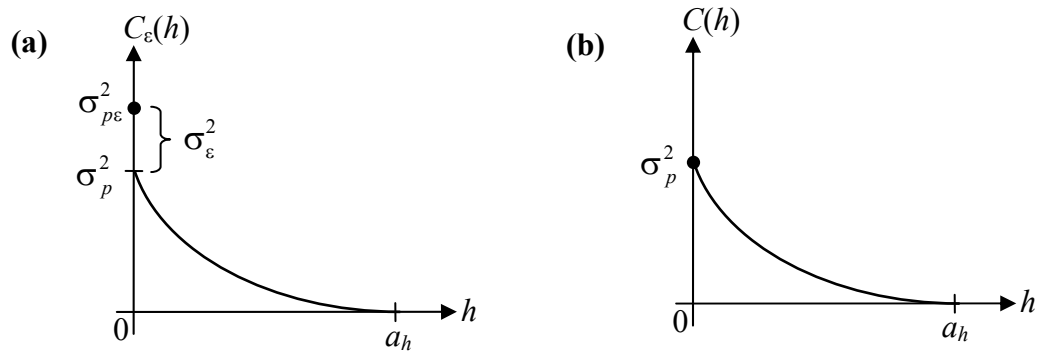

Figure 5-3. Difference between $C_\varepsilon(h)$ and $C(h)$. $C_\varepsilon(h)$ and $C(h)$ are identical except for $C_\varepsilon(0) = \sigma^2_{p\varepsilon}$ and $C(0) = \sigma^2_p$.

Using ordinary kriging, R_{g1} may be predicted from known R_{mi} as

$$R^*_{g1} = \sum_{i=1}^{n_g} w_i R_{mi} \tag{5.5}$$

where the sum of the kriging weights $\sum_{i=1}^{n_g} w_i = 1$. Under the assumption that $C(h) = 0$ between different pile groups (i.e., possible spatial correlation only within pile groups), w_i are found from the ordinary kriging system,

$$\begin{bmatrix} \sigma^2_{m1} + \dfrac{\sigma^2_\varepsilon}{n_{m1}} & 0 & \cdots & 0 & 1 \\ 0 & \sigma^2_{m2} + \dfrac{\sigma^2_\varepsilon}{n_{m2}} & \ddots & \vdots & \vdots \\ \vdots & \ddots & \ddots & 0 & \vdots \\ 0 & \cdots & 0 & \sigma^2_{mng} + \dfrac{\sigma^2_\varepsilon}{n_{mng}} & 1 \\ 1 & \cdots & \cdots & 1 & 0 \end{bmatrix} \begin{bmatrix} w_1 \\ w_2 \\ \vdots \\ w_{ng} \\ \mu \end{bmatrix} = \begin{bmatrix} \sigma^2_{mg1} \\ 0 \\ \vdots \\ 0 \\ 1 \end{bmatrix} \tag{5.6}$$

with

$$\sigma^2_{mi} = \frac{1}{n^2_{mi}} \sum_{j=1}^{n_{mi}} \sum_{k=1}^{n_{mi}} C(h_{jk}) \tag{5.7}$$

$$\sigma_{mg1}^2 = \frac{1}{n_{p1} n_{m1}} \sum_{j=1}^{n_{m1}} \sum_{k=1}^{n_{p1}} C(h_{jk}) \tag{5.8}$$

where h_{jk} is the lag distance between the j-th and k-th piles in the i-th group and μ is the Lagrangian operator. Equation 5.7 represents nothing but the mean value of $C(h)$ between all possible pairs of monitored piles, which is identical to the mean of all elements in the variance–covariance matrix between all monitored piles in group i. In analogy, Equation 5.8 is nothing but the mean value of $C(h)$ between all possible pairs of a monitored pile in the 1st group and every pile (both monitored and unmonitored) in the 1st group. As such, for the example of Figure 5-1a, Equation 5.7 corresponds to averaging over the darkly shaded portion of the variance–covariance matrix depicted in Figure 5-4 while Equation 5.8 corresponds to averaging over both the darkly and lightly shaded portions.

In order to simplify Equation 5.6 and to arrive at a closed form solution, it is assumed in Equation 5.7 that spatial correlation within the groups is large enough, such that $C(h_{jk}) \approx C(0) = \sigma_p^2$ can be used for $i > 1$ leading to Figure 5-2b and

$$\begin{bmatrix} \sigma_{m1}^2 + \frac{\sigma_\varepsilon^2}{n_{m1}} & 0 & \cdots & 0 & 1 \\ 0 & \sigma_p^2 + \sigma_\varepsilon^2 & \ddots & \vdots & \vdots \\ \vdots & \ddots & \ddots & 0 & \vdots \\ 0 & \cdots & 0 & \sigma_p^2 + \sigma_\varepsilon^2 & 1 \\ 1 & \cdots & \cdots & 1 & 0 \end{bmatrix} \begin{bmatrix} w_1 \\ w_2 \\ \vdots \\ w_2 \\ \mu \end{bmatrix} = \begin{bmatrix} \sigma_{mg1}^2 \\ 0 \\ \vdots \\ 0 \\ 1 \end{bmatrix} \tag{5.9}$$

		Monitored				Unmonitored				
	j	**1**	**2**	**3**	**4**	**5**	**6**	**7**	**8**	**9**
Monitored	**1**	C_{11}	C_{12}	C_{13}	C_{14}	C_{15}	C_{16}	C_{17}	C_{18}	C_{19}
	2	C_{21}	C_{22}	C_{23}	C_{24}	C_{25}	C_{26}	C_{27}	C_{28}	C_{29}
	3	C_{31}	C_{32}	C_{33}	C_{34}	C_{35}	C_{36}	C_{37}	C_{38}	C_{39}
	4	C_{41}	C_{42}	C_{43}	C_{44}	C_{45}	C_{46}	C_{47}	C_{48}	C_{49}
Unmonitored	**5**	C_{51}	C_{52}	C_{53}	C_{54}	C_{55}	C_{56}	C_{57}	C_{58}	C_{59}
	6	C_{61}	C_{62}	C_{63}	C_{64}	C_{65}	C_{66}	C_{67}	C_{68}	C_{69}
	7	C_{71}	C_{72}	C_{73}	C_{74}	C_{75}	C_{76}	C_{77}	C_{78}	C_{79}
	8	C_{81}	C_{82}	C_{83}	C_{84}	C_{85}	C_{86}	C_{87}	C_{88}	C_{89}
	9	C_{91}	C_{92}	C_{93}	C_{94}	C_{95}	C_{96}	C_{97}	C_{98}	C_{99}

Figure 5-4. Variance–covariance matrix between all piles of the example in Figure 5-1a ($n_{pi} = 9$ and $n_{mi} = 4$). Index j is bold and C_{jk} is short for $C(h_{jk})$. The mean of all elements in the darkly shaded portion corresponds to Equation 5.7. The mean of all elements in the darkly and lightly shaded portions corresponds to Equation 5.8. The mean of all 9 × 9 elements corresponds to Equation 5.16.

This is equivalent to increasing the uncertainty about the data values from all pile groups, except the one of interest ($i = 1$). As a consequence, this results in a larger uncertainty about the final group resistance estimate as well as a higher kriging weight for R_{m1} (whose variance is not increased). Equation 5.9 may be expanded into the following set of equations:

$$\begin{aligned} &\left(\sigma_{m1}^2 + \frac{\sigma_\varepsilon^2}{n_{m1}}\right) w_1 + \mu = \sigma_{mg1}^2 \\ &\left(\sigma_p^2 + \sigma_\varepsilon^2\right) w_2 + \mu = 0 \\ &w_1 + \left(n_g - 1\right) w_2 = 1 \end{aligned} \tag{5.10}$$

Note that $w_i = w_2$ for $i > 1$. Solving for w_1, w_2 and μ gives

$$w_1 = \frac{\alpha_{mg1}\left(n_g - 1\right) + \alpha_\varepsilon + 1}{\alpha_{m1}\left(n_g - 1\right) + \alpha_\varepsilon\left(\frac{n_g - 1}{n_{m1}} + 1\right) + 1}$$

$$w_2 = \frac{\alpha_{m1} + \frac{\alpha_\varepsilon}{n_{m1}} - \alpha_{mg1}}{\alpha_{m1}\left(n_g - 1\right) + \alpha_\varepsilon\left(\frac{n_g - 1}{n_{m1}} + 1\right) + 1} \tag{5.11}$$

and

$$\mu = \sigma_p^2 \frac{\alpha_{mg1} - \alpha_{m1} - \frac{\alpha_\varepsilon}{n_{m1}}}{\alpha_{m1}\left(n_g - 1\right) + \alpha_\varepsilon\left(\frac{n_g - 1}{n_{m1}} + 1\right) + 1} \tag{5.12}$$

where $\alpha_{m1} = \sigma_{m1}^2 / \sigma_p^2$, $\alpha_{mg1} = \sigma_{mg1}^2 / \sigma_p^2$, and $\alpha_\varepsilon = \sigma_\varepsilon^2 / \sigma_p^2$. Substituting Equation 5.11 into Equation 5.5 results in

$$R_{g1}^* = W_1 R_{m1} + \left(1 - W_1\right)\mu_p \tag{5.13}$$

with

$$W_1 = \frac{\alpha_{mg1} n_g - \alpha_{m1} + \alpha_\varepsilon\left(1 - \frac{1}{n_{m1}}\right) + 1}{\alpha_{m1}\left(n_g - 1\right) + \alpha_\varepsilon\left(\frac{n_g - 1}{n_{m1}} + 1\right) + 1} \tag{5.14}$$

From Isaaks and Srivastava (1989), the ordinary kriging variance (i.e., estimation error variance) may be expressed as $\sigma_\varepsilon^2 = \sigma_{g1}^2 - w_1\sigma_{mg1}^2 - \mu$ leading to

$$\alpha_e = \alpha_{g1} - \frac{\alpha_{mg1}^2\left(n_g - 1\right) + 2\alpha_{mg1} - \alpha_{m1} + \alpha_\varepsilon\left(2\alpha_{mg1} - \alpha_{m1} - \frac{1}{n_{m1}}\right) - \frac{\alpha_\varepsilon^2}{n_{m1}}}{\alpha_{m1}\left(n_g - 1\right) + \alpha_\varepsilon\left(\frac{n_g - 1}{n_{m1}} + 1\right) + 1} \tag{5.15}$$

where $\alpha_e = \sigma_e^2 / \sigma_p^2$, $\alpha_{g1} = \sigma_{g1}^2 / \sigma_p^2$ and

$$\sigma_{g1}^2 = \frac{1}{n_{p1}^2} \sum_{j=1}^{n_{p1}} \sum_{k=1}^{n_{p1}} C(h_{jk}) \tag{5.16}$$

Equation 5.16 is nothing but the mean value of $C(h)$ over all possible pairs of piles (both monitored and unmonitored) in the 1st pile group. For the example of Figure 5-1a, this is equivalent to the averaging of all elements of the variance–covariance matrix in Figure 5-4.

5.4 Discussion of Results

5.4.1 No Pile Monitored in Group of Interest ($n_{m1} = 0$)

It may occur that none of the piles in a group is monitored, such that $n_{m1} = 0$. This leads to the non-existence of the first rows in Equations 5.6, 5.9 and 5.10 and to

$$w_2 = \frac{1}{n_g - 1} \tag{5.17}$$

$$\alpha_e = \alpha_{g1} + \frac{1 + \alpha_\varepsilon}{n_g - 1} \tag{5.18}$$

in Equations 5.11 and 5.15. This means that all the available data from other $n_g - 1$ pile groups is evenly weighted and $R_{g1}^* = \mu_p$; α_e collapses to the form for the scenario where limited data is available and none of them is nearby for conditioning; n_g has to be larger than one in this case, as no data is available from the first pile group. Limits for $\alpha_\varepsilon = 0$ and $n_g >> 1 + \alpha_\varepsilon$ are easily found from Equation 5.18.

5.4.2 One Pile Monitored in Group of Interest ($n_{m1} = 1$)

In case a single pile is monitored in the group of interest, such that $n_{m1} = 1$, Equations 5.14 and 5.15 become

$$W_1 = \frac{\alpha_{mg1}}{1 + \alpha_\varepsilon} \tag{5.19}$$

$$\alpha_e = \alpha_{g1} + \frac{1+\alpha_\varepsilon}{n_g} - \alpha_{mg1}\left[\frac{\alpha_{mg1}\left(n_g - 1\right)}{n_g\left(1+\alpha_\varepsilon\right)} + \frac{2}{n_g}\right] \tag{5.20}$$

since $\alpha_{m1} = 1$. If in addition $n_{p1} >> 1$ (i.e., a single pile monitored out of many piles in a group), then $\alpha_{mg1} \approx 0$ and Equation 5.13 yields $R^*_{g1} \approx \mu_p$, which reflects a low degree of monitoring and uniform weighting of data from all pile groups. Equation 5.20 then becomes $\alpha_e \approx \alpha_{g1} + (1 + \alpha_\varepsilon)/n_g$. In the presence of a single pile group, i.e., $n_g = 1$, $\alpha_e = \alpha_{g1} + 1 + \alpha_\varepsilon - 2\alpha_{mg1}$. Note that W_1 is not a function of n_g in this case (this can be shown to be generally the case when the same number and pattern of piles is monitored in each group) and that it decreases as α_ε increases. That is, the larger the measurement errors, the more uniformly kriging weights are distributed over all data and $R^*_{g1} \approx \mu_p$. For $\alpha_\varepsilon = 0$, Equation 5.20 yields $\alpha_e = \alpha_{g1} + 1/n_g - \alpha_{mg1}[\alpha_{mg1}(n_g - 1)/n_g + 2/n_g]$ and for $n_g >> 1+\alpha_\varepsilon$, $\alpha_e = \alpha_{g1} - \alpha^2_{mg1}/(1+\alpha_\varepsilon)$.

5.4.3 All Piles Monitored in Group of Interest ($n_{m1} = n_{p1}$)

Here, $\alpha_{m1} = \alpha_{mg1} = \alpha_{g1}$ and Equations 5.14 and 5.15 become

$$W_1 = \frac{\alpha_{m1}\left(n_g - 1\right) + \alpha_\varepsilon\left(1 - \frac{1}{n_{p1}}\right) + 1}{\alpha_{m1}\left(n_g - 1\right) + \alpha_\varepsilon\left(\frac{n_g - 1}{n_{p1}} + 1\right) + 1} = 1 - \frac{\alpha_\varepsilon \frac{n_g}{n_{p1}}}{\alpha_{m1}\left(n_g - 1\right) + 1 + \alpha_\varepsilon\left(1 - \frac{1}{n_{p1}} + \frac{n_g}{n_{p1}}\right)} \tag{5.21}$$

$$\alpha_e = \frac{\alpha_\varepsilon\left[\frac{\alpha_{m1}}{n_{p1}}\left(n_g - 1\right) + \frac{1}{n_{p1}}\left(1+\alpha_\varepsilon\right)\right]}{\alpha_{m1}\left(n_g - 1\right) + 1 + \alpha_\varepsilon\left(1 - \frac{1}{n_{p1}} + \frac{n_g}{n_{p1}}\right)} \tag{5.22}$$

For $n_g = 1$ this gives $\alpha_e = \alpha_\varepsilon/n_{p1}$, while for $n_g >> 1 + \alpha_\varepsilon$ one finds $W_1 = \alpha_{m1}/(\alpha_{m1} + \alpha_\varepsilon/n_{p1})$ and $\alpha_e = \alpha_\varepsilon\alpha_{m1}/(n_{p1}\alpha_{m1} + \alpha_\varepsilon)$. In the theoretical scenario of no measurement error ($\alpha_\varepsilon = 0$) Equations 5.21 and 5.22 reduce to $W_1 = 1$ and $\alpha_e = 0$.

In case $\alpha_\varepsilon >> 1$, α_e has to become very large, independent of the particular scenario and all other parameters. Moreover for $n_g = 1$, i.e., in the presence of a single pile group, $R^*_{g1} = R_{m1} = \mu_p$ always independent of W_1.

5.4.4 Single Pile Group without Spatial Correlation ($n_g = 1$ and $a_h = 0$)

In this case, only monitored data from the pile group of interest is considered, except for CV_{Rp} which may be based on all monitored data at a site. Thus, Equation 5.13 becomes $R^*_{g1} = R_{m1}$ independent of a_h, which may be unconservative for pile groups where $R_{m1} > \mu_p$. In the hypothetical case that both $n_g = 1$ and $a_h = 0$ (such that $\alpha_{g1} = \alpha_{mg1} = 1/n_{p1}$ and $\alpha_{m1} = 1/n_{m1}$), Equation 5.15 reduces to the simple form,

$$\alpha_e = \frac{1+\alpha_\varepsilon}{n_{m1}} - \frac{1}{n_{p1}} \tag{5.23}$$

This nicely illustrates how α_e grows with α_ε and n_{p1} and how it decreases with n_{m1}. However, as seen later in Figures 5-9b and 5-10b (top continuous graphs of each color), the case of $a_h = 0$ is not a universal worst case scenario.

5.5 Worst Case Scenarios of Unknown a_h

The behavior of W_1 from Equation 5.15 is graphically illustrated by the dashed lines in Figures 5-5 through 5-10, where black, blue and red correspond to $\alpha_\varepsilon = CV_\varepsilon^2 \big/ CV_p^2 = \{0, 0.1, 0,3\}$. Black circles in the pile groups indicate the monitored piles and D_s is an arbitrary fundamental pile separation distance (center-to-center; e.g., D_s = 3 times pile diameter). From top to bottom, the dashed lines correspond to $n_g = \{1, 5, 100\}$, i.e., the larger n_g the larger the weight on μ_p in Equation 5.14. Moreover, it may be observed that W_1 possesses a minimum value W_{1min} and a maximum value W_{1max} at $a_h/D_s >> 1$. The latter may be generally expressed as

$$W_{1\max} = 1 - \frac{\alpha_\varepsilon n_g}{n_g n_{m1} + \alpha_\varepsilon \left(n_g + n_{m1} - 1\right)} \tag{5.24}$$

while a simple equation for the former may only be found for the configurations of Figures 5-5 through 5-8 where W_{1min} consistently occurs at $a_h/D_s < 1$. Since in these cases W_{1min} occurs when there is no more correlation between individual piles in the group, Equations 5.7, 5.8 and 5.16 simplify leading to $\alpha_{g1} = \alpha_{mg1} = 1/n_{p1}$, $\alpha_{m1} = 1/n_{m1}$ and

$$W_{1\min} = \frac{\frac{n_{m1}}{n_{p1}} n_g}{\left(n_g + n_{m1} - 1\right)\left(1 + \alpha_\varepsilon\right)} + \frac{n_{m1} - 1}{n_g + n_{m1} - 1} \tag{5.25}$$

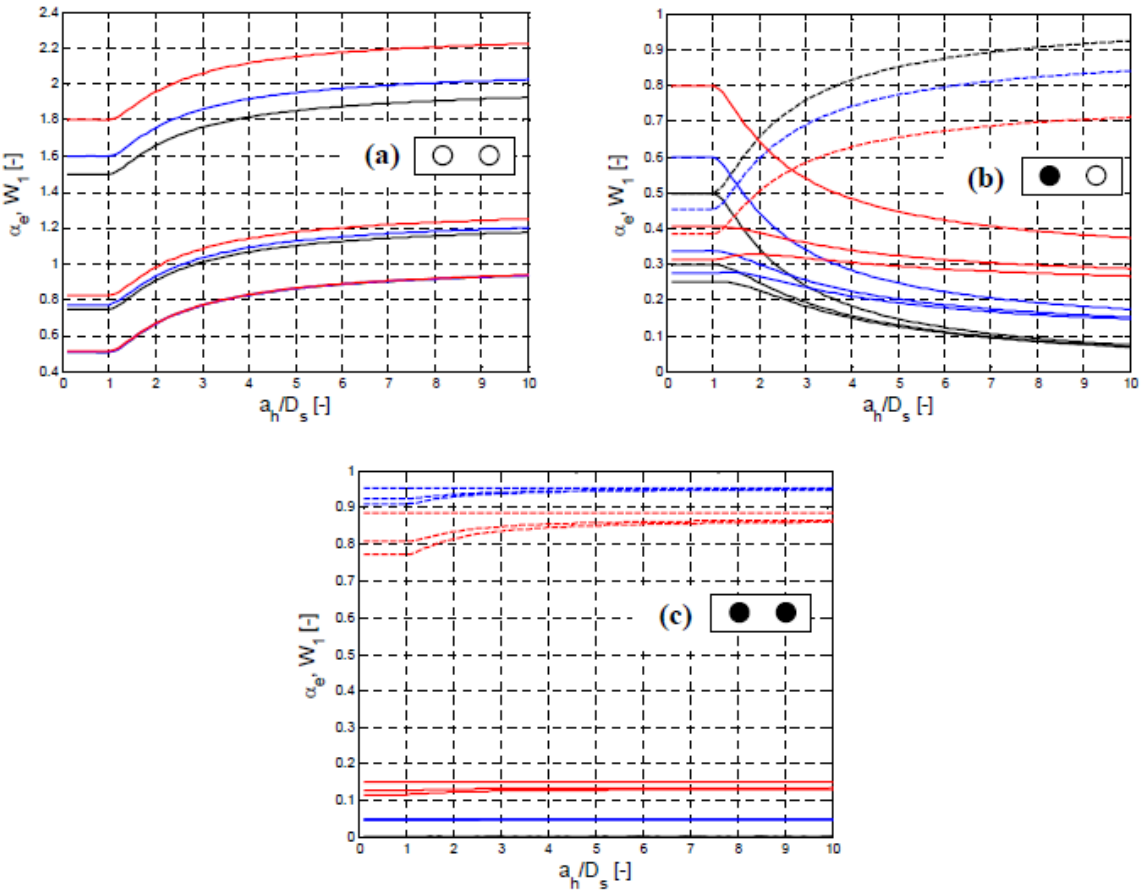

Figure 5-5. Terms W_1 (dashed, except for (a), where W_1 does not exist as no pile is monitored in the group) and α_e (continuous) as functions of a_h/D_s from Equations 5.14 and 5.15 for a double pile group. Black circles indicate monitored piles. Colors black, blue and red correspond to α_ε = {0, 0.1, 0.3}, respectively. For each color and line type there are three graphs corresponding to n_g = {1, 5, 100} from top to bottom, except for (a) where n_g = {2, 5, 100}. Graphs for W_1 and different n_g are identical whenever $n_{m1} = 1$ (compare Equation 5.19).

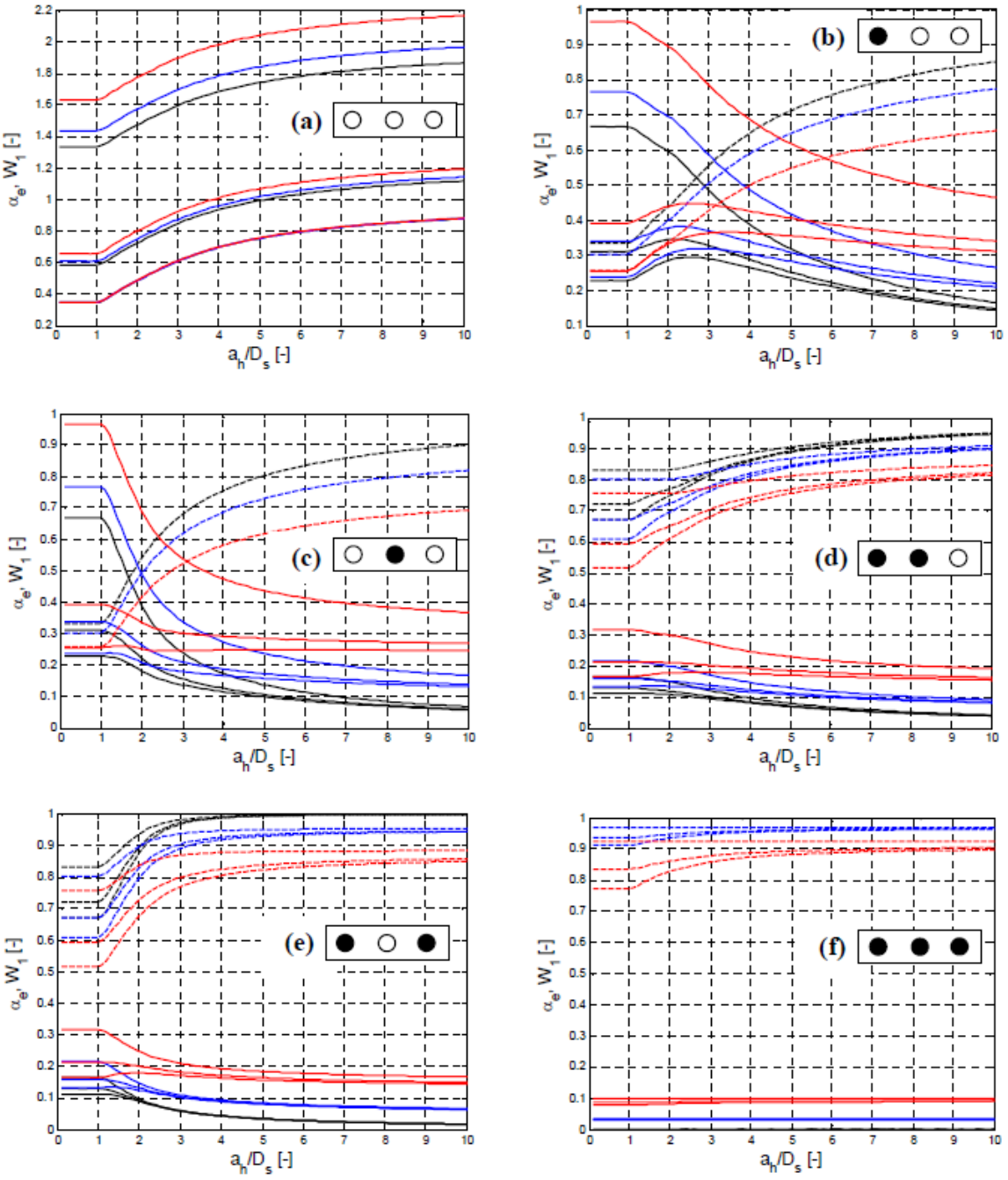

Figure 5-6. Analogous to Figure 5-5 for tripe pile groups in a line and different monitoring configurations.

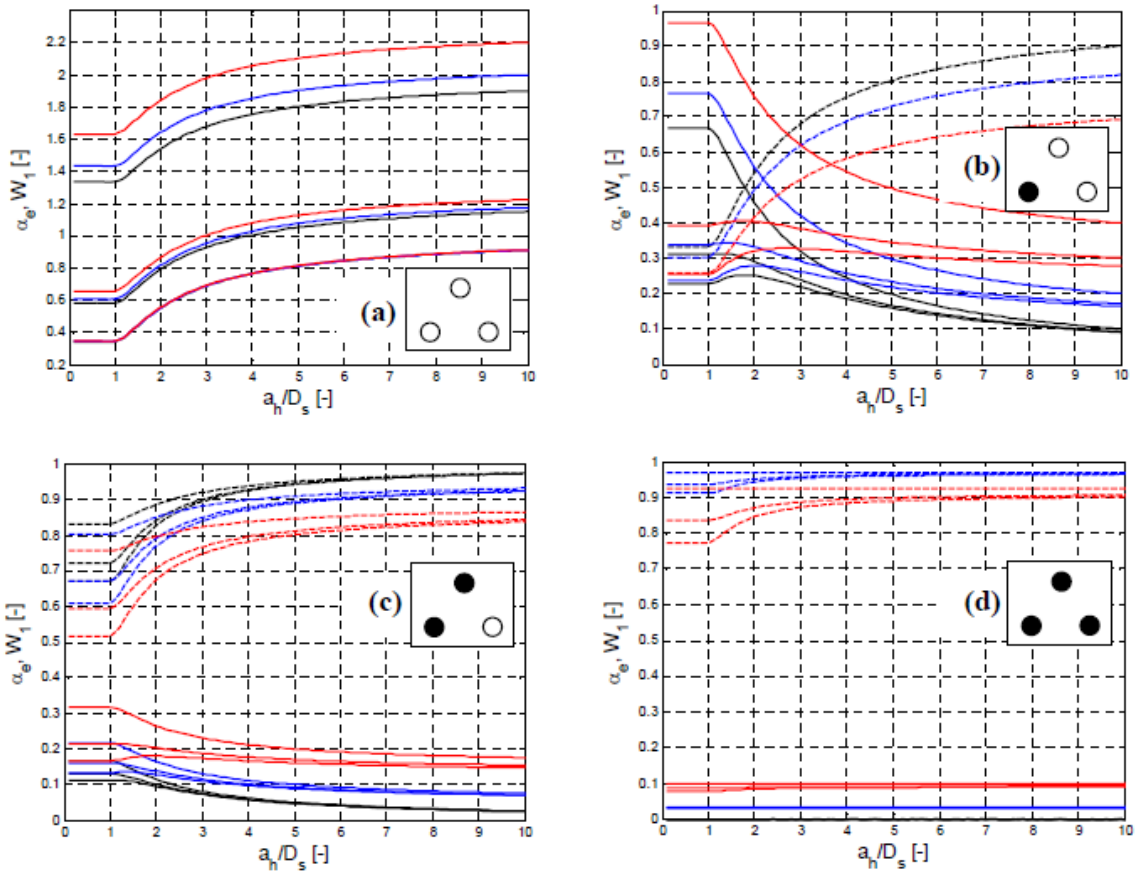

Figure 5-7. Analogous to Figure 5-5 for tripe pile groups in a triangle and different monitoring configurations.

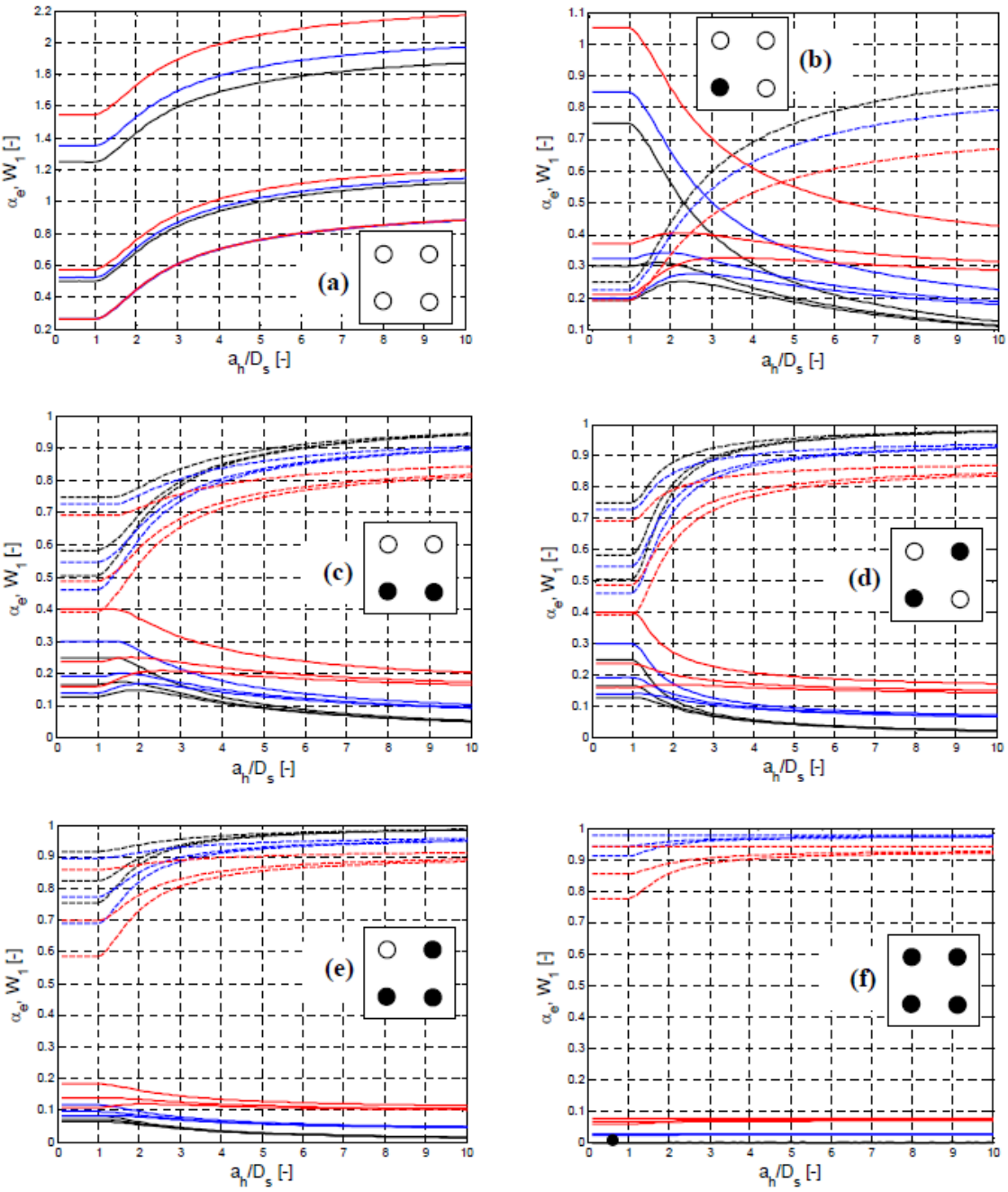

Figure 5-8. Analogous to Figure 5-5 for 2 × 2 pile groups and different monitoring configurations.

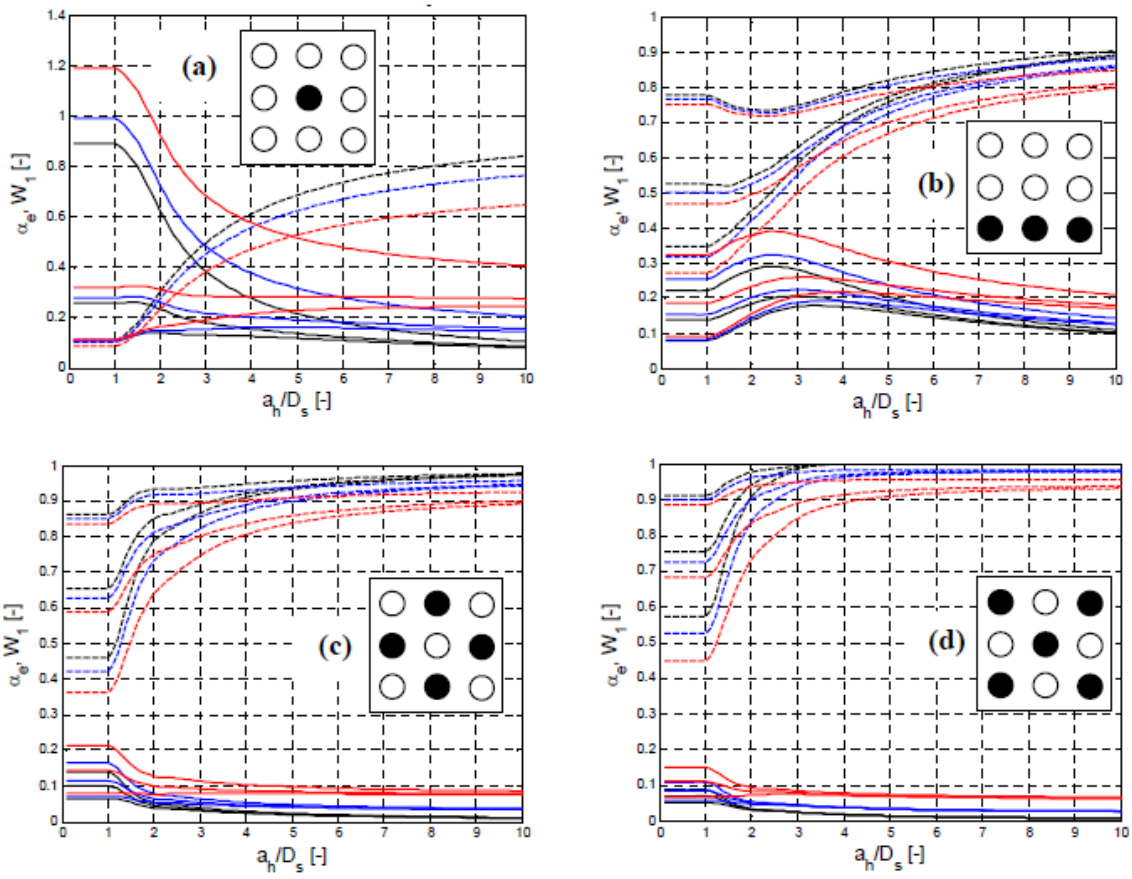

Figure 5-9. Analogous to Figure 5-5 for 3 × 3 pile groups and different monitoring configurations.

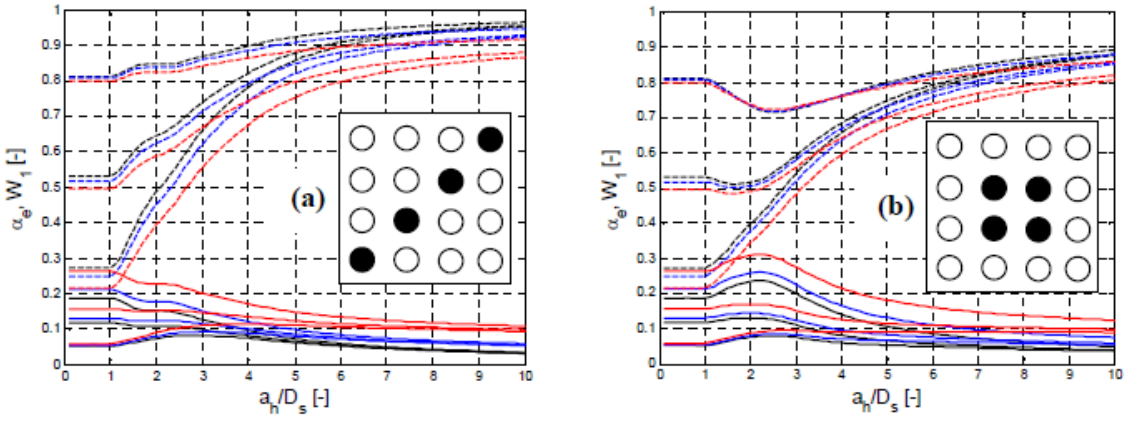

Figure 5-10. Analogous to Figure 5-5 for 4 × 4 pile groups and different monitoring configurations.

In more complex configurations of Figures 5-9 and 5-10, minima in W_1 may occur at different locations and are best determined graphically. In case a_h is not available for explicit computation of W_1, a worst case prediction R^*_{g1w} may hence be defined as

$$R^*_{g1w} = \min\left[W_{1\max}R_{m1} + \left(1 - W_{1\max}\right)\mu_p, W_{1\min}R_{m1} + \left(1 - W_{1\min}\right)\mu_p\right] \tag{5.26}$$

In other words, $R^*_{g1w} = W_{1max}R_{m1} + (1\text{-}W_{1max})\mu_p$ if $R_{m1} \leq \mu_p$, and $R^*_{g1w} = W_{1min}R_{m1} + (1\text{-}W_{1min})\mu_p$, if $R_{m1} > \mu_p$. This shows that for an increasing degree of monitoring (i.e., $n_{m1} \rightarrow n_{p1}$) W_{1min} approaches $n_g + (n_{m1} - 1)(1 + \alpha_\varepsilon)/[(n_g + n_{m1} - 1)(1 + \alpha_\varepsilon)]$ which is one for $\alpha_\varepsilon = 0$, such that the worst case prediction R^*_{g1w} approaches R_{m1}. With $n_{m1} = 1$, Equation 5.25 collapses to $W_{1min} = 1/[n_{p1}(1 + \alpha_\varepsilon)]$, while for large n_g it may be found that $W_{1min} = n_{m1}/[n_{p1}(1 + \alpha_\varepsilon)]$.

For computation of LRFD Φ (e.g., through AASHTO, Equation 4.10, assuming log-normal distributions of load and resistance), CV_{Rg1} is required which may be found from Equation 5.15 by $CV_{Rg1} = \alpha_e^{1/2} CV_{Rp}$, where $CV_{Rp} = \sigma_p/\mu_p$. For $n_g = 1$, Equation 5.15 collapses to $\alpha_e = \alpha_{g1} + \alpha_{m1} - 2\alpha_{mg1}$, while for large n_g, $\alpha_e \approx \alpha_{g1} - \alpha^2_{mg1}/\alpha_{m1}$. Although a mathematical model for $C(h)$, e.g., spherical or exponential, may be adopted to find closed form expressions of Equations 5.7 through 5.16 by simple algebraic manipulations, this process is extremely lengthy, needing to be repeated for every single combination of pile group type and monitoring configuration. Useful (i.e., sufficiently short /simple) results for practical application are not expected. Instead, in the same way as W_1 from Equation 5.14, Equation 5.15 is evaluated numerically and results are investigated graphically for several example configurations in Figures 5-5 through 5-10 (continuous lines). From top to bottom, the lines correspond to $n_g = \{1, 5, 100\}$, i.e., the larger n_g the smaller α_e and the larger will be Φ. Black, blue and red

again correspond to $\alpha_\varepsilon = CV_\varepsilon^2 / CV_p^2 = \{0, 0.1, 0.3\}$ where larger values of α_ε clearly lead to larger uncertainty and α_e.

It may be observed that, in general, an increase in the number n_{mi} of monitored piles leads to a more substantial reduction in α_e than a comparable increase in the number n_g of pile groups. This is, the number of data available outside the pile group of interest is less important than the number of data available within the pile group of interest. This is further reflected by the fact that as a_h / D_s grows, α_e becomes increasingly independent of n_g. It is also observed that it is advantageous to locate monitored piles near the center of pile groups (compare Figures 5-6a and 5-6b) as well as not immediately adjacent to each other (compare Figures 5-6c and 5-6d as well as Figures 5-8b and 5-8c). Worst case values α_{ew} for unknown a_h are seen to mostly occur at $a_h / D_s \leq 1$, i.e., when no correlation is present between individual piles. However, exceptions are when n_g is large and n_{m1} is small, such that "humps" in the graphs become evident at $a_h / D_s \approx 2$. Unfortunately, these humps become more pronounced as $\alpha_\varepsilon > 0$ and α_{ew} is best determined graphically.

5.6 Practical Example

To better illustrate the outcome and implications of the previous section, an example is worked. Consider a bridge site with five pile groups (n_g), where for the group of interest (i=1, or group 1) the number of piles monitored (n_{m1}) are 1, 2, or 3, and the mean of the monitored pile resistance (R_{m1}) of group 1 is 1.6 MN as given,

μ_p = 2 MN
CV_{Rp} = 0.5
R_{m1} = 1.6 MN
σ_ε = 0
$C(h)$ is spherical with a_h / D_s = 3
n_g = 5
Square pile group with n_{m1} = 1, 2, 3
Reliability index β = 3

Given in Table 5-1 are the results where italic numbers are read from the respective figures. It may be observed that Φ consistently grows as n_{m1} increases. However, the variable of ultimate interest, the design load $Q_{(w)}$, also depends on the ratio R_{m1}/μ_p and general conclusions are hence more difficult to make. Finally, it is noted that the present worst case investigation is based on a separate minimization of R^*_{g1} and Φ. In cases where the two minima do not occur at equal values of a_h/D_s (e.g., in the present scenario R^*_{g1w} is obtained at $a_h/D_s >> 1$ and α_{ew} at $a_h/D_s \approx 1$), a more favorable worst case design load Q_w may be obtained by direct (numerical) minimization of the product ΦR^*_{g1} as a function of a_h/D_s (as shown in Chapter 4). This is equivalent to assuming different possible values of a_h and finding respective values of Q from which the minimum is chosen as Q_w. It is recalled that the resistance Q represents the entire pile group.

Table 5-1. Summary of Results from Practical Example.

n_{m1}	Fig.	W_1	R^*_{g1}	α_e	CV_{Rg1}	Φ	**Q**	W_{1min}	R^*_{g1w}	α_{ew}	CV_{Rg1w}	Φ_w	**Q_w**
-	-	-	MN	-	-	-	**MN**	-	MN	-	-	-	**MN**
1	5-7a	*0.60*	1.76	*0.28*	0.26	0.59	**4.16**	0.25	1.6	*0.31*	0.28	0.54	**3.46**
2	5-7b	*0.79*	1.68	*0.13*	0.18	0.72	**4.84**	0.58	1.6	*0.18*	0.21	0.67	**2.28**
2	5-7c	*0.89*	1.64	*0.08*	0.14	0.80	**5.26**	0.58	1.6	*0.17*	0.21	0.67	**2.28**
3	5-7d	*0.94*	1.62	*0.04*	0.10	0.89	**5.78**	0.82	1.6	*0.08*	0.14	0.80	**5.12**
			Eqn. 5.13		$\alpha_e^{1/2} CV_{Rp}$	AASHTO	$n_{p1}\,\Phi\,R^*_{g1}$	Eqn. 5.25	Eqn. 5.26		$\alpha_{ew}^{1/2} CV_{Rp}$	AASHTO	$n_{p1}\,\Phi\,R^*_{g1w}$

CHAPTER 6
UNMONITORED, PARTIALLY AND FULLY MONITORED PILE GROUPS – REGRESSION APPROACH

6.1 Background

The previous two chapters consider estimation of driven pile group resistance and uncertainty based on SPT/CPT data (for side friction only) and directly monitored data (EDC, PDA; side + tip resistance). Fundamental assumptions in both cases are that SPT/CPT estimates of local strength in the former case and monitored pile resistances in the latter case may be regarded as random functions in space. As such, the approach in Chapter 5 requires some common characteristic of all monitored and unmonitored piles (e.g., equal embedment depths or blow counts). This may be in accordance with design practice if other load scenarios other than pure axial load are dominant (e.g., lateral loading requiring minimum embedment depth). In general, however, piles are driven until a desired design resistance is reached with the number of hammer blow counts, i.e., blows/ft, etc., varying from pile to pile. Beside this, the use of SPT/CPT data (i.e., Chapter 4) from the design phase prior to any (test) for pile driving/monitoring introduces more complexity.

Due to the conceptual limitations (i.e., equal pile capacity/blows) of Chapter 5 and added complexity of SPT/CPT data of Chapter 4, the present chapter seeks an alternative solution based on two modifications: (1) Blow count data during pile installations is incorporated as an additional piece of information to more closely emulate construction practice; and (2) spatial correlation between monitored pile resistances is neglected to avoid conceptual limitations (approach more flexible/adaptive to different design situations) and to make results more designer friendly. As such, Chapters 5 and 6 may be regarded as two particular simplifications of a general co-kriging approach, which would consider monitored pile resistances and pile blow count data as primary and secondary variables, respectively. While Chapter 5 neglects the

collocated secondary variable (blow counts are ignored), Chapter 6 neglects spatial correlation of the primary variable (spatial correlation of monitored resistances is ignored). Since blow count data is known to be well correlated with "true" resistances from static load tests (and, hence, also with monitored pile resistances), the loss of information (increase in uncertainty) through neglecting spatial correlation of monitored resistances is quite insignificant (see Appendix for an illustrative example). Before developing the approach, an overview is given of different relationships which have been used between blow counts and pile capacities.

6.2 Examples of Relationships between Blow Count and Pile Capacities

Relationships between static pile capacity R and hammer blow counts measured during pile driving go back to the earlier 1800s. Generally, the early relationships were linear and the later representations were nonlinear (Paikowsky 2004). For instance, one of the most popular capacity estimations is the Engineering News-Record (ENR) formula by Wellington (Paikowsky 2004),

$$R = \frac{e_h W_H H}{FS(s + C)} \tag{6.1}$$

where W_H is the weight of the hammer ram expressed in the same units as R; e_h the energy loss of the hammer; H the height of fall of the ram (i.e., its stroke); s the pile permanent set; and C the energy loss per hammer blow. Values H, s and C are in inches, where $C = 1$ inch for drop hammers and $C = 0.1$ inches for all other hammers. FS is a factor of safety, generally ranging from 2 to 6.

Another popular approach is the FHWA Gates relationship (Paikowsky 2004) expressed as

$$Q_u = 1.75\sqrt{W_H H}\log(10\,N) - 100 \tag{6.2}$$

where Q_u is the ultimate pile resistance in kips; W_H the weight of the hammer ram in pounds; H the height of fall of the ram (i.e., its stroke) in feet; and N the driving resistance in blows/inch. Both approaches are generally used where high strain rate measurement devices are not employed (Paikowsky 2004). Their characterization of a Delmag D22 (60 kip-ft) hammer with various blow counts is shown in Figure 6-1 (ENR: $FS = 4$, $e_h = 0.85$). Evident from Figure 6-1, both approaches are nonlinear; however, the ENR results could be approximated as linear. Also, both approaches differ the most at low and high blow counts, but both methods would be characterized as linear in a log-log plot.

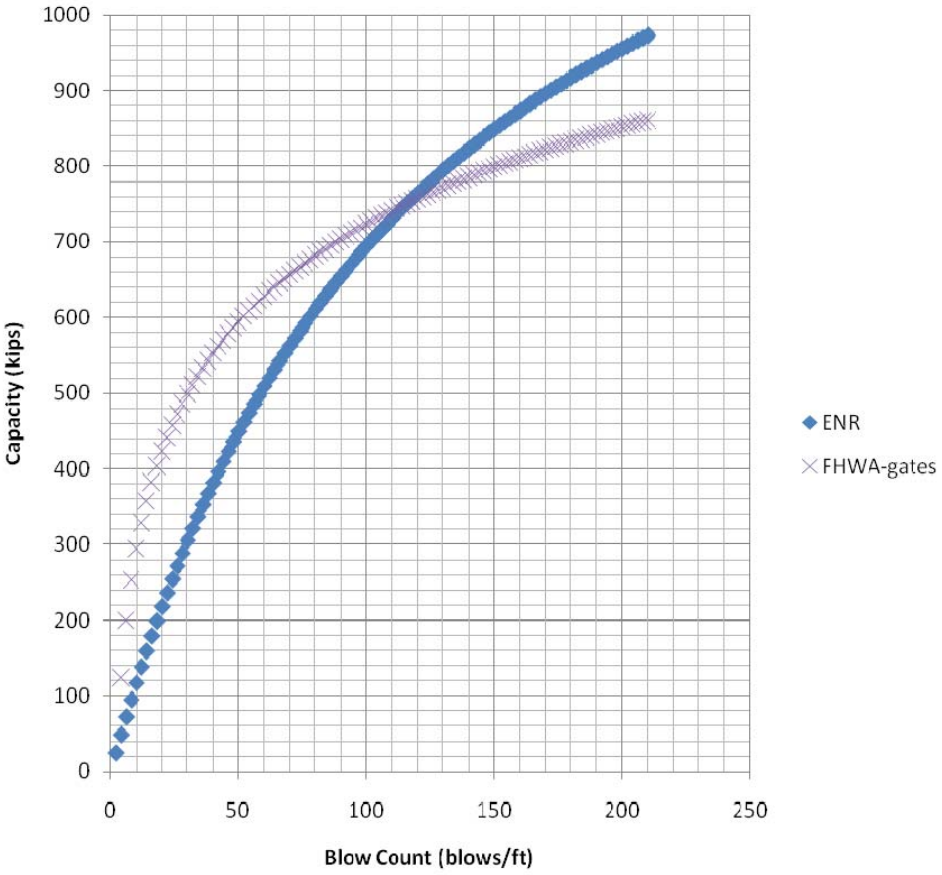

Figure 6-1. Comparison of ENR and FHWA-Gates for Delmag D22.

National Cooperative Highway Research Program (*NCHRP*) *Report 507* (Paikowsky 2004) evaluated both approaches with a database of measured versus predicted static resistances.

Shown in Table 6-1 (AASHTO, 2009) under "Dynamic Equations" are both ENR and FHWA-Modified Gates summary statistics (bias, standard deviation and ratio CV). As evident, the ENR appears more conservative (higher bias) with more scatter (CV) versus the FHWA-Modified Gates. Also note the high strain rate predictions approaches (e.g., PDA-CAPWAP) have lower coefficient of variation than the simpler Dynamic Equation approaches (ENR, FHWA-Gates), e.g., PDA/CAPWAP (CV = 0.453), ENR (CV = 0.910) and FHWA-Gates (CV = 0.502).

Table 6-1. Summary Statistics for ENR and FHWA-Modified Gates (AASHTO, 2009; Note: "COV" in this table is equivalent to "CV" in the rest of the report)

Method		Time of Driving	No. of Cases	Mean	Standard Deviation	COV	Resistance Factors for a given Reliability Index, β		
							2.0	2.5	3.0
Dynamic Measurements	CAPWAP	General	377	1.368	0.620	0.453	0.68	0.54	0.43
		EOD	125	1.626	0.797	0.490	0.75	0.59	0.46
		EOD - AR < 350 & Bl. Ct. < 16 BP10cm	37	2.589	2.385	0.921	0.52	0.35	0.23
		BOR	162	1.158	0.393	0.339	0.73	0.61	0.51
	Energy Approach	General	371	0.894	0.367	0.411	0.48	0.39	0.32
		EOD	128	1.084	0.431	0.398	0.60	0.49	0.40
		EOD - AR < 350 & Bl. Ct. < 16 BP10cm	39	1.431	0.727	0.508	0.63	0.49	0.39
		BOR	153	0.785	0.290	0.369	0.46	0.38	0.32
Dynamic Equations	ENR	General	384	1.602	1.458	0.910	0.33	0.22	0.15
	Gates	General	384	1.787	0.848	0.475	0.85	0.67	0.53
	FHWA modified Gates	General	384	0.940	0.472	0.502	0.42	0.33	0.26
		EOD	135	1.073	0.573	0.534	0.45	0.35	0.27
		EOD Bl. Ct. < 16BP10cm	62	1.306	0.643	0.492	0.60	0.47	0.37
WEAP		EOD	99	1.656	1.199	0.724	0.48	0.34	0.25

Notes: EOD = End of Driving; BOR = Beginning of Restrike; AR = Area Ratio; Bl. Ct. = Blow Count; ENR = Engineering News Record Equation; BP10cm = Blows per 10cm; COV = Coefficient of Variation; Mean = ratio of the static load test results (Davisson's Criterion) to the predicted capacity = K_{SX} = λ =bias

The present chapter aims at discussing the statistical implications of using blow count data for estimating static pile resistances and using linear relationship between blow count and capacity. This is in agreement with a preliminary data analysis from two different sites (four piles). However, a generalization to include non-linear relationships is straightforward (see Section 2.1 on estimation bias) and is one of the advantages of the approach.

6.3 List of Variables for Chapter 6

For developing Chapter 6, the following variables have been used and are collected together for accessibility:

Φ LRFD resistance factor.

β Reliability index.

Q Nominal design load.

CV_Q Coefficient of variation of design load distribution.

n_p Total number of piles in group of interest.

n_m Number of monitored piles in group of interest.

n_0 Number of previously driven piles in group of interest.

L Pile embedment depth in general.

N_h Number of hammer strikes per meter pile advance (blow count).

N_{hi} Blow count of i-th pile at production depth.

R_m Monitored total (side + tip) pile resistance.

R_m^* Prediction of R_m using N_h.

R_{mi} Monitored total (side + tip) pile resistance of the i-th pile at production depth.

R_p Nominal total (side + tip) pile resistance.

R_g Nominal total (side + tip) resistance of the pile group of interest.

σ_g^2 Variance of pile group resistance distribution.

CV_g σ_g / R_g.

R_0 Combined nominal resistance of all previously installed piles in the group of interest.

σ_0^2 Variance of combined resistance of all previously installed piles in the group of interest.

CV_0 σ_0 / R_0.

$CV_{\varepsilon m}$ Coefficient of variation of error between predicted total (side + tip) pile resistances R_m from monitoring (e.g., from EDC or PDA) and true total pile resistances (e.g., from static load test).

$CV_{\varepsilon h}$ Coefficient of variation of error between predictions of monitored total (side + tip) pile resistances R_m^* and monitored pile resistances R_m.

$\sigma_{\ln m}^2$ Variance of natural logarithms of R_m.

R^2 Coefficient of determination of a linear regression model in general.

$R_{\ln}^2$ Coefficient of variation of the linear regression model of the log-transformed data.

i Index denoting different piles in the group of interest.

a, b, $c^{(\prime)}$, $d^{(\prime)}$, e, f, g, h, A, B, C, X are auxiliary variables used in intermediate equations.

6.4 The Regression Approach

Typically, a nominal design load Q with a respective coefficient of variation CV_Q is given in combination with a desired level of reliability β. These values are defined for a whole pile group consisting of n_p piles, an arbitrary number n_m of which may be monitored (side + tip resistance, e.g., through EDC or PDA). For a chosen monitoring method, the measurement error with respect to true pile resistances (e.g., from static load tests) is known and expressed by a constant coefficient of error variation $CV_{\varepsilon m}$ (i.e., measurement errors are proportional to resistance). While driving monitored piles, both monitored pile resistances R_m and the number of hammer strikes, N_h per meter pile advance (i.e., blow count) are recorded as functions of depth L. This is illustrated by an example in Figure 6-2 using data from a 30-in. × 70-ft. pile at Bent 7 at Caminida Bay, Louisiana. Figure 6-2a shows depth profiles of R_m and N_h as recorded in the field where R_m was obtained with Case's (i.e., *Jc*) Equation. Figure 6-2b is a general comparison, i.e., cloud of data points (scatter plot) of R_m versus N_h for all depths. This further allows for linear correlation/regression analysis of raw data and of the log-data (i.e., after taking the natural logarithms; Caminida pile 7 example of Figure 6-2c). Other, e.g., non-linear, relationships may also be considered at this stage as an additional bias correction before regression analysis (see Section 2.1). From the raw data scatter plot a linear regression relationship was found between the arbitrary blow count N_h (within the range of data points) and the associated expected (or predicted) value R_m^* of R_m as

$$R_m^* = a + bN_h \tag{6.3}$$

where a and b are the regression coefficients. Since the scatter of the data points about the regression line is seen to be approximately proportional to N_h, the scatter plot of log-data is used to find a constant coefficient of error variation $CV_{\varepsilon h}$ between R_m^* and R_m, i.e., between monitored resistances predicted from blow counts (Equation 6.3) and the truly monitored resistances from EDC or PDA. Assuming the distributions of N_h and R_m are approximately log-normal, $CV_{\varepsilon h}$ may be found from the following equation:

$$CV_{\varepsilon h} = \sqrt{\exp\left[\sigma^2_{\ln m}\left(1 - R^2_{\ln}\right)\right] - 1} \tag{6.4}$$

with $\sigma^2_{\ln m}$ being the variance of $\ln(R_m)$ and $R^2_{\ln}$ the coefficient of determination of the log-regression relationship (e.g., R^2 in Caminida pile 7 shown in Figure 6-2c).

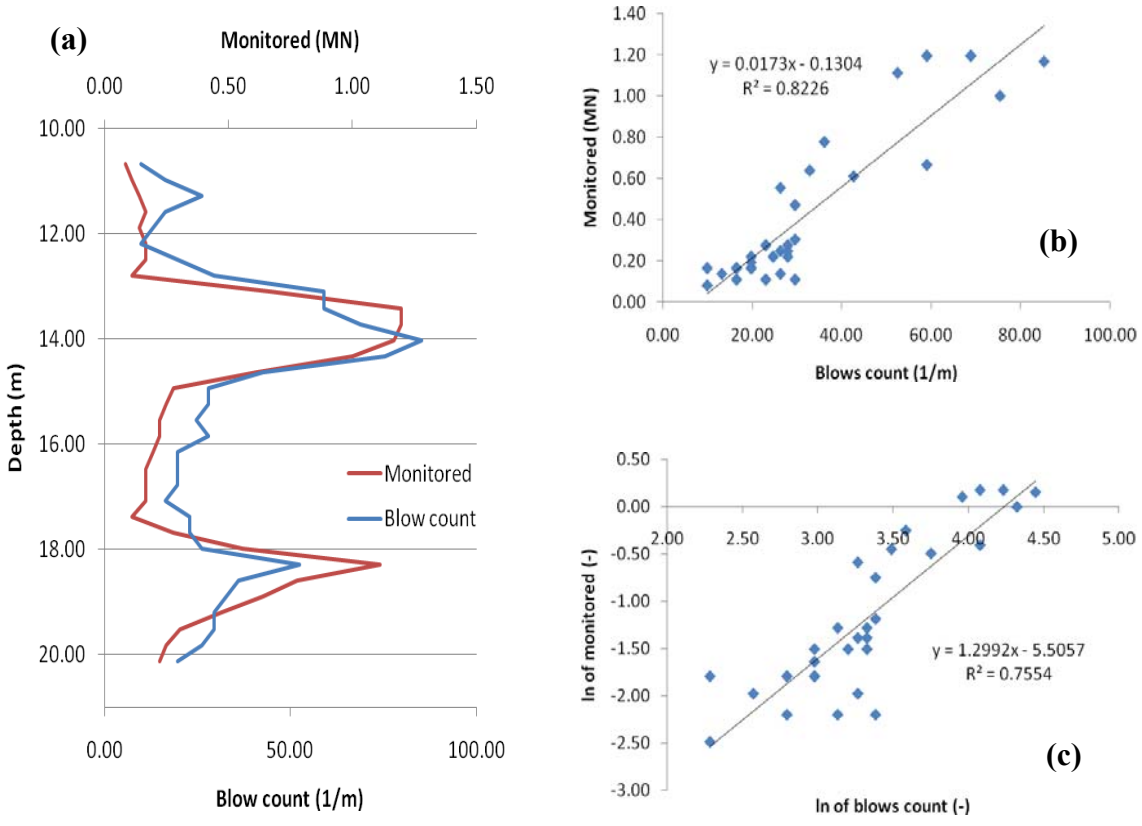

Figure 6-2. Example data from driving of a single pile (pile 7) at Caminida. (a) Depth profiles of monitored resistance R_m and blow count N_h; (b) Scatter plot and linear regression between N_h and R_m; and (c) Scatter plot and linear regression between $\ln(N_h)$ and $\ln(R_m)$.

Designating all n_p piles in a group by different values of an index i, which ranges from 1 to n_m for monitored piles and from $n_m + 1$ to n_p for unmonitored piles, the total resistance of the group may be written as

$$R_g = \sum_{i=1}^{n_m} R_{mi} + \sum_{i=n_m+1}^{n_p} (a + bN_{hi}) \tag{6.5}$$

where R_{mi} are the monitored pile resistances to which the monitored piles are driven, and N_{hi} are the blow counts to which the unmonitored piles are driven. The variance σ_g^2 about R_g is then

$$\sigma_g^2 = \sum_{i=1}^{n_m} (CV_{\varepsilon m} R_{mi})^2 + \sum_{i=n_m+1}^{n_p} \left\{ (CV_{\varepsilon m} R_{mi})^2 + [CV_{\varepsilon h} (a + bN_{hi})]^2 \right\} \tag{6.6}$$

such that $CV_g = \sigma_g / R_g$. Note, the first summation represents the uncertainty of monitored piles in terms of static resistance, and the second summation represents the uncertainty of unmonitored piles. To represent the uncertainty of the unmonitored piles in terms of static resistance, it must first be expressed in terms of the monitored piles (2nd term in 2nd summation) and then in terms of static load tests (1st term in 2nd summation). Subsequently, the LRFD Φ (AASHTO equation; assuming log-normal load and resistance distributions) may be found after all piles in a group are driven and a, b (Equation 6.5) and $CV_{\varepsilon h}$ found from data analysis (Equations 6.3 and 6.4) from one or more monitored piles. With this, LRFD leads to a nominal design load of $Q = \Phi R_g$.

However, as initially stated, it is a more typical design scenario to determine R_g for a given Q. Under purely axial load, it is also reasonable to assume that all piles should have the same nominal resistance R_p such that Equation 6.5 and 6.6 become $R_g = n_p R_p$ and $\sigma_g^2 = R_p^2 [n_p CV_{\varepsilon m}^2 + (n_p - n_m) CV_{\varepsilon h}^2]$. This leads to

$$CV_g = \sqrt{\frac{1}{n_p} \left[CV_{\varepsilon m}^2 + \left(1 - \frac{n_m}{n_p} \right) CV_{\varepsilon h}^2 \right]} \tag{6.7}$$

which is independent of R_p and LRFD Φ (to be obtained from CV_g and AASHTO equation). Consequently, $R_g = Q/\Phi$ or $R_p = R_g/n_p$ may be directly determined. Knowing this, the monitored piles in a group are driven until $R_m = R_p$ is reached and the unmonitored piles are driven until $R_m^* = R_p$ is reached, or from Equation 6.3, until a blow count of $N_h = (R_p - a)/b$.

Useful in the sequel (and perhaps for various other purposes) will be an approximation to the full AASHTO equation (black lines in Figure 6-3) as a linear form $\Phi \approx c - d*CV_g$, where $c = e + f*\beta$ and $d = g + h*\beta$. Optimizing the constants e through h gives

$$\Phi \approx 1.25 - 0.082\beta - (0.80 + 0.31\beta)CV_g \tag{6.8}$$

which is depicted through red lines in Figure 6-3 and is valid for the range $CV_g \geq 0.05$, $\Phi > 0.4$ and $2 \leq \beta \leq 4$. For the common requirement of $\beta = 3$, Equation 6.8 becomes

$$\Phi \approx 1 - 1.73CV_g \tag{6.9}$$

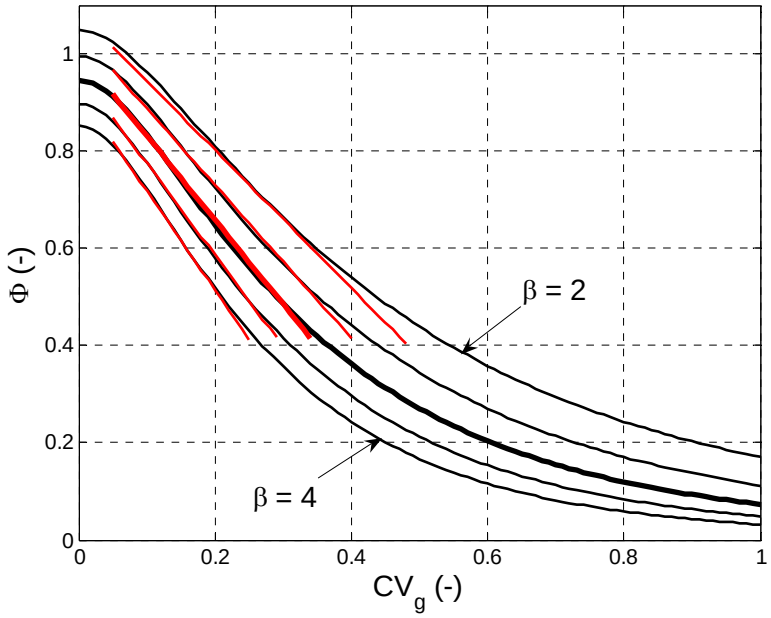

Figure 6-3. Term Φ (with $\lambda_R = 1$ and for $\beta = \{2, 2.5, 3, 3.5, 4\}$) as a function of CV_g from full AASHTO equation (black) and linear approximations (red) from Equation 6.8 for the range $CV_g \geq 0.05$, $\Phi > 0.4$ and $2 \leq \beta \leq 4$. Lines for $\beta = 3$ are bold.

Another good approximation may be of the form $\Phi \approx 1/(c' + d' * CV_g^2)$, where c' and d' are again (linear) functions of β. However, except for elimination of the square root in Equation 6.7, no significant advantages of the latter approximation over Equation 6.8 are found. Combining Equations 6.7 and 6.8 leads to the following compact expression for Φ as a function of group size n_p, degree of monitoring n_m/n_p as well as the prediction errors $CV_{\varepsilon m}$ and $CV_{\varepsilon h}$,

$$\Phi \approx 1 - 1.73\sqrt{\frac{1}{n_p}\left[CV_{\varepsilon m}^2 + \left(1 - \frac{n_m}{n_p}\right)CV_{\varepsilon h}^2\right]} \tag{6.10}$$

In general, it may happen that not all piles are driven to the same nominal resistance. For example, monitored test piles may be driven prior to design of the remaining piles and to larger depths for more reliable site exploration. In this case, n_0 denotes the number of previously driven piles such that $n_p - n_0$ is the number of remaining piles in the group for which a uniform nominal pile resistance R_p is sought. The expression $R_0 = \sum_{i=1}^{n_0} R_{mi}$ is then the known sum of the monitored resistances of the previously driven piles, which is associated with a known variance $\sigma_0^2 = \sum_{i=1}^{n_0} \left(CV_{\varepsilon m} R_{mi}\right)^2$. Equations 6.5 and 6.6 remain valid in the forms

$$R_g = R_0 + \left(n_p - n_0\right)R_p \tag{6.11}$$

$$\sigma_g^2 = \sigma_0^2 + \left[\left(n_p - n_0\right)CV_{\varepsilon m}^2 + \left(n_p - n_m\right)CV_{\varepsilon h}^2\right]R_p^2 \tag{6.12}$$

CV_g is now a function of R_p and Φ may not be found directly as above. However, it is known from Equation 6.8 that

$$\Phi = \frac{Q}{R_g} \approx c - dCV_g \tag{6.13}$$

is a good approximation from which by substituting R_g and $CV_g = \sigma_g/R_g$ from Equations 6.11 and 6.12, a quadratic equation in R_p is obtained. Defining the auxiliary variable

$X = (n_p - n_0)R_p/R_0$ as the multiple of R_0 that the piles still to be driven have to contribute, an equation in the form of $AX^2 + BX + C = 0$ may be written where

$$A = \frac{d^2}{n_p - n_0}\left(CV_{\varepsilon m}^2 + \frac{n_p - n_m}{n_p - n_0}CV_{\varepsilon h}^2\right) - c^2$$
$$B = 2c\left(\frac{Q}{R_0} - c\right) \tag{6.14}$$
$$C = d^2 CV_0^2 - \left(\frac{Q}{R_0} - c\right)^2$$

and $CV_0 = \sigma_0/R_0$. With this, X and R_p are found as

$$X = -\frac{B}{2A} + \sqrt{\left(\frac{B}{2A}\right)^2 - \frac{C}{A}} \tag{6.15}$$

$$R_p = \frac{XR_0}{n_p - n_0} \tag{6.16}$$

The relevant solution for the present purpose is characterized by $R_g > Q$. The second solution of the quadratic system leads to $R_g < Q$ and most likely corresponds to the relevant situation, where the upper tail of the resistance distribution overlaps the lower tail of the load distribution (i.e., the opposite of a regular design situation).

Knowing required values of $R_m = R_p$ for monitored piles and $N_h = (R_p - a)/b$ for unmonitored piles, expected pile embedment depth (and possibly uncertainties) may be determined from available depth profiles of R_m and N_h. An optimization of the degree of pile monitoring (e.g., n_m/n_p in Equation 6.10) versus cost of monitoring, pile construction, driving, etc., is most easily obtained by assuming different scenarios of n_m/n_p and comparing expected costs. Results are expected to heavily depend on site specific conditions (e.g., degree of heterogeneity and layering) and no general guideline may be given at this point.

Before any pile monitoring data is available at a site, $CV_{\varepsilon h}$ given in Equation 6.10 must be assessed. A number of potential solutions are viable: (1) collect existing data for a variety of site conditions (e.g., soil types and hammers) to define the possible worst case values of $CV_{\varepsilon h}$ to be used if site specific monitoring data is not available for regression analysis; and (2) collect explicit site specific blow count versus monitored capacities from which $CV_{\varepsilon h}$ may be established. Due to the large number of individual blow count versus monitored capacities with depth for an individual pile, two to three monitored piles per site would be sufficient to establish $CV_{\varepsilon h}$ for a given site. Equally important and more expensive in obtaining is the evaluation of $CV_{\varepsilon m}$ or the uncertainty between the static load test capacity and the monitored pile capacity. The latter may be a function of soil type and evaluation time (e.g., end of drive (EOD) versus beginning of redrive (BOR), etc.). For instance, Table 6-1 suggests a value of 0.339 at BOR for all soils in the U.S. For Florida silts, sands, and limestone, a value of 0.25 will be used (Section 6.5). Also note, the site exploration data, e.g., SPT or CPT, are used to set the design embedment pile lengths with a computed uncertainty and LRFD Φ, whereas in construction, pile monitoring and measured blow counts will be used to assess a different LRFD Φ (Equation 6.10) and associated uncertainty and final installed pile length.

6.5 Practical Example

In order to apply the theoretical development from above, data from pile driving at Caminida Bay, Louisiana (piles 1 and 7) and SR 810, Dixie Highway (piles 1 and 8) over Hillsboro Canal in Broward County, Florida, are analyzed. While Figure 6-2 already represents data from Caminida pile 7 as an example to illustrate the above development, Figure 6-4 contains the depth profiles of monitored resistances and blow counts of the other three piles. It is noted that the scales of monitored resistances and blow counts are different (the two variables possess different dimensions), which disallows a direct comparison of magnitudes in Figures 6-2a and

6.4. However, this is of actual interest for the present problem. Figures 6-2a and 6-4 demonstrate that the fluctuations in monitored resistances and blow counts seem to be positively correlated to some degree (i.e., "peaks" and "valleys" mostly coincide for both). This supports the suggestions in Section 6.2 that blow count may be a reasonable predictor for monitored resistances. This is further analyzed in Figure 6-5 containing combined scatter plots of R_m against N_h from all four piles with corresponding linear regression fits (compare Figures 6-2b and 6-2c which represent the same for a single pile).

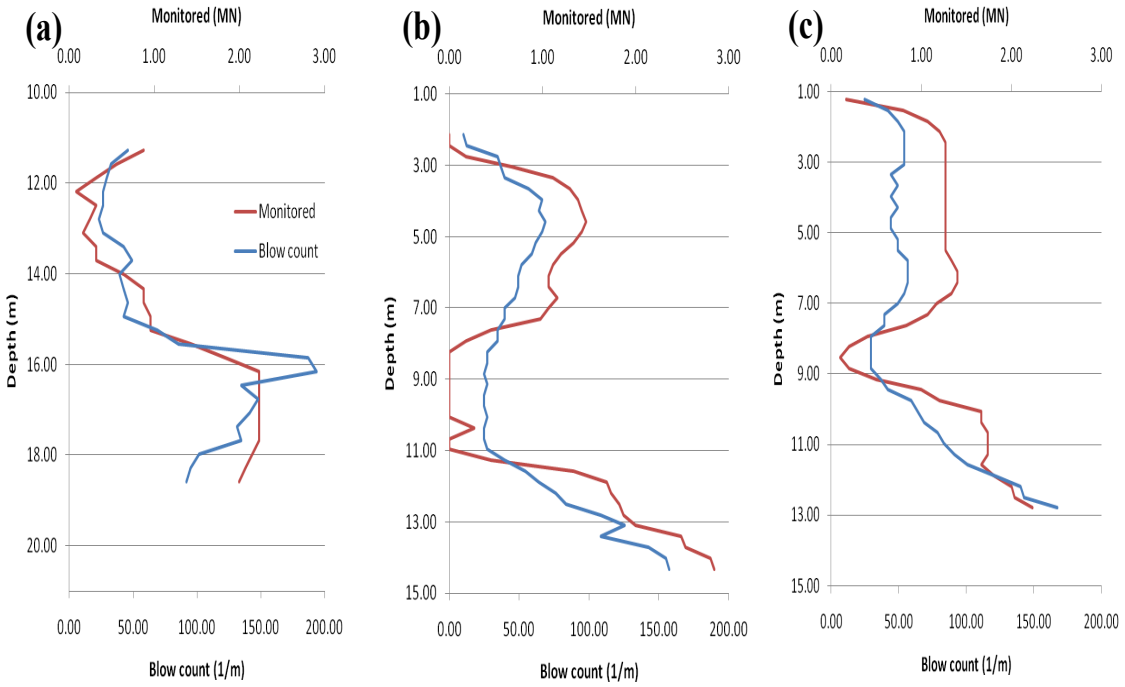

Figure 6-4. Depth profiles of monitored resistances R_m and blow counts N_h for: (a) Caminida pile 1; (b) Dixie pile 1; and (c) Dixie pile 7.

The data of both sites and all four piles is seen to form a single cloud indicating that the relationships between R_m and N_h at Caminida and Dixie are basically the same. This may be a reflection of similar site conditions or of N_h actually being a convenient predictor for R_m even under variable conditions between sites. Moreover, the data cloud is relatively narrow around the regression line and application of Equation 6.4 with $\sigma^2_{\ln m} = 0.92$ and $R^2_{\ln} = 0.77$ (Figure 6-5b)

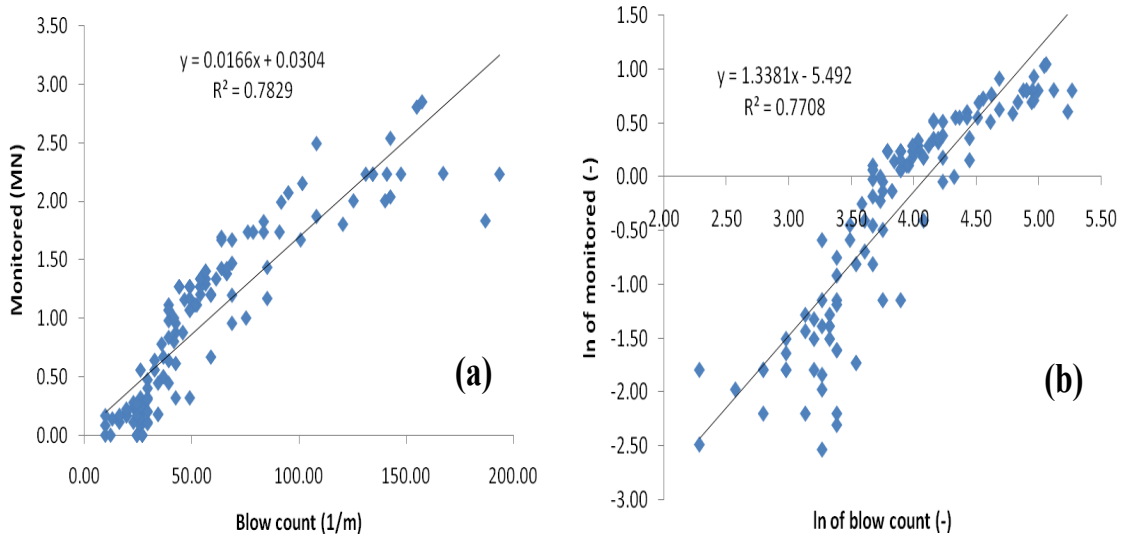

Figure 6-5. Combined scatter plots and linear regression fits of monitored resistance R_m versus blow count N_h data from Caminida piles 1 + 8 and Dixie piles 1 + 7: (a) Raw data; and (b) log-transformed data.

gives $CV_{\varepsilon h} = 0.48$. The coefficients a and b of Equation 6.3 result from Figure 6-5a as 0.030 and 0.017, respectively. Repeating the same analysis only for piles 1 and 8 at Caminida gives $CV_{\varepsilon h} = 0.44$ and only for piles 1 and 7 at Dixie $CV_{\varepsilon h} = 0.45$ (regression charts not shown). Respective values of a and b are also similar.

For the resulting $CV_{\varepsilon h} = 0.48$, a value of $CV_{\varepsilon m} = 0.25$ and $\beta = 3$. Figure 6-6 graphically represents LRFD Φ as a function of the degree of monitoring in groups of different pile numbers. Using the relative portion of piles monitored (Figure 6-6b), it is observed that larger pile groups have consistently larger Φ which is due to the larger amount of averaging (variance reduction) among a larger number of individual piles (positive and negative measurement error cancel out to a larger degree). In turn, smaller pile groups present a larger increase in Φ with additional monitoring. Note that results only depend on n_p and n_m/n_p, but not on the actual geometric arrangement of piles in a group. The continuous lines in Figure 6-6b are approximations obtained from Equation 6.10 and show excellent agreement with exact results from the full

AASHTO equation indicated by dots. This is a consequence of the fact that all data points in Figure 6-6 lie within the range established for the approximate Equations 6.8 and 6.9.

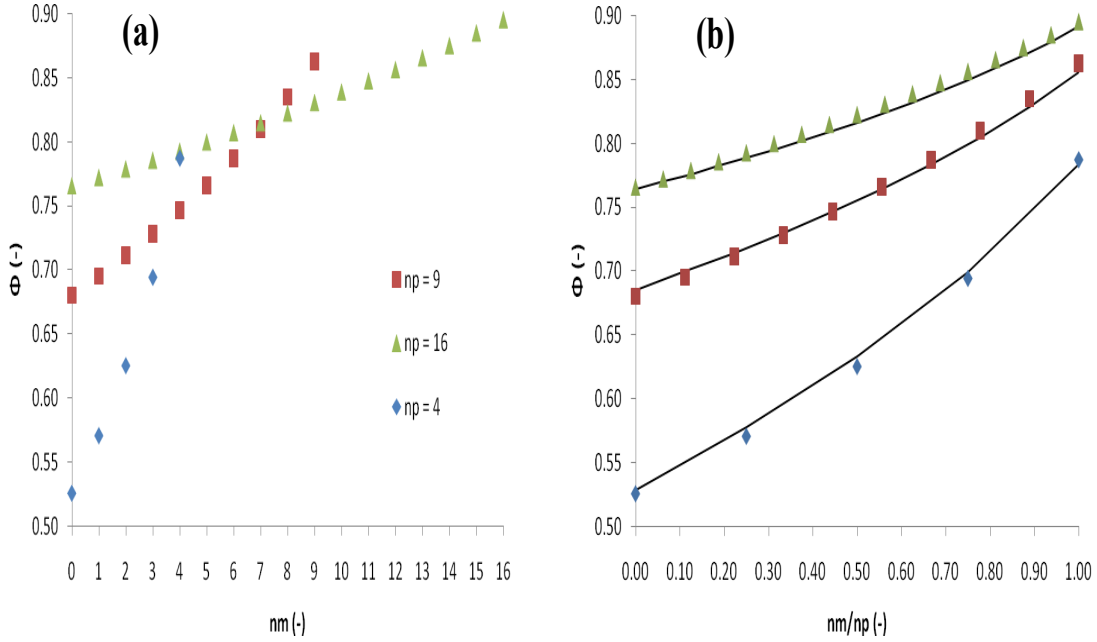

Figure 6-6. LRFD Φ as a function of degree of monitoring for different numbers of piles in a group (see legend) using $CV_{\varepsilon m} = 0.25$, $CV_{\varepsilon h} = 0.48$ and $\beta = 3$. (a) $\Phi = f(n_m)$ and (b) $\Phi = f(n_m/n_p)$. Dots are from full AASHTO equation, while continuous lines are from Equation 6.10.

Figure 6-7 displays the effect of variable $CV_{\varepsilon h}$ on Φ for different values of n_p and n_m/n_p. Evidently, Φ consistently decreases as $CV_{\varepsilon h}$ increases and vice-versa. The influence of $CV_{\varepsilon h}$, however, decreases gradually as the degree of monitoring increases and it has to become zero for full monitoring ($n_m/n_p = 1$). Moreover, averaging of prediction errors over a larger number of piles makes the sensibility of Φ to changes in $CV_{\varepsilon h}$ smaller for larger pile groups (graphs closer together). Effects of $CV_{\varepsilon m}$ on Φ are of the same nature as those of $CV_{\varepsilon h}$, however, they do not depend so much on n_m/n_p and correspond more to a vertical shifting of the curves in Figure 6-7.

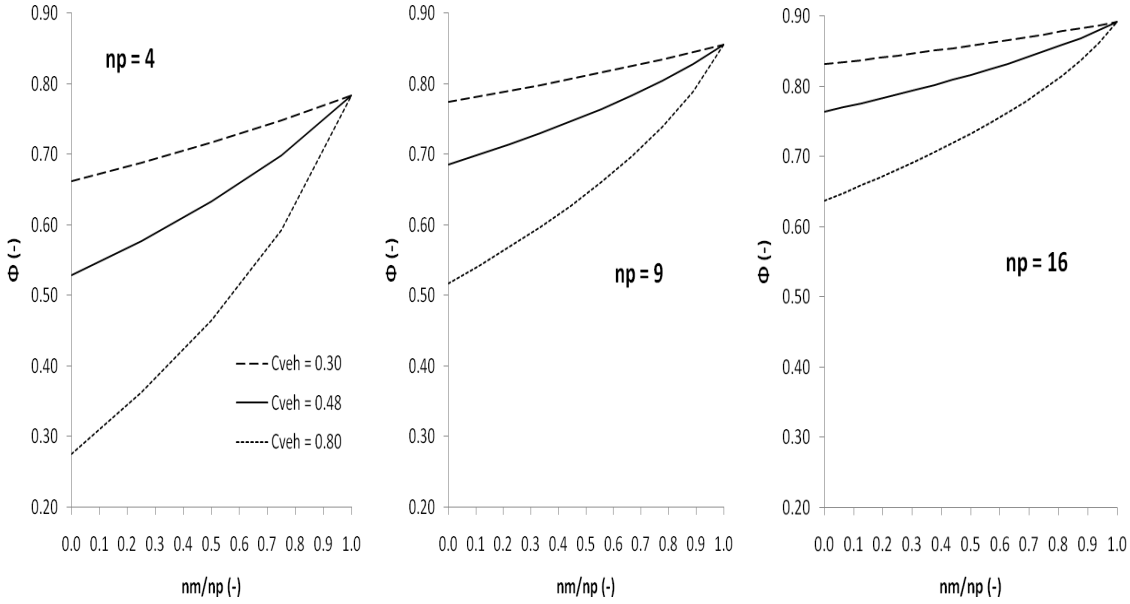

Figure 6-7. Term Φ as a function of degree of monitoring n_m/n_p for n_p = {4, 9, 16} and $CV_{\varepsilon h}$ = {0.30, 0.48, 0.80} (see legend). Continuous lines are identical to those in Figure 6-6b.

Assuming a nominal load Q = 15 MN of a group of nine piles, four of which it is intended to monitor, Figure 6-6 or Equation 6.10 give Φ = 0.75 leading further to R_g = 15/0.75 = 20 MN and R_p = 20/9 = 2.22 MN. This means that the four monitored piles are driven until a monitored resistance of 2.22 MN is reached, while the unmonitored piles are driven until a blowcount of $N_h = (R_p - a)/b$ = (2.22 – 0.030)/0.017 = 129 blows/m is reached, for which the expected monitored resistance is again 2.22 MN (regression relationship, Figure 6-5a). If it is further assumed that one pile of the group has already been installed to a monitored resistance R_0 = 3 MN ($CV_0 = CV_{\varepsilon m}$ = 0.25 for n_0 = 1), then the problem is to find R_p for the eight remaining piles (three monitored plus five unmonitored). For this purpose, Equations 6.14, 6.15 and 6.16 (with c = 1 and d = 1.73 as obtained for β = 3; Equation 6.9) may be used to find R_p = 2.11 MN which is smaller than 2.22 MN from above, as to be expected. For R_0 = 2.22 MN, i.e., when the first pile happened to be driven to the uniformly distributed nominal pile resistance, then $R_p = R_0$ = 2.22 MN is also correctly obtained. In case R_0 = 1.5 MN, i.e., the first pile was driven

too short, then R_p = 2.34 MN is required for each of the other eight piles. This example also illustrates the flexibility of the regression approach in being conceptually appropriate for a variety of design situations.

CHAPTER 7
SUMMARY AND CONCLUSIONS

The final length of a driven pile is proportional to its load and resistance factor design (LRFD) Φ factor which is a function of: (1) uncertainty of the capacity assessment approach, e.g., SPT, PDA, EDC; (2) spatial variability issues, i.e., change of properties from monitored to unmonitored pile; and (3) target reliability or probability of failure of pile group that the pile is located within. Recommended LRFD Φ factor for the design of driven piles using in situ SPT testing vary from 0.35 to 0.45 (e.g., AASHTO Table 10.5.5.2.3-1 – uncertainty of method: Tomlinson versus Meyerhof). In construction, for high strain rate field monitoring, LRFD Φ factor of 0.65 is recommended (PDA and CAPWAP: FDOT Structures Design Guidelines), if approximately 10% of the piles are monitored during driving. Others (AASHTO 2009) also use pre-defined Φ depending on number of piles monitored, type of monitoring, and whether static load testing is performed. For example, Φ = 0.75 if all piles are monitored and Φ = 0.80 if 20% are monitored, as well as one static load test will be performed.

Evidently, all of the approaches do not explicitly account for the spatial heterogeneity that generally exists between individual piles (monitored and unmonitored) in a group, number of piles monitored within a group, and the possibility of combined methods (i.e., high strain rate with hammer blow counts, etc.). Also, due to the typical dimensions of driven piles and expected vertical loads, piles are generally combined underneath a rigid pile cap to form a pile group foundation. For such a pile group foundation, none, some, or all of the individual piles may be monitored resulting in different pile group resistance uncertainty and, hence, different design LRFD resistance factors Φ for the group. Typically, the larger the number of piles monitored, the smaller should be the coefficient of variation of group resistance CV_R leading to higher Φ for the group.

The work presented begins with a discussion of probability of failure (POF) of a bridge and defines failure in terms of redundant and non-redundant systems. Generally, piers may be considered non-redundant (i.e., one pier failure then bridge fails), whereas, the group of piles (n_g>3) beneath a rigid cap could be considered as redundant, i.e., if one pile fails the group may not fail. It was found that the number of piles in a pier may play an important role for the POF of a bridge (see Chapter 2). As a consequence, the very fundamental question arises about what structural level (e.g., pile, pier or bridge) are design reliabilities or POF valid for. From a transportation point of view, it would make most sense to apply them to entire highway sections possibly including more than a single bridge. However, this would require an integrated approach of many engineering disciplines at the highest level of complexity which is currently out of reach. Instead, the geotechnical engineer involved in bridge foundation design is typically expected to determine pier dimensions for a given (pier or pile group) design load. Consequently, we believe that design and, hence, LRFD Φ must be based on the POF of the whole pier by accounting for the number of piles within the group and what is monitored and unmonitored within the group.

Next, the effort (Chapter 3) looked at spatial uncertainty (skin + tip resistance) of a single pile using in situ SPT data. Here, site data (SPT borings) were considered in assessing the spatial uncertainty of a pile (Figure 3-4) in terms of a site's SPT blow count N summary statistics (i.e., mean and standard deviation), and covariance (expressed in terms of correlation length a_v). Subsequently, the work was expanded to spatial group uncertainty (Chapter 4) for the case of pile skin friction. The effort also introduced kriging, which considered different weights for individual borings and group layouts (e.g., double, triple, quads, etc.) to assess group uncertainty CV_R. The work also focused on identifying worst case design scenarios for typically unknown horizontal correlation lengths.

Using the kriging approach, the work (Chapter 5) then moved to assessing uncertainty, i.e., spatial and method error (predicted versus static load test) using high strain rate field measurements. The effort developed charts identifying the uncertainty (variance) reduction (α_e) for a specific group based on number and geometric configuration of piles monitored within a group, total piles within the group, and number of pile groups at the site (see Figures 5-5 through 5-7). Once the variance reduction α_e for a specific group has been assessed, it may be multiplied by the variance of individual total pile capacity R_p (e.g., variance of all monitored piles) to give the variance of group resistance from which CV_R and LRFD Φ of the group may be found. Unfortunately, no simple analytical expression for variance reduction in terms of pile group layouts (e.g., group size, versus number and layout of monitored piles) could be developed. In addition, the development assumed that all piles within the group had approximately the same capacity on a horizontal plane where the pile tips were founded. And, the approach is specifically one directional, i.e., for a specific pile layout, monitoring, etc., the group uncertainty and LRFD Φ of the group is assessed along with the total group resistance Q which always increases with monitoring (see Table 5-1). Of interest for practice is the inverse solution where a specific axial design load is given and LRFD Φ for a group supported by driven piles of possibly different lengths and resistances needs to be assessed.

Due to the conceptual limitations of the kriging approach (Chapter 5), an alternative solution based on: (1) the use of blow count data recorded during pile installations as an additional piece of pile information currently used in construction practice; and (2) dropping spatial correlation between monitored pile resistances in favor of blow counts on every pile in order to avoid conceptual limitations. This allowed the approach to be more flexible/adaptive to different design situations and more designer friendly. Due to the very good correlation observed between blow count data and monitored resistances, the disregarding of spatial

correlation between monitored piles was shown to have a rather insignificant effect on group resistance uncertainties. As with prior work, the uncertainty of the pile group was expressed in terms of monitored (high strain rate data: EDC, PDA, etc.) and unmonitored piles (hammer blow count measurements) uncertainties. In terms of the unmonitored piles within a group, their uncertainty was assessed by linear correlation between blow count data and EDC/PDA capacities. Justification for the latter is supported in the literature by a series of formulae (ENR, Gates, etc.) between static pile capacity and hammer blow counts. Using both the monitored pile resistances and blow count predicted resistances, the total group resistance and its associated uncertainty (variance σ_g^2) was expressed in terms of monitoring uncertainty $CV_{\varepsilon m}$ (coefficient of variation between high strain rate testing and static load testing) and unmonitored uncertainty ($CV_{\varepsilon h}$ expressed the uncertainty between measured hammer blow count and high strain rate testing). Therefore, knowing the total group resistance R_g (Equation 6.5) and its associated uncertainty (Equation 6.6), its coefficient of variation CV_R may be readily assessed which when combined with a representative probability of failure (Chapter 2) a relatively simple LRFD Φ equation may be developed (Equation 6.10).

The applicability of Equation 6.10 versus current practice (i.e., FDOT, AASHTO) was investigated on two different sites: 1) Caminida Bay, Louisiana (piles 1 and 7); and 2) SR 810, Dixie Highway (piles 1 and 8) over Hillsboro Canal in Broward County, Florida. Using the hammer blow count data for two piles at each site versus EDC/PDA data, the uncertainty of the unmonitored piles $CV_{\varepsilon h}$ was assessed. Using an uncertainty of monitored piles $CV_{\varepsilon m}$ = 0.25, LRFD Φ (Equation 6.10) was assessed for 2×2 to 4×4 with variable pile monitoring (Figure 6-6). Interestingly, full monitoring gives LRFD Φ values similar to literature (i.e., AASHTO, FDOT); however, shown in the figure and not reported in the literature is the influence of pile group size (Chapter 2). Of additional importance is the flexibility of Equation 6.10 which allows

for different resistances of piles within group (see Equations 6.11 and 6.12), as well as nonlinear regressions between blow count and high strain rate capacities (see Chapters 2 and 6). Also of interest, and not discussed, are end of drive (EOD), beginning of restrike (BOR) high strain rate capacity assessment versus static axial capacity. The latter could readily be accounted for in $CV_{\varepsilon m}$.

Finally, the development of Equation 6.10 allows different considerations: (1) EOD versus BOR; (2) number of monitored piles; (3) variability of axial capacity within a group (Equations 6.11 through 6.16); and (4) equipment (EDC and PDA), site and soil specific conditions (e.g., $CV_{\varepsilon m}$, $CV_{\varepsilon h}$), both the contractor and owner have a multitude of options when designing/constructing a deep foundation. Of great interest to each will be the consideration of optimization, which results in the safest and most economical foundation.

REFERENCES

AASHTO. (2004). *LRFD Bridge Design Specifications*, 3rd ed., American Association of State Highway and Transportation Officials, Washington, D.C.

AASHTO. (2009). *LRFD Bridge Design Specifications, Customary U.S. units,* American Association of State Highway and Transportation Officials, Washington, D.C.

FDOT. (2009) *Temporary Design Bulletin C09-04,* "Mandatory Utilization of Embedded Data Collectors (EDC) in All Bridge Proects with Square Prestressed Concrete Pile Foundations.

Isaaks, E. H., and Srivastava, R. M. (1989). *An Introduction to Applied Geostatistics*, Oxford University Press.

Journel, A. G., and Huijbregts, C. J. (1978). *Mining Geostatistics*, The Blackburn Press.

Journel, A. G., and Rossi, M. E. (1989). "Do we need a trend model in kriging?," *Mathematical Geology*, Vol. 21, No. 7, pp. 715–739.

Klammler, H., McVay, M., Horhota, D., and Lai, P. (2010a). "Influence of spatially variable side friction on single drilled shaft resistance and LRFD resistance factors," *Journal of Geotechnical and Geoenvironmental Engineering*, Vol. 136, No. 8, pp. 1114–1123.

Klammler, H., McVay, M., Lai, P., and Horhota, D. (2010b). "Incorporating geostatistical aspects in LRFD design for deep foundations," In: *GeoFlorida 2010: Advances in Analysis, Modeling and Design*, E. O. Fratta, B. Muhunthan, and A. J. Puppala, eds., ASCE Geotechnical Special Publication N^{o} 199, ISBN 978-0-78441-095-0, CD-ROM.

Paikowsky, S. (2004). "Load and Resistance Factor Design (LRFD) for deep foundations," *NCHRP Report 507*, National Cooperative Highway Research Program, Washington, DC.

Zhang, L. M., Tang, W. H., and Ng, C. W. W. (2001). "Reliability of axially loaded driven pile groups," *Journal of Geotechnical and Geoenvironmental Engineering*, Vol. 127, No. 12, pp. 1051–1060.

APPENDIX A
SPATIAL CORRELATION VERSUS COLLOCATED SECONDARY DATA

This appendix attempts to illustrate the relationship between the approaches of Chapters 5 and 6 by regarding the simplest possible co-kriging scenario of monitored and blow count data for a two-pile foundation with one monitored (assuming $CV_{\varepsilon m} = 0$) and one unmonitored pile. Known are the spatial auto correlation functions C_{mm} of monitored resistance R_m with R_m, C_{hh} of blow count predictions $R_m^* = a + bN_h$ with R_m^* and the spatial cross correlation function C_{mh} of R_m with R_m^*. Since R_m^* is a linear regression predictor of R_m we know that the variances σ_{mm}^2 and σ_{hh}^2 of R_m and R_m^*, respectively, are related by $\sigma_{hh} = \rho_{mh}\sigma_{mm}$ (the slope of the regression line between R_m^* and R_m is one) with ρ_{mh} being the respective correlation coefficient. The covariance σ_{mh}^2 between R_m and R_m^* is known as $\rho_{mh}\,\sigma_{mm}\,\sigma_{hh} = \rho_{mh}^2\,\sigma_{mm}^2$. The spatial auto and cross correlation functions also need to meet certain criteria. In the simplest case they are all proportional with the same range, such that $C_{hh} = \rho_{mh}^2 C_{mm}$ and $C_{mh} = \rho_{mh} C_{mm}^{1/2} C_{hh}^{1/2} = \rho_{mh}^2 C_{mm}$, as shown in Figure A-1.

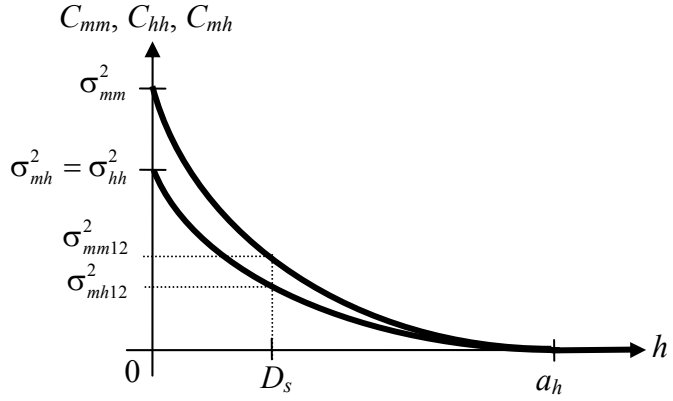

Figure A-1. C_{mm} (top curve) and $C_{mh} = C_{hh} = \rho_{mh}^2 C_{mm}$ (bottom curve).

With this, co-kriging of the monitored (= true because error assumed zero) resistance of the unmonitored pile can be done. There are different types of co-kriging and the one with a single bias condition as discusses in Isaaks and Srivastava (1989, Equation 17.15) is chosen here. The ordinary co-kriging system results as

$$\begin{bmatrix} \sigma^2_{mm} & \sigma^2_{mh12} & 1 \\ \sigma^2_{mh12} & \sigma^2_{hh} & 1 \\ 1 & 1 & 0 \end{bmatrix} \begin{bmatrix} w_1 \\ w_2 \\ \lambda \end{bmatrix} = \begin{bmatrix} \sigma^2_{mm12} \\ \sigma^2_{mh} \\ 1 \end{bmatrix} \tag{A.1}$$

where σ^2_{mh12} is the covariance between R_m at the first (monitored) pile and R^*_m at the second (unmonitored) pile which are separated by a distance D_s. In analogy, σ^2_{mm12} is the covariance between values of R_m at the two piles. From Figure A-1, it becomes clear that $\sigma^2_{mh12} = \rho_{mh}\sigma^2_{mm12}$. While λ is the Lagrangian operator; w_1 and w_2 are the weights assigned to the monitored resistance R_{m1} of the first pile and of the predicted resistance R^*_{m2} of the second pile. They are used in Equation A.2 to find an estimate R^{**}_{m2} of the monitored resistance R_{m2} of the second pile as

$$R^{**}_{m2} = w_1 R_{m1} + w_2 R^*_{m2} \tag{A.2}$$

Note that $w_1 + w_2 = 1$ and that a single asterisk "*" denotes a regression estimate only from collocated blow count information N_h, while double asterisks "**" denotes a co-kriging estimate including information from monitored piles at other locations (here R_{m1}).

Equation 1 may be solved for w_1, w_2 and λ or, alternatively, using Cramer's rule one can directly express the ratio w_1/w_2 as

$$\frac{w_1}{w_2}=\frac{\begin{vmatrix}\sigma^2_{mm12} & \sigma^2_{mh12} & 1\\ \sigma^2_{mh} & \sigma^2_{hh} & 1\\ 1 & 1 & 0\end{vmatrix}}{\begin{vmatrix}\sigma^2_{mm} & \sigma^2_{mm12} & 1\\ \sigma^2_{mh12} & \sigma^2_{mh} & 1\\ 1 & 1 & 0\end{vmatrix}}=\frac{\sigma^2_{mh12}+\sigma^2_{mh}-\sigma^2_{hh}-\sigma^2_{mm12}}{\sigma^2_{mm12}+\sigma^2_{mh12}-\sigma^2_{mh}-\sigma^2_{mm}} \tag{A.3}$$

With the relationships of Figure A-1 and by also introducing a spatial correlation coefficient $\rho_s = \sigma^2_{mm12}/\sigma^2_{mm} = \sigma^2_{mh12}/\sigma^2_{mh}$ as the auto correlation that persists over a lag distance D_s between the piles, Equation A.3 simplifies to

$$\frac{w_1}{w_2}=\frac{\rho_s\left(1-\rho^2_{mh}\right)}{\left(1-\rho_s\right)\left(1+\rho^2_{mh}\right)} \tag{A.4}$$

which is shown by contour lines in Figure A-2. In Chapter 5, R^*_{m2} is disregarded in Equation A.2, which is equivalent to using a large value of w_1/w_2 as it occurs in the yellow zone in Figure A-2. This zone is located where $\rho_s >> \rho_{mh}$, i.e., where spatial correlation is dominant. In Chapter 6, the opposite is the case and R_{m1} is eliminated from Equation A.2. This corresponds to small values of w_1/w_2 and the green zones in Figure A-2, i.e., where $\rho_{mh} >> \rho_s$ and blow count correlation dominates over spatial correlation. Interestingly from the data used in Chapter 6, it is evident that the green zone is relevant (see arrow at $\rho_{mh} \approx 0.85$) and neglecting R_{m1} will not have a large impact ($w_1 << w_2$; i.e., w_1 would be close to zero anyway). Neglecting R_{m1} is also conservative as the estimation uncertainty should somewhat increase, but again not by much as the weight of R_{m1} in estimation would not be very significant. One can also see that for $\rho_{mh} \approx 0.85$, it does not make a large difference what particular ρ_s there is unless it is really close to 1, which is irrelevant for practice. It is recalled that the error of the monitoring method was neglected here; this error would always decrease ρ_s. Moreover, in many situations the values of

ρ_s are not even reliably known (e.g., unknown horizontal correlation length). Note that Figure A-2 also indicates $w_2 >> w_1$ for both $\rho_{mh} \approx \rho_s \approx 0$. This is an artifact of the fact that the regression estimate in the present form does not consider uncertainty due to limited data (from a single unmonitored pile).

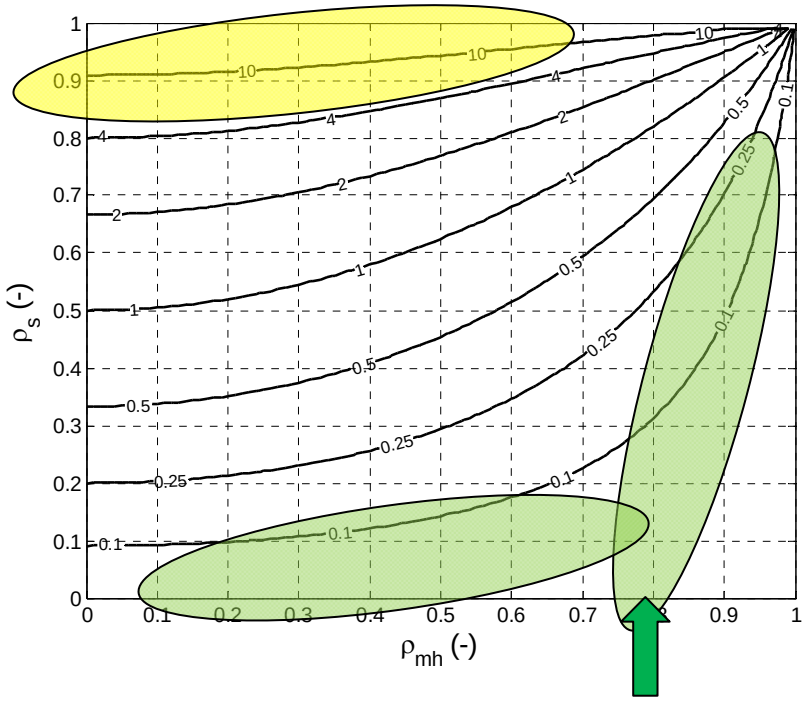

Figure A-2. w_1/w_2 as a function of ρ_{mh} and ρ_s. Yellow zone is where spatial correlation is dominant (previous approach), green zone is where correlation between blow count and monitored resistance is dominant. Green arrow indicates $\rho_{mh} \approx 0.85$ from Caminida and Dixie data.

Overall, this is a very simple "elementary" example, but if the conclusion holds for a single monitored and a single unmonitored pile, then it should also hold in some form for more complex configurations.